Front. Phys., 2011, 6(1): 15–45
DOI 10.1007/s11467-010-0155-y

REVIEW ARTICLE

Quantum superchemistry of de Broglie waves: New wonderland at ultracold temperature

Hui JING (景辉)†, **Ya-jing JIANG** (蒋亚静), **Yuan-gang DENG** (邓元刚)

Department of Physics, Henan Normal University, Xinxiang 453007, China

E-mail: †*jinghui73@gmail.com*

Received September 24, 2010; accepted October 8, 2010

The experimental realization of atomic Bose–Einstein condensation at ultracold temperature has led to rapid advances in creating and manipulating cold molecules, and which has given birth to a new research field of quantum matter-wave superchemistry. Contrary to the classical Arrhenius law, the tunneling-dominated ultracold reactions can be realized through the highly-controlled magneto–optical technique. Novel quantum effects have been identified in these cold reactions, such as the super-selectivity rule in dissociating triatomic molecules, and the quantum size (vessel-shape) effect. In this review, we focus on a variety of new achievements in this fascinating matter-wave wonderland, including the quantum finite-number effect and double-slit interference in assembling cold molecules, the quantum noise in triggering collective abstraction reaction, and the magnetic phase transition in a laser-catalyzed quantum spin-mixing gas. The practical applications of matter-wave superchemistry are also introduced, such as the optical information storage via quantum photo-association, and the laser-enhanced creation of spinor or even chiral molecules.

Keywords superchemistry, laser-catalyzed, collective abstraction reaction

PACS numbers 03.67.Lx, 03.65.Yz, 82.56.Jn

Contents

1 Introduction

Quantum control of atoms and molecules is essential for a broad range of research fields, from high-precision measurement to quantum information science [1]. The recent realization of Bose–Einstein condensate (BEC) [2–4] in dilute atomic gases, for example, has led to a number of advances with implications well past the confines of traditional atomic, molecular and optical (AMO) physics [5]. A particularly related achievement is *superchemistry* or quantum control of matter-wave reactions at ultracold temperature [6]. Contrary to the classical Arrhenius law in collision-dominated chemistry, the tunneling-induced cold reactions can be actively initiated and then collectively enhanced in a highly-controlled manner. This non-Arrehenius feature has

been identified in, i.e., the Bose-enhancement effect in creating cold molecules with bosonic or fermionic atoms by applying the magnetic Feshbach resonance (FR) [7, 8] or the optical photoassociation (PA) [9] technique. Cooperative many-body effects [10] have also been extensively studied in superchemistry, such as the efficient creation of fermionic molecules from an atomic Bose–Fermi mixture [11], the quantum-entangled pairs generation through three-body recombination [12–14] or dissociating the molecular condensate [15], and the Efimov many-body bound-state resonance [16–18]. Most recently, two groups first reported their wonderful experiments on cold abstraction reaction [19, 20] (with an atom–molecule mixture) or quantum conversion between homonuclear and heteronuclear molecules. Clearly, superchemistry of de Broglie waves is still in its golden age, and the purpose of this review is to introduce some new developments and their potential applications.

In the past ten years, the experiments have been focused on creating cold molecules via FR or PA technique, especially the simplest diatomic molecules, such as $^6Li_2$ [21–26], $^7Li_2$ [27], Na_2 [28], $^{40}K_2$ [29, 30], $^{85}Rb_2$ [31, 32], $^{87}Rb_2$ [33–37], Cs_2 [38–41], and their heteronuclear counterparts $^6Li^7Li$ [42, 43], $^6Li^{23}Na$ [44, 45], $^6Li^{40}K$ [46], $^6Li^{87}Rb$ [47, 48], $^7Li^{87}Rb$ [49], $^7Li^{133}Cs$ [50], NaCs [51], $^{39}K^{85}Rb$ [52], $^{40}K^{87}Rb$ [53–61], $^{85}Rb^{87}Rb$ [62], $^{85}RbCs$ [63–66]. Thereby, superchemistry mainly refers to coherent atom–dimer conversion ($a+a \rightarrow d$). Extensive works have been done for this simplest process, such as the generalized stimulated Raman adiabatic passage (STIRAP) technique [67–72] and the reactant diagnosis through quantum correlations of created molecules. In Section 2, we will show the quantum nature of superchemistry through a simple example, i.e., finite-number molecular formation.

Nevertheless, superchemistry certainly includes more complex couplings like $a+a+a \rightarrow g$ [73–76] or $a+a \rightarrow d$, $a+d \rightarrow g$ [77, 79], where a, d, g denote the atom, dimer, and trimer, respectively. In fact, the indirect evidence for three-body or four-body bound states has been observed, such as $^6Li_3$ [74], $^{40}K_3$ [75], Cs_3 [16–18], $^{87}Rb^{40}K^6Li$ [80], and $^{133}Cs_4$ [81]. In view of their novel anisotropic properties [82, 83], quantum control of triatomic molecule is of particular interest as it may lead to intriguing developments such as the realization of a triatomic molecular matter-wave amplifier [84] or quantum computing with a trimer lattice [58, 85, 86]. In Section 3, we will introduce the concept of atom–molecule dark state [87–92] and its applications in creating molecular trimer A_2B. An important result is that the creation of heteronuclear trimers can be significantly enhanced by constructive interference of two reaction channels leading to their formation.

The dissociation of cold molecules, i.e., $^{87}Rb_2$ or $^{23}Na_2$ into bosonic atomic pairs ($B_2 \rightarrow B + B$) [93, 94], turns out to be the matter-wave analog of the familiar parametric down-conversion process in quantum optics [95–99]. In contrast to this, the dissociation of bosonic molecules $^{40}K_2$ into fermionic atoms is governed by quantum many-body physics and closely related to the BEC–BCS crossover [100–103]. This process was demonstrated to be useful in precision measurement [15] and in providing quantum-entangled sources [99]. By considering coherent multichannel dissociation of bosonic trimer ABC, Moore and Vardi further showed the Bose-enhanced super-selectivity rule between different reaction channels [104, 105]. The dependence of dissociation on the size or shape of the trapping vessel was also revealed [106].

In Section 4, we will introduce coherent abstraction reaction or bimolecular reactive scattering $A + B_2 \rightarrow AB + B$ [107, 108], where A, B, B_2, and AB denote either bosonic or fermionic atoms or dimers. This reaction is an important benchmark system in chemical physics. Its dynamics has received much attention in recent studies of reactive resonance or low-energy non-Born–Oppenheimer reactivity through a crossed-beam scattering method [109, 110]. A particularly noteworthy contribution is the study by Shapiro and Brumer [111–113] of the coherent control of single-molecular PA or bimolecular collisions through interference of reactive pathways. Extending these considerations to the case of ultracold matter waves, we show that the coherent abstraction reaction can be realized efficiently and controlled in a PA pulse sequence [114, 115] such that the intermediate states are dark states. An important characteristic of this process is that it is triggered by quantum noise, leading to large shot-to-shot quantum fluctuations that invalidate the use of the Gross-Pitaevskii equation (GPE) in the initial stages. That equation can be used only at later times when the product reactant channels become macroscopically occupied. This is somewhat similar to the dissociation reaction or various quantum-optics examples such as the laser [116], optical and matter-wave super-radiance [117, 118], and molecular matter-wave amplifier [84], but in contrast to the molecular combination reaction [119].

In realizing the collective reaction $A + B_2 \rightarrow AB + B$, the basic idea is to first create weakly bound trimers AB_2 via an entrance-channel atom–dimer FR and then to dissociate them into a closed-channel bound dimer and atom via PA. This scheme, which is specific to quantum-degenerate matter waves, is different from a purely collision-induced reaction [12] and from the non-degenerate single-pair dynamics of reactive scattering [111–113]. As such it represents a promising advance in the ongoing development of superchemistry (see the recent experiment about $2KRb \rightarrow K_2 + Rb_2$ [20]). A key aspect of the coherent population trapping (CPT)scheme is of involving a trimer intermediate state which remains

almost unpopulated throughout the conversion process. Such an atom–molecule dark state does not exist in other schemes that involve, e.g., an intermediate two-species atomic state. In Section 5, we will confirm the existence of CPT states by calculating the nonlinear adiabatic condition of cold reactions, including the synthesis and the abstraction reactions.

Superchemistry is not only an important new playground for exploring the quantum nature of degenerate matter waves, but also has some fascinating applications, like quantum simulations or logical gate based on cold molecules. In Section 6, we will introduce an interesting example of this kind, i.e., encoding (and then decoding) the optical information of a quantized PA light into (and then from) the atom–molecule dark state. This nonlinear quantum memory, exploiting slow-light propagation through chemical reaction (first PA and then photodissociation) instead of linear atomic transitions, has several advantages of, e.g., much slower group velocity with the same atomic population. For the atom-heteronuclear molecule dark state, one also can study the role of populations imbalance of two atomic species and even the formation of splitting molecular soliton-laser beams.

Up to now, almost all the studies have been confined within the scalar atomic reactants. With the rapid advances in creating and manipulating multi-component spinor condensates [120, 121], the spin degrees of freedom of the polarized ultracold particles become accessible when a far-off-resonant optical trap is used to provide the confinement for all Zeeman states. The anharmonic spin oscillations under the influence of an external magnetic field can be well described by an effective nonrigid-pendulum model [122], which were experimentally confirmed in an antiferromagnetic condensate of ^{23}Na atoms [123, 124]. It is thus fascinating to further study the role of PA in quantum spin dynamics or even the creation of spinor molecules.

In Section 7, we will demonstrate theoretically the optical control of atomic spin mixing and laser-induced phase transition in a spin-1 Bose gas. In the proposed method the optical fields induce virtual PA processes in the atoms, for example via a dark molecular state. This step, which can be intuitively coined a laser-catalyzed spin-exchange process (SEP), opens up an efficient and well-controlled optical channel for spin mixing. By tuning the strength ratio of these two channels of optical SEP and spin collisions, three different regimes are identified, i.e., going from the collision-dominated regime to the no-spin-mixing regime, and to the laser-induced antiferromagnetic regime, which is reminiscent of the prominent role of long-range dipole–dipole interaction (DDI) in a dipolar spin gas (by changing the ratio of spin collision and DDI).

In a very recent experiment, Kobayashi *et al*. observed the spin-selective formation of spinor molecules in ferromagnetic atoms ^{87}Rb [125]. We will show that, due to the interplay of atomic spin-dependent collisions and the optical PA, an effective three-body spin-exchange interaction can dominate the atom-molecule spin dynamics, leading to the creation of quantum-entangled spinor atom–molecule pairs. The antiferromagnetic instability and the role of nonzero magnetization in creating spinor molecules are also discussed.

Finally, in Section 8, we give our summary and conclusion of this review, together with some prospects about the next on the agenda of quantum superchemistry.

2 Finite-number atom–molecule conversion

2.1 Finite N (total atomic number)

By constructing an exact quantum dark state, Zhao *et al*. in their recent work re-examined the atom–molecule conversion system with *finite*-number N of initial atoms [73]. They showed that the particles' population exhibit interesting quantum deviations from the mean-field approach (MFA) results, which turns out to be quite significant for the few-N cases. Hence, the classical GPE completely breaks down in the quantum few-N cases. The exact quantum solutions of atom–molecule dark state also allow one to study the higher-order matter-wave statistical properties. In the following, we focus on the exact quantum solutions of the atom-heteronuclear molecule dark state by considering the two-color PA process. We will show that the populations imbalance $\mathcal{M} \neq 0$ of the two-species atoms also play an important role in this system [126]. With large $\mathcal{M}$, the exact quantum result is very *close* to the classical one even for few N.

2.2 Finite $\mathcal{M}$ (population imbalance)

Without any loss of generality, we take the Rabi frequency of pumping or dumping laser $\Omega_{\rm p,d}$ to be real and positive whose phase factor can be absorbed by a global gauge transformation of the field operators [127]. Δ and δ are the single- and two-photon detunings of the frequencies of two lasers, respectively. In order to compare with that of Ref. [73], here we ignore the collisions of a dilute or FR tuned gas, a safe approximation for short molecular lifetime [73, 91]. In the interaction picture, the Hamiltonian of this system can be written in the simplest level as ($\hbar = 1$):

$$\hat{H} = \Delta\hat{\psi}_e^\dagger\hat{\psi}_e + \frac{1}{2}\left(\Omega_p\hat{\psi}_e^\dagger\hat{\psi}_a\hat{\psi}_b + \Omega_d\hat{\psi}_e^\dagger\hat{\psi}_g + h.c.\right) \qquad (1)$$

where $\hat{\psi}_i$ or $\hat{\psi}_i^\dagger$ is the bosonic annihilation or creation operator ($i = a,\ b,\ e,\ g$). The standard MFA is valid if the number of particles is significantly large and then

the operators can be replaced by the c-numbers ψ_i or ψ_i^*. Then, the mean-field dark state is computed,

$$|D\rangle_{\rm MF} = \left(\psi_a^0, \psi_b^0, \psi_e^0, \psi_g^0\right)^{\rm T} = \left(\psi_a^0, \psi_b^0, 0, \psi_g^0\right)^{\rm T}$$

with

$$\begin{aligned}
&|\psi_a^0|^2 + |\psi_b^0|^2 + 2|\psi_g^0|^2 = N \\
&|\psi_a^0|^2 - |\psi_b^0|^2 = \mathcal{M} > 0 \\
&2|\psi_{a,b}^0|^2 = -1/\chi^2 \pm \mathcal{M} \\
&\qquad + \sqrt{(N + 1/\chi^2)^2 - (N^2 - \mathcal{M}^2)}
\end{aligned}$$

and $\chi = \Omega_{\rm p}/\Omega_{\rm d}$. Clearly, by tuning $\chi(t)$, the atoms can be converted into the ground-state molecules without any population in the excited state $|e\rangle$. This picture is also true for *quantum* CPT state

$$|D\rangle_Q = |0\rangle_e |\Psi\rangle_{\mu\in(a,b,g)}$$

From the eigenequation $\hat{H}|D\rangle_Q = 0$,

$$(\chi\hat{\psi}_a\hat{\psi}_b + \hat{\psi}_g)|\Psi\rangle_\mu = \hat{\psi}_g e^{\chi\hat{\psi}_g^\dagger\hat{\psi}_a\hat{\psi}_b}|\Psi\rangle_\mu = 0 \tag{2}$$

The quantum dark state is then

$$|D\rangle_Q = C(\chi, N, \mathcal{M}) e^{-\chi\hat{\psi}_g^\dagger\hat{\psi}_a\hat{\psi}_b}|N_a, N_b, 0, 0\rangle \tag{3}$$

with the normalization factor $C(\chi, N, \mathcal{M})$ and the Fock state basis $|N_a, N_b, N_e, N_g\rangle$. By expanding the exponential operator, we have another form of the superposition state, i.e.,

$$|D\rangle_Q = \sum c_n |N_a - n, N_b - n, 0, n\rangle$$

The comparisons between the quantum and the MFA results about the populations of closed-channel molecules A_2 (homonuclear) or AB (heteronuclear) are shown in Fig. 1, for $\mathcal{M} = 0$ (but with different values of N). In this case, as is expected, quantum effects are significant in the few-N situations and the conversion rate is always *higher* than the mean-field results, for both heteronuclear and the homonuclear cases. We note that the quantum deviations are always *larger* in creating heteronuclear molecules AB.

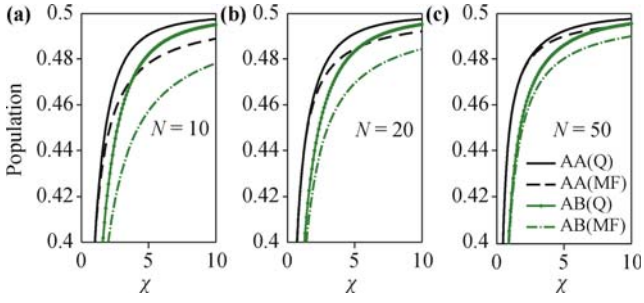

Fig. 1 The population of ground-state molecules A_2 or AB as the function of Rabi frequencies ratio χ, for different initial atomic number $N = 10,\ 20,\ 50$. Reproduced from Ref. [127], Copyright © 2010 The American Physical Society.

Figure 2(a) is the result for a small number $N = 10$ but $\mathcal{M} \neq 0$. Clearly, even for finite total number of *imbalanced* two-species atoms, the mean-field conversion rate still can be remarkably close to the exact quantum results. This feature is impossible to be observed in creating homonuclear dimers. In Fig. 2(b), it also can be seen that for both large $N = 100$ and small $N = 10$, the mean-field and exact quantum lines are almost overlapped ($N_b = 4$ for both cases). In fact, for large N_a, this system is reduced to a linear one since the operator $\hat{\psi}_a$ can be replaced by a c-number.

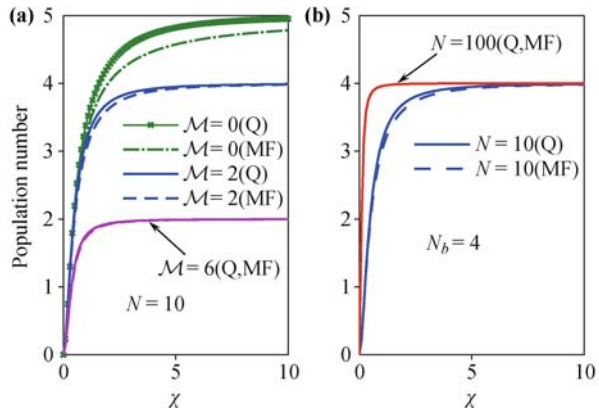

Fig. 2 **(a)** is the population number of molecules AB as the function of χ, for different initial number of N_b, at $N = 10$. **(b)** adds a line of $N = 100, N_b = 4$. In all figures both the quantum and mean-field solution are presented. Reproduced from Ref. [127], Copyright © 2010 The American Physical Society.

Now we consider the second-order correlations,

$$g_i^{(2)} = \frac{\langle\hat{\psi}_i^\dagger\hat{\psi}_i^\dagger\hat{\psi}_i\hat{\psi}_i\rangle}{\langle\hat{\psi}_i^\dagger\hat{\psi}_i\rangle^2} = \frac{\langle\hat{\psi}_i^\dagger\hat{\psi}_i^\dagger\hat{\psi}_i\hat{\psi}_i\rangle}{n_i^2}, \quad \mathcal{C}_{ig} = \frac{\langle\hat{n}_i\hat{n}_g\rangle}{n_i n_g}$$

For $\mathcal{M} = 0$ with large N, the classical Poissonian distribution can be reached for both the homonuclear and the heteronuclear dimers [73, 126, 128].

For the general case $\mathcal{M} \neq 0$, we have

$$\begin{aligned}
&\lim_{\chi\to 0} g_{a,b}^{(2)} = 1 - \frac{1}{N_{a,b}} \\
&\lim_{\chi\to 0} g_{\rm AB}^{(2)} = \frac{(N_a - 1)(N_b - 1)}{N_a N_b}
\end{aligned} \tag{4}$$

$$\begin{aligned}
&\lim_{\chi\to\infty} g_a^{(2)} = 1 - \frac{1}{\mathcal{M}}, \quad \lim_{\chi\to\infty} g_{AB}^{(2)} = 1 - \frac{1}{N_b} \\
&\lim_{\chi\to\infty} g_b^{(2)} = 1 - \frac{N + \mathcal{M} + 2}{(N - \mathcal{M})(\mathcal{M} + 2)}
\end{aligned} \tag{5}$$

Figure 3(a) and (b) shows the numerical results for evolutions of quantum matter-wave correlations with a finite small number $N = 10$. We can observe that, by increasing the imbalance value $\mathcal{M}$, $g_a^{(2)}$ can be significantly increased and tends to the classical value $g_a^{(2)} \to 1$. In contrast, the non-classical feature becomes more evident for the created molecules, i.e., $g_{\rm AB}^{(2)} \to 0$. The most interesting result turns out to be that of $g_b^{(2)}$, which first increases to some maximum value for

$$\mathcal{M}_{\max} = \sqrt{2N(N+2)} - (N+2)$$

and then decreases to 0. This feature also can be seen in Fig. 3(c) for $N = 50$. Clearly, $\mathcal{M}_{\max} \sim 4$ for $N = 10$ and $\mathcal{M}_{\max} \sim 20$ for $N = 50$.

The role of populations imbalance also can be observed by probing the atom–molecule quantum correlations. In the two limits of χ,

$$\begin{aligned} &\lim_{\chi\to 0} \mathcal{C}_{ag} = 1 - \frac{1}{N_a}, \quad \lim_{\chi\to\infty} \mathcal{C}_{ag} = 1 \\ &\lim_{\chi\to 0} \mathcal{C}_{bg} = 1 - \frac{1}{N_b}, \quad \lim_{\chi\to\infty} \mathcal{C}_{bg} = 1 - \frac{1}{N_b} < 1 \end{aligned} \tag{6}$$

The distinction between $\mathcal{C}_{ag}$ and $\mathcal{C}_{bg}$ is obvious, since one tends to the classical value 1 but the other tends to a non-classical value relying on the initial atomic number. This feature, as numerically confirmed in Fig. 3(d), does *not* exist both in the homonuclear case or in the heteronuclear (balanced) case with $\mathcal{M} = 0$.

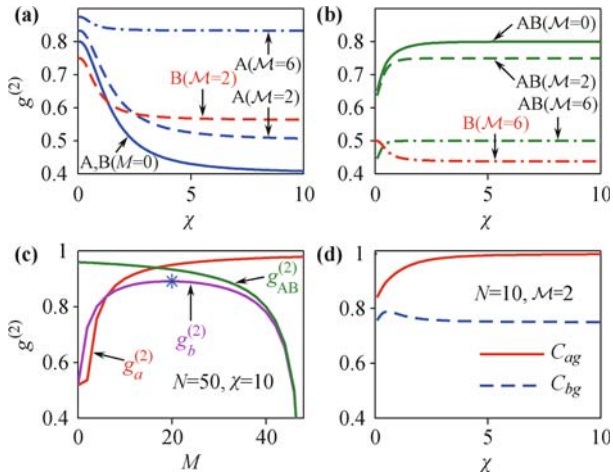

Fig. 3 **(a)**, **(b)** Quantum correlation functions $g^{(2)}$ as a function of χ for $N = 10$, and **(c)** as a function of populations imbalance $\mathcal{M}$ for $N = 50$, $\chi = 10$; **(d)** the atom–molecule correlation $\mathcal{C}_{ag,bg}$ as a function of χ. Reproduced from Ref. [127], Copyright © 2010 The American Physical Society.

2.3 Adiabatic fidelity

The quantum solutions also allow us to study the full energy spectrum and the adiabatic fidelity [129, 130] of the atom-heteronuclear molecule conversion. To see this point, we performed the simulations by choosing two Gaussian pulses (with width T, centered at $t_{\rm p,d}$, $t_{\rm d} < t_{\rm p}$)

$$\Omega_{\rm p,d}(t) = \Omega_0 \mathrm{e}^{-(t-t_{\rm p,d})^2/T^2} \tag{7}$$

Figure 4 shows the adiabatic fidelity between $|\psi(t)\rangle$ and the instantaneous dark state $|D(t)\rangle_Q$. In the ideal case, the fidelity should be close to 1. However, for $\Delta = 0$, the system departs from $|D(t)\rangle_Q$ even for finite number of atoms N. This problem can be overcame either by choosing a larger detuning, i.e. $\Delta = 0.5$ (see Fig. 4), or more interestingly, by choosing larger populations imbalance, e.g., $\mathcal{M} = 15$, $\Delta = 0$ (with a fixed value of N_b). We note that larger total particles number N (with a fixed value of N_b) leads to improved adiabatic fidelity. This is in contrast to that of the homonuclear system (the adiabatic fidelity is worse for larger N [73]). Clearly, the parameter $\mathcal{M}$ provides an additional freedom to control quantum dark-state evolutions of the system.

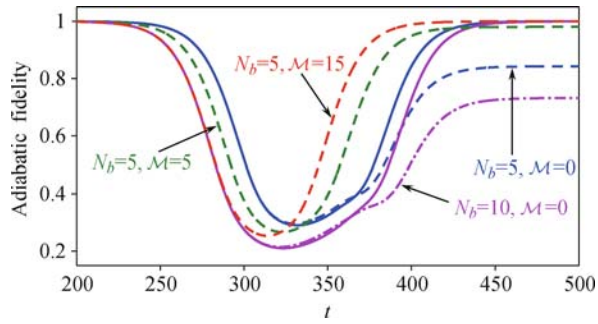

Fig. 4 The adiabatic fidelity $|\langle\psi(t)|D(t)\rangle_Q|^2$ as the function of time, for $\Delta = 0$ (*dashed lines*, $N_b = 5$, $\mathcal{M} = 0,\ 5,\ 15$) and $\Delta = 0.5$ (indistinguishable solid lines for different values of N and $\mathcal{M}$). Other parameters: $\Omega_0 = 5$, $T = 100$, $t_{\rm d} = 250$, and $t_{\rm p} = 450$. Reproduced from Ref. [127], Copyright © 2010 The American Physical Society.

3 Interfering for the better assembly

The combination of magnetic FR and optical PA techniques has recently been shown to be able to achieve the efficient and stable conversion of atoms into molecular dimers [87]. In this Chapter, we demonstrate that this STIRAP method can in principle be extended to the generation of molecular trimer. An important new result is that the creation of *heteronuclear* trimer can be significantly enhanced by the constructive interference of different quantum channels leading to their formation from atomic condensate.

3.1 Double-slit-like interference

The formation of heteronuclear trimers A_2B can be realized through two different paths that involve intermediate dimers A_2 (channel I, path AA) or AB (channel II, path AB), respectively. To set the stage we consider first the single-channel case I (or II), whereby AA (or AB) dimers formed via FR are photoassociated with an atom B (or A) to form the trimer A_2B. The essence of the idea is to minimize the occupation of intermediate dimers by exploiting an atom–molecule dark state that permits the direct association of atoms into trimers without the formation of a substantial dimer population in the process [91]. The dynamics of the system can be described by the model Hamiltonian

$$\begin{aligned} \hat{\mathcal{H}}_{I,II} = -\hbar \int \mathrm{d}r \Big\{ &\sum_{m,n} \chi_{mn} \hat{\psi}_m^\dagger(r) \hat{\psi}_n^\dagger(r) \hat{\psi}_n(r) \hat{\psi}_m(r) \\ &+\delta \hat{\psi}_{d_i}^\dagger(r) \hat{\psi}_{d_i}(r) + \lambda_i' \big[\hat{\psi}_d^\dagger(r) \hat{\psi}_a(r) \hat{\psi}_{a,b}(r) + h.c.\big] \\ &+(\Delta+\delta) \hat{\psi}_g^\dagger(r) \hat{\psi}_g(r) - \Omega_i' \big[\hat{\psi}_g^\dagger(r) \hat{\psi}_{d_i} \hat{\psi}_{b,a} + h.c.\big] \Big\} \end{aligned}$$

where $m, n = a, b, d_i, g$ and $i = 1$ or 2 for the case I or II. Denoting the strength of the atom-dimer coupling with detuning δ by λ_1', the Rabi frequency of the PA laser by Ω_1' and its detuning by Δ, and the collision terms proportional to χ_{ij} describe s-wave collisions between these species. The nonlinear bound–bound coupling between dimers and trimers is typically induced by a narrow–frequency, continuous-wave PA laser, for which the Franck–Condon factor can be calculated by resonant scattering theory [114, 115, 131] and be tuned by laser pumping methods [9, 132].

We assume in the following that the main features of the dynamics are adequately described by a mean-field analysis, $\hat{\psi}_i \to \sqrt{n}\psi_i$, where n is the initial atomic density. In this limit, the system is described by the equations of motion ($\hbar = 1$)

$$\begin{aligned}
\frac{\mathrm{d}\psi_a}{\mathrm{d}t} &= 2\mathrm{i}n\sum_m \chi_{am}|\psi_m|^2\psi_a + 2\mathrm{i}\lambda_1\psi_{d_1}\psi_a^* \\
\frac{\mathrm{d}\psi_b}{\mathrm{d}t} &= 2\mathrm{i}n\sum_m \chi_{bm}|\psi_m|^2\psi_b - \mathrm{i}\Omega_1\psi_{d_1}^*\psi_g \\
\frac{\mathrm{d}\psi_{d_1}}{\mathrm{d}t} &= -(\gamma - \mathrm{i}\delta)\psi_{d_1} + 2\mathrm{i}n\sum_m \chi_{d_1m}|\psi_m|^2\psi_{d_1} \\
&\quad +\mathrm{i}\lambda_1\psi_a^2 - \mathrm{i}\Omega_1\psi_b^*\psi_g \\
\frac{\mathrm{d}\psi_g}{\mathrm{d}t} &= 2\mathrm{i}n\sum_m \chi_{gm}|\psi_m|^2\psi_g + \mathrm{i}(\Delta+\delta)\psi_g - \mathrm{i}\Omega_1\psi_{d_1}\psi_b
\end{aligned} \tag{8}$$

where $\lambda_1 = \lambda_1'\sqrt{n}$, $\Omega_1 = \Omega_1'\sqrt{n}$ and the decay rate γ accounts for the loss of untrapped dimers. To reduce these losses we exploit a CPT technique that relies on the existence of an approximate atom–molecule dark state. Such techniques are well known in the case of linear systems, where they permit the transfer of population from an initial to a final state via an intermediate state that remains unpopulated at all times. This is the basis for STIRAP, which achieves this goal via a so-called counter-intuitive sequence of pulses [114, 115].

By using the steady-state ansatz

$$\begin{aligned}
&\psi_a = |\psi_{a,s}|\mathrm{e}^{\mathrm{i}\theta_a}\mathrm{e}^{-\mathrm{i}\mu_a t}, \quad \psi_{d_1} = |\psi_{d_1,s}|\mathrm{e}^{2\mathrm{i}\theta_a}\mathrm{e}^{-2\mathrm{i}\mu_a t} \\
&\psi_b = |\psi_{b,s}|\mathrm{e}^{\mathrm{i}\theta_b}\mathrm{e}^{-\mathrm{i}\mu_b t}, \quad \psi_{d_2} = |\psi_{d_2,s}|\mathrm{e}^{\mathrm{i}(\theta_a+\theta_b)}\mathrm{e}^{-\mathrm{i}(\mu_a+\mu_b)t} \\
&\psi_g = |\psi_{g,s}|\mathrm{e}^{\mathrm{i}(2\theta_a+\theta_b)}\mathrm{e}^{-\mathrm{i}(2\mu_a+\mu_b)t}
\end{aligned}$$

it is easily shown that under the generalized two-photon resonance condition

$$\begin{aligned}
\Delta_{\mathrm{I}} = \Delta_{\mathrm{II}} &= -\delta + (4\chi_{ag} + 2\chi_{bg} - 2\chi_g)N_g^0 \\
&\quad +(4\chi_a + 4\chi_{ab} - 2\chi_{ag} + \chi_b - \chi_{bg})N_a^0 \qquad (9) \\
\mu_{a;b}^{\mathrm{II}} = \mu_{a;b}^{\mathrm{III}} &= 2(\chi_{aa;bb}N_{a,s;b,s} + \chi_{ab}N_{b,s;a,s} + \chi_{ag;bg}N_{g,s})
\end{aligned}$$

Eqs. (8) admit a steady-state solution with no dimer population,

$$N_{g,s} = \frac{1}{3}\cdot\frac{k(\lambda_i/\Omega_i)^2}{1 + k(\lambda_i/\Omega_i)^2} \tag{10}$$

where $i = 1$ and $k = 4$. For the path AB, Eq. (10) remains the same, but with $i = 2$ and $k = 1$, so that $N_{g,s}^{\mathrm{AB}} < N_{g,s}^{\mathrm{AA}}$ for the same external parameters.

One can show both numerically and also via an approximate analytical treatment that the increase in deviation from the optimal CPT values as a function of time is different for the two cases. To demonstrate this point we numerically simulate the creation of trimer A_2B, including two-body collisions.

Figure 5 shows that results of numerical simulations that consider the channels AA and AB separately. In the specific example of the figure atom A is ^{41}K and atom B is ^{87}Rb, two atoms for which good scattering parameters are available [133], λ_i=4.718 × 10^4 s^{-1}, and

$$\Omega_i(t) = \Omega_{i,0}\mathrm{sech}(t/\tau) \tag{11}$$

with $\Omega_{i,0}/\lambda_i = 20$, $\lambda_i\tau = 20$. In units of λ_i/n, the parameters: $\chi_a = 0.3214$, $\chi_b = 0.5303$, $\chi_{ab} = 0.8731$, and the other collision parameters are taken as 0.0938 (in units of λ_l/n). As expected, the two reaction channels lead to different dynamical behaviors.

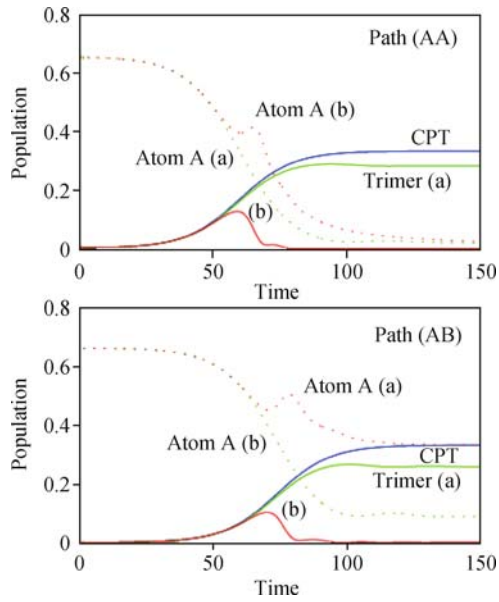

Fig. 5 Heteronuclear trimer population for (a) $\delta = -3$ (*in green*) or (b) $\delta = 3$ (*in red*) and their corresponding numbers of atom A. Time is in units of λ_l^{-1}, and $\gamma = 1$. The dimer population (A_2 or AB) remains essentially zero at all times and is not shown. The line labelled "CPT" shows the ideal, analytically derived trimer population. The evolution of the atoms B is also not shown. Reproduced from Ref. [78], Copyright © 2008 The American Physical Society.

We now proceed to demonstrate that when acting in concert, the two channels can yield a significantly larger conversion rate and approach the ideal CPT yield of 1/3, see Fig. 6. Here, the coexistence of the two channels provides considerable additional flexibility in approaching the ideal CPT value for trimer formation. Note however that this approach either requires an accidental coincidence of FRs for the dimers formation, or might be real-

izable by applying a magnetic field gradient [134] across the coexisting (A, B) condensates.

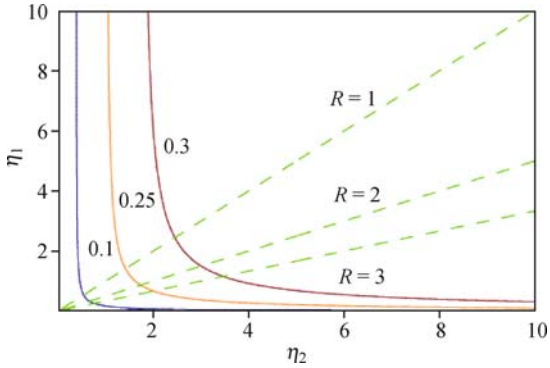

Fig. 6 Normalized CPT trimer population as a function of $\eta_l = \lambda_l/\Omega_l, l = 1, 2$. Also shown are three values of $R = \eta_2/\eta_1$. At constant ratios $\Omega_2(t)/\Omega_1(t)$ the counterintuitive evolution of the system is along lines of constant R starting from the origin. Reproduced from Ref. [77], Copyright © 2007 The American Physical Society.

Figure 6 plots the steady-state trimer number $N_{g,s}$ as a function of $\eta_l = \lambda_l/\Omega_l, l = 1, 2$, as well as the parameter

$$R = \eta_2/\eta_1 \tag{12}$$

(Note that there is no CPT solution for $R < 0$.) As the STIRAP PA pulses $\Omega_1(t)$ and $\Omega_2(t)$ are applied, η_1 and η_2 increase and if the ratio of their amplitudes remains constant the system evolves along a line of constant R. However, it is not obvious that this should still be the case in the presence of collisions. In fact, each of the individual paths leading to the formation of trimers is characterized by an increasing departure of the population transfer from the CPT solution as time evolves. This is where quantum interferences come into play: the freedom of choice of R, which is a unique feature of the two-channel scheme, provides us with additional flexibility in attempting to approach the ideal CPT value via the interference of the two paths.

We found numerically that $R = 2$ leads to a trimer production that most closely approaches the ideal CPT solution, and is significantly larger than in the single-channel situation of Fig. 5. This is illustrated in Fig. 7 for $\delta = 0$ and $\delta = -3$. Note the insensitivity of trimer production to the detuning in that case. These results should be contrasted to Fig. 7(b), which shows the evolution of the trimer population in case $R = 1$, again for $\delta = 0$ and $\delta = -3$. Here, the trimer production is very significantly reduced, and depends strongly on the value of the detuning. Similar results have been obtained for the other values of R and the other sets of collision parameters that we have considered, which does not depend on the details of the trimer potential function [135].

3.2 Assembling trimer ^{87}Rb^{40}K^{6}Li

Very recently, Taglieber *et al.* realized experimentally for the first time a quantum-degenerate three-species Bose–Fermi–Fermi mixture ^{87}Rb-^{40}K-^{6}Li [80]. This provides a promising new platform for the study of creating ABC trimer as well as the investigation of Fermi–Fermi or Bose-Fermi mixtures within one sample [76].

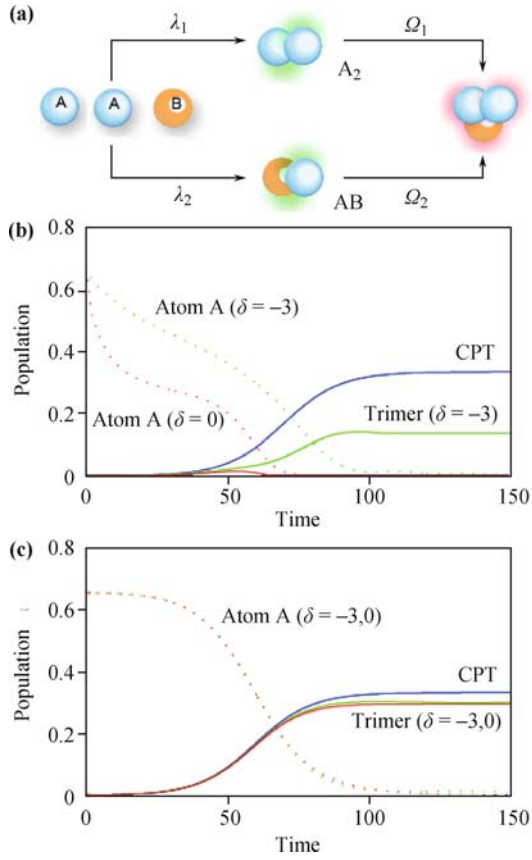

Fig. 7 **(a)** Two-channel creation of trimers. The time dependence of the populations of the trimer (*solid*) and of atom A (*dotted*) are shown for **(b)** $R = 1$ or **(c)** $R = 2$. Reproduced from Ref. [78], Copyright © 2008 The American Physical Society.

The purpose of this section is to show that, by starting from a ^{87}Rb-^{40}K-^{6}Li mixture, one can exploit a constructive multi-path interference in the atom–molecule conversion. In particular, the triple-path case can be almost ideal and far more efficient than the single- or double-path cases. Also, the choice of the external fields needs to account for the initial atomic populations imbalance in order to keep the dimer states unpopulated, that is, to guarantee an (approximate) dark state. While the proposed scheme is experimentally challenging, recent progress in the manipulation of atom–dimer or dimer–dimer resonances [64, 81–83, 136] indicates that it may become possible in the not too distant future.

3.2.1 *Interfering for the best*

As illustrated in Fig. 8, there are three different paths that lead to the creation of the heteronuclear trimer ABC in a ^{87}Rb-^{40}K-^{6}Li mixture via the FR-assisted PA method. They involve the intermediate fermionic dimers

AB or AC or the bosonic dimer BC, respectively. The existence of CPT dark state makes it possible to eliminate the collision losses that would otherwise significantly reduce the conversion process. The energy density corresponding to the path-AB case is given in the Hartree approximation by [137]

$$\begin{aligned} E_{\rm AB} = & \sum_{i\neq j}\frac{1}{2}\chi'_{ij}|\psi_i|^2|\psi_j|^2+\delta|\psi_{d_1}|^2 \\ & +\lambda'_1\left(\psi^*_{d_1}\psi_a\psi_b+h.c.\right) \\ & +(\Delta+\delta)|\psi_g|^2-\Omega'_1\left(\psi^*_g\psi_{d_1}\psi_c+h.c.\right) \\ & +\sum_{i=(a,g)}\frac{1}{2}\chi'_i|\psi_i|^4+\sum_{f=(b,c,d_1)}\frac{3}{5}A'_f|\psi_f|^{10/3} \end{aligned} \tag{13}$$

Here, λ'_1, Ω'_1, δ, and Δ are same as section 3.1, the indices $i,j=a,b,c,d_1,g$ stand for the atoms, dimers or trimers, respectively, and $A'_f=(6\pi^2)^{2/3}/(2M_f)$, with M_f $(f=b,c,d_1)$ denoting the mass of the fermionic components. The terms proportional to $\chi'_{ij}=2\pi a_{ij}/M_{ij}$ describe the s-wave collisions between the species i and j, a_{ij} is the s-wave scattering length, and $M_{ij}=M_iM_j/(M_i+M_j)$ is the reduced mass ($\chi'_i=\chi'_{ii}$). Note that there are no s-wave collisions between fermionic atoms of the same species, so that the kinetic energy dominates the intra-species interaction. Hence, it is a good approximation to consider only the kinetic energies for same-species fermions, but to assume that the collisions are the dominating terms for the bosons and for inter-species fermion-fermion interactions.

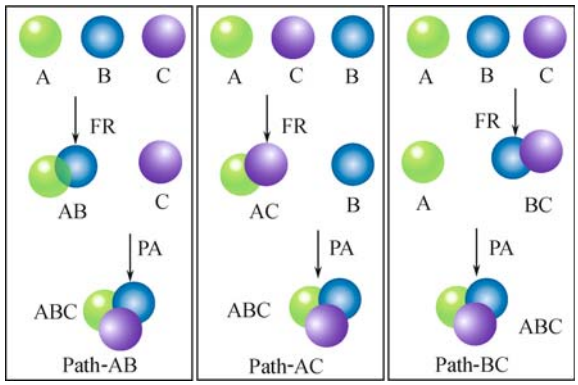

Fig. 8 The possible path for the coherent association of the heteronuclear trimer ABC in the ^{87}Rb-^{40}K-^{6}Li mixture via the intermediate fermionic dimers AB and AC or the bosonic dimer BC. Here, A, B, or C denote the atoms ^{87}Rb, ^{40}K, or ^{6}Li, respectively. Reproduced from Ref. [79], Copyright © IOP Publishing Ltd. and Deutsche Physikalische Gesellschaft.

The ordinary mean-field approach [138, 139] is suitable to treat systems with large numbers of condensed bosonic particles, but is of course inadequate for fermions. Here we follow the approach of Ref. [137] by starting from the mean-field Lagrangian density [140, 141] and using the Euler–Lagrange equations to derive mean-field dynamical equations. We then consider a single evolution equation for each particle species, noting that due to the different nature of the self-interaction terms, though, there are important differences between the mean-field dynamical equations for fermions and those for bosons. With these considerations in mind we introduce the mean-field Lagrange density

$$\mathcal{L}=\frac{\mathrm{i}}{2}\sum_i\left(\psi^*_i\frac{\partial\psi_i}{\partial t}-\psi_i\frac{\partial\psi^*_i}{\partial t}\right)-E_{\rm AB} \tag{14}$$

for the system, and substitute it into the Euler–Lagrange equations

$$\frac{\partial\mathcal{L}}{\partial\psi^*_i}-\partial_\mu\left(\frac{\partial\mathcal{L}}{\partial(\partial_\mu\psi^*_i)}\right)=0 \tag{15}$$

This yields a set of coupled evolution equations for each species. For example the path-AB is described by the following equations of motion, with $\phi_i=\psi_i/\sqrt{n}$ and n the initial particle density:

$$\begin{aligned} \frac{\mathrm{d}\phi_a}{\mathrm{d}t} &= -\mathrm{i}\sum_j\chi_{aj}|\phi_j|^2\phi_a-\mathrm{i}\lambda_1\phi_{d_1}\phi^*_b \\ \frac{\mathrm{d}\phi_b}{\mathrm{d}t} &= -\mathrm{i}\sum_{j\neq b}\chi_{bj}|\phi_j|^2\phi_b-\mathrm{i}\lambda_1\phi^*_a\phi_{d_1}-\mathrm{i}A_b|\phi_b|^{4/3}\phi_b \\ \frac{\mathrm{d}\phi_c}{\mathrm{d}t} &= -\mathrm{i}\sum_{j\neq c}\chi_{cj}|\phi_j|^2\phi_c+\mathrm{i}\Omega_1\phi_g\phi^*_{d_1}-\mathrm{i}A_c|\phi_c|^{4/3}\phi_c \\ \frac{\mathrm{d}\phi_{d_1}}{\mathrm{d}t} &= -\mathrm{i}\sum_{j\neq d_1}\chi_{d_1j}|\phi_j|^2\phi_{d_1}-\mathrm{i}\lambda_1\phi_a\phi_b+\mathrm{i}\Omega_1\phi_g\phi^*_c \\ & \quad -(\gamma+\mathrm{i}\delta)\phi_{d_1}-\mathrm{i}A_{d_1}|\phi_{d_1}|^{4/3}\phi_{d_1} \\ \frac{\mathrm{d}\phi_g}{\mathrm{d}t} &= -\mathrm{i}\sum_j\chi_{gj}|\phi_j|^2\phi_g-\mathrm{i}(\Delta+\delta)\phi_g+\mathrm{i}\Omega_1\phi_{d_1}\phi_c \end{aligned} \tag{16}$$

Here $\chi_{ij}=\chi'_{ij}n, A_f=A'_fn^{2/3}, \lambda_l=\lambda'_l\sqrt{n}, \Omega_l=\Omega'_l\sqrt{n}$ $(l=1,2,3)$, and the decay rate γ is introduced phenomenologically to simulate the loss of dimers, based on the assumption that this decay dominates all other loss mechanisms, such as, e.g., non-resonant scattering. As already mentioned this decay can be minimized by exploiting the CPT dark state technique, which ideally permits the full transfer of the entrance-channel atoms to the closed-channel molecules while keeping the intermediate dimer state unpopulated at all times [88].

In order to support our analysis we numerically solved Eqs. (16) by assuming that initially the atomic populations are the same and that there are no molecules present. Typical results are shown in Fig. 9. In that specific example, the external fields are $\lambda_l=9.07\times10^5$ s^{-1} ($l=1$ for the path AB). The collision parameters are chosen [137] as $\chi_{aa}=0.0056\lambda_l$, $\chi_{ab}=0.23\lambda_l$, $\chi_{ac}=\chi_{bc}=0.0098\lambda_l$, and $A_b=0.3\lambda_l$, $A_c=0.5762\lambda_l$, $A_{d_1}=0.09\lambda_l$, $A_{d_2}=0.1\lambda_l$. All other collision values are taken as zero due to the lack of good estimates in current experimental conditions. Figure 9(a) shows the creation of trimers ABC for $\delta=\pm1$ when considering only the single-path AB. We also carried out simulations

for $\delta = \pm 2$ and $\delta = \pm 3$, and the final conversion rate $|\phi_g(t = \infty)|^2$ was found to always exceed 0.22 in those cases for negative detunings (the maximum theoretical value is of course 0.33).

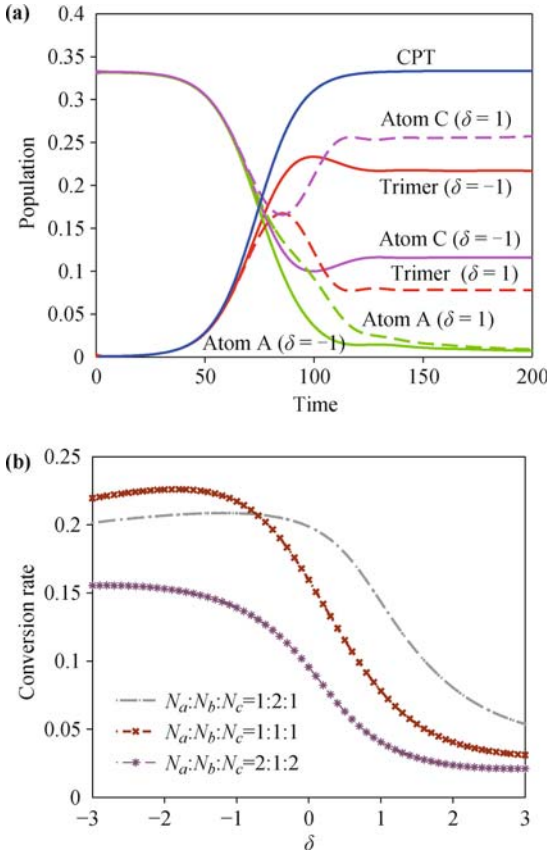

Fig. 9 **(a)** Trimer population along the path AB with $\delta = \pm 1$, and corresponding numbers of atoms A and C. The evolution of the population of atoms B is identical to A, and the "CPT" line shows the ideal analytical solution of the trimer number. **(b)** Conversion rate $|\phi_g(t = \infty)|^2$ as a function of δ. The scaled time is in units of λ_1^{-1}. Reproduced from Ref. [79], Copyright © IOP Publishing Ltd. and Deutsche Physikalische Gesellschaft.

Figure 9(b) shows the conversion rate as the function of δ for various ratios of the initial particle numbers, i.e., $N_a, N_b, N_c = 1:1:1,\ 1:2:1$, or $2:1:2$, respectively, illustrating the significant effect of any initial population *imbalance*. We conclude the single-path part by pointing out that similar results can be found for the other paths AC and BC, with the *same* CPT state and the same two-photon resonance condition [107, 108].

We now show that any two of the three single paths can be combined to achieve a significantly enhanced conversion rate, a result of constructive quantum interferences between these paths. As a concrete example, we consider the two paths AC and BC, for which we calculate the CPT value of the trimer population

$$|\phi_g^0|^2 = \frac{(\lambda_3/\Omega_3)(\lambda_2/\Omega_2)^2}{\lambda_3/\Omega_3 + 2\lambda_2/\Omega_2 + 3(\lambda_3/\Omega_3)(\lambda_2/\Omega_2)^2} \qquad (17)$$

We now introduce the ratio $R_1 = \eta_2/\eta_3$ (with $\eta_l = \Omega_l/\lambda_l$) of the external fields of the two paths, and observe that the freedom of choice of R_1 provides additional flexibility in attempting to approach the ideal CPT conditions via the constructive interference between these paths.

Figure 10(a) shows an example of a numerical simulation of the mean-field dynamics for $R_1 = 1$ and $\delta = \pm 1$. It illustrates the significant enhancement in trimer production as compared to the single-path situation (for $\delta = 1$, the final conversion rates are 0.078 or 0.234 for the single- or double-path cases). We found a similar enhanced atom–trimer conversion for $\delta = \pm 2$ and $\delta = \pm 3$ when choosing $R_1 = 1$. Note that $R_1 = 1$ is the optimal choice for the conditions of these simulations.

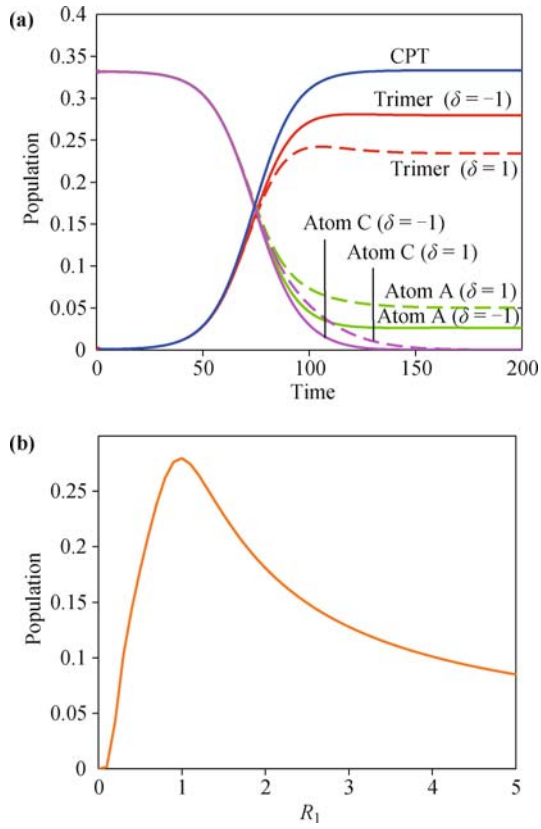

Fig. 10 Interfering for the better in atom–trimer conversion. **(a)** shows the population of the trimers and of atoms A and C for $\delta = \pm 1$. Here, $A_{d_2} = 0.1$ and all other parameters are as in the single-path case. **(b)** shows the final trimer population $|\phi_g(t = \infty)|^2$ as the function of R_1 for $\delta = -1$. Reproduced from Ref. [79], Copyright © IOP Publishing Ltd. and Deutsche Physikalische Gesellschaft.

We finally turn to the triple-path formation of trimers. A point of particular importance is to determine the quantum interference of all three channels with multi-dark states (AB, AC and BC), so that an almost ideal conversion rate can be approached even for positive detunings.

Figure 11(a) plots the result of typical numerical simulations for $R_1 = R_2 = 1$, where

$$R_1 = \eta_2/\eta_3, \quad R_2 = \eta_1/\eta_2 \qquad (18)$$

and $\eta_l = \Omega_l/\lambda_l$ $(l = 1, 2, 3)$. In contrast to the single- or

double-path cases, the triple-path interference can lead to an almost ideal conversion rate, especially for $\delta = 1$. In fact, we can almost not distinguish the cases $\delta = 1$ and $\delta = -1$ in Fig. 11(a), both of which reach a final population of 0.2836. This indicates a significant improvement even over the double-path situation. Figure 11(b) shows the final conversion rate $|\phi_g(t = \infty)|^2$ as a function of R_1 and R_2 for $\delta = -1$.

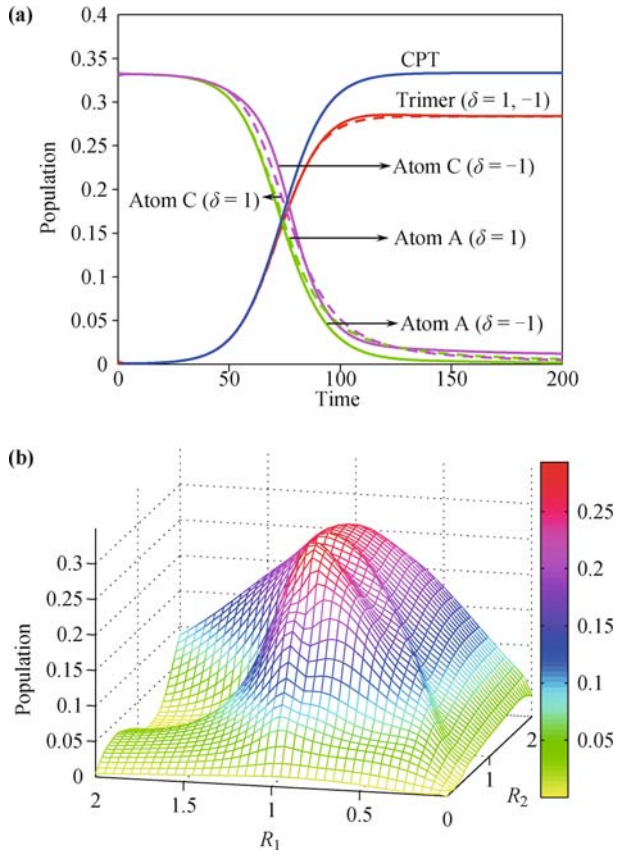

Fig. 11 Interfering for the *best* in the triple-path creation of trimers ABC. **(a)** shows the populations of the trimer and of atoms A and C for $R_1 = R_2 = 1$. **(b)** shows the final trimer population variation with R_1 and R_2 for $\delta = -1$. Reproduced from Ref. [79], Copyright © IOP Publishing Ltd. and Deutsche Physikalische Gesellschaft.

3.2.2 Role of populations imbalance

Population imbalance often plays an important role in the physics of ultracold matter waves. For example, by starting from a two-spin-state mixture of ultracold fermionic atoms, the population imbalance can result in a superfluid to normal phase transition [142]. In the following we show that an initial population imbalance can also significatly affect the dynamics of atom–molecule conversion. To this end we introduce parameters P and Q to characterize the initial atomic population imbalance as:

$$P = \frac{n_a - n_b}{n_a + n_b + n_c}, \quad Q = \frac{n_a - n_c}{n_a + n_b + n_c} \tag{19}$$

where n_a, n_b, n_c are the atomic densities. Since the total particle number is conserved we have that

$$|\phi_a^0|^2 + |\phi_{d_1}^0|^2 + |\phi_{d_2}^0|^2 + |\phi_g^0|^2 = \frac{1+P+Q}{3} \tag{20}$$

$$|\phi_b^0|^2 + |\phi_{d_1}^0|^2 + |\phi_{d_3}^0|^2 + |\phi_g^0|^2 = \frac{1-2P+Q}{3} \tag{21}$$

$$|\phi_c^0|^2 + |\phi_{d_2}^0|^2 + |\phi_{d_3}^0|^2 + |\phi_g^0|^2 = \frac{1+P-2Q}{3} \tag{22}$$

and from the steady-state conditions we obtain

$$\begin{aligned} &|\phi_a^0|^2 = \eta_1\eta_2|\phi_g^0|^2, \quad |\phi_b^0|^2 = \eta_1\eta_3|\phi_g^0|^2 \\ &|\phi_c^0|^2 = \eta_2\eta_3|\phi_g^0|^2 \end{aligned} \tag{23}$$

The CPT solution for the general case is then

$$\begin{aligned} |\phi_g^0|^2 &= \frac{(1+P+Q)/3}{1+\eta_1\eta_2} = \frac{(1-2P+Q)/3}{1+\eta_1\eta_3} \\ &= \frac{(1+P-2Q)/3}{1+\eta_2\eta_3} \end{aligned} \tag{24}$$

which can be reexpressed as:

$$P = \frac{\eta_1\eta_2 - \eta_3\eta_1}{3 + \eta_1\eta_2 + \eta_2\eta_3 + \eta_3\eta_1} \tag{25}$$

$$Q = \frac{\eta_1\eta_2 - \eta_2\eta_3}{3 + \eta_1\eta_2 + \eta_2\eta_3 + \eta_3\eta_1} \tag{26}$$

Obviously, $P = Q = 0$ for $\eta_1 = \eta_2 = \eta_3$, a property closely related to the fact that in that case the trimer conversion rate is dramatically improved in the double-path case for $R_1 = \eta_2/\eta_3 = 1$ [see Fig. 10(b)] and in the triple-path case for $R_1 = \eta_2/\eta_3 = 1, R_2 = \eta_1/\eta_2 = 1$.

In our earlier part on the creation of the trimer A_2B [77, 78] we found that $R = 2$ leads to an optimal conversion rate. The present discussion clarifies the fact that this specific value is a result of the fact that our simulations assumed an initial ratio of 2 between atoms A and B. This value, quite different from the value of $R = 1$ found for equal initial populations, illustrates clearly the crucial role of the initial atomic population imbalance in any multi-dark state scheme of atom–molecule conversion.

3.3 Tetramer $^{133}Cs_4$ with dark state

We consider two different schemes for creating the molecular tetramers [143]. Firstly, we study the bright-state scheme with intermediate dimer state A_2 (I):

$$A + A \rightarrow A_2, \quad A_2 + A_2 \rightarrow A_4$$

In this case, a point of particular interests is that the atom–molecular CPT or dark state does *not* exist and the atom–tetramer conversion is unstable since the intermediated dimer state A_2 formed by a magnetic FR *can not* be kept unpopulated (see the recent experiment by Chin *et al.* [81]).

Figure 12 gives a specific example of such kind of numerical simulation by using the collision parameters

of atomic ^{87}Rb with the s-wave scattering length 5.77 nm. We see that the nonzero populations of intermediate dimers are largely oscillated and thereby the atom–tetramer conversion is unstable for any detuning.

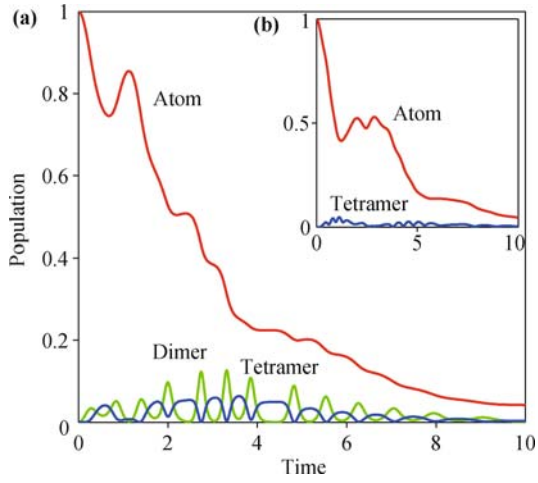

Fig. 12 Particle populations for **(a)** $\delta = 3$ or **(b)** $\delta = -3$ via the dimer-intermediated bright-state scheme. Here, the effective time $\tau = \lambda t = 20$. We note that, after $\tau = 10$, the population of molecular tetramers is almost zero, which is not shown here. Reproduced from Ref. [143], Copyright © 2008 The American Physical Society.

Now, we turn to the dark-state scheme with intermediate trimer state A_3 (II):

$$A + A + A \rightarrow A_3, \quad A + 3 + A \rightarrow A_4$$

Our purpose is to find the atom-molecule CPT dark state with zero occupation of intermediate trimers, through which more and efficient atom-tetramer conversion can be made possible. The experimental evidence of ER was already observed recently by Grimm *et al.* in a cesium atomic BEC at temperatures ranging from 10 to 500 nK, for both large negative and small positive atomic scattering lengths [18].

In the interaction picture the Heisenberg equations of motion of this system can be written as:

$$\begin{aligned}
\frac{\mathrm{d}\psi_a}{\mathrm{d}t} &= 2\mathrm{i}n\sum_j \chi_{aj}|\psi_j|^2\psi_a + 3\mathrm{i}\lambda\psi_m\psi_a^{*2} - \mathrm{i}\Omega\psi_g\psi_m^* \\
\frac{\mathrm{d}\psi_m}{\mathrm{d}t} &= 2\mathrm{i}n\sum_j \chi_{mj}|\psi_j|^2\psi_m + (\mathrm{i}\delta - \gamma)\psi_m \\
&\quad + \mathrm{i}\lambda\psi_a^3 - \mathrm{i}\Omega\psi_g\psi_a^* \\
\frac{\mathrm{d}\psi_g}{\mathrm{d}t} &= 2\mathrm{i}n\sum_j \chi_{gj}|\psi_j|^2\psi_g + \mathrm{i}(\Delta + \delta)\psi_g - \mathrm{i}\Omega\psi_m\psi_a
\end{aligned} \tag{27}$$

Here, $\lambda = \lambda'\sqrt{n}$, $\Omega = \Omega'\sqrt{n}$, λ', Ω' denote the strength of pumping and dumping fields, and γ denotes the loss of the dimers. By using the steady-state ansatz, it really supports a steady CPT solution:

$$|\psi_a^0|^2 = \frac{2}{\sqrt{1 + 16\ (\lambda/\Omega)^2} + 1} = 1 - 4|\psi_g^0|^2 \tag{28}$$

under the the "two-photon" resonance condition

$$\begin{aligned}
\Delta &= -\delta + (8\chi_{aa} - 2\chi_{ga})n|\psi_a^0|^2 + (8\chi_{ag} - 2\chi_{gg})n|\psi_g^0|^2 \\
\mu_a &= -2n(\chi_{aa}|\psi_a^0|^2 + \chi_{ag}|\psi_g^0|^2) \\
\mu_a &= -2n(\chi_{aa}|\psi_a^0|^2 + \chi_{ag}|\psi_g^0|^2)
\end{aligned} \tag{29}$$

We emphasize that the "two-photon" resonance plays a key role in maintaining the atom–molecule CPT state. As Ling *et al.* showed [87], the CPT state technique can compensate the collisional mean-field shifts and thereby, contrary to the previous belief, the conversion needs not limited by the collisions.

By comparing the results in Figs. 12 and 13, we see that the bright-state scheme only leads to a small oscillating number of tetramers in very short time limits ($\tau < 10$) for both $\delta = 3$ and $\delta = -3$, which approaches zero in later times. However, in the dark-state scheme, large occupation of tetramers can be reached even for the unstable case of $\delta = 3$ ($\tau \sim 76$); for the stable case of $\delta = -3$, an almost ideal CPT value can be approached.

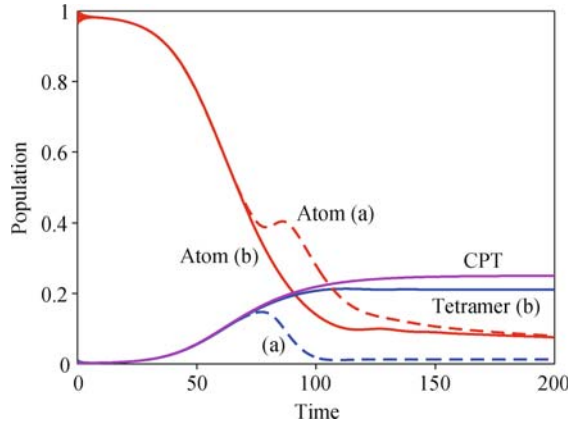

Fig. 13 Populations of atoms (*colored in red*) and molecular tetramers (*colored in blue*) for (a) $\delta = 3$ or (b) $\delta = -3$ via the trimer-intermediated dark-state scheme. The CPT value for the tetramers is also shown (*colored in purple*). The populations intermediate trimer are kept as zero at all times. Reproduced from Ref. [143], Copyright © 2008 The American Physical Society.

We note that the evidence of molecular tetramer was recently observed via the dimer–dimer FR [81] where the conversion efficiency is not very high and tends to rapidly decay. The present ER-aided CPT scheme may have potential advantages since more stable atom–tetramer conversion is possible by keeping the intermediate state unpopulated in the process.

Finally, the above method also can be steadily generalized to the assembly of fermionic tetramers in an atomic Bose–Fermi mixture by using the substitution [137]:

$$\chi_{jj}|\psi_j|^2 \rightarrow A_j|\psi_j|^{4/3}$$

for the fermionic components j in the equations of motion for the matter waves [with $A_j = (6\pi^2)^{2/3}/(4M_j)$ and M_j denoting the particle mass], provided that the s-wave collisions of fermionic particles can be ignored and

only their kinetic energy is taken into account.

4 Quantum noise in abstraction reaction

This section extends the toolbox of superchemistry to the coherent abstraction reaction $A + B_2 \rightarrow AB + B$. This reaction is an important benchmark system in chemical physics. Its dynamics has attracted much interest in recent studies of reactive resonance [109, 110] or coherent control of PA through the interference of reactive pathways [111–113].

4.1 Short-time quantum dynamics

As Fig. 14 shows, the intermediate trimers AB_2 are created via FR, and then photodissociated into bound molecules AB and atoms B. This CPT scheme, which is specific to quantum-degenerate matter waves, is different from purely collision-induced reactive scattering [12, 111–113]. The Hamiltonian of this system is

$$\hat{\mathcal{H}} = -\int \mathrm{d}r\Big\{\sum_{i,j}\chi'_{i,j}\hat{\psi}_i^\dagger(r)\hat{\psi}_j^\dagger(r)\hat{\psi}_j(r)\hat{\psi}_i(r) + \lambda'[\hat{\psi}_m^\dagger(r)\hat{\psi}_a(r)\hat{\psi}_{b_2}(r) + H.c.] + (\Delta+\delta)\hat{\psi}_{ab}^\dagger(r)\hat{\psi}_{ab}(r) - \Omega'[\hat{\psi}_{ab}^\dagger(r)\hat{\psi}_b^\dagger(r)\hat{\psi}_m(r) + H.c.] + \delta\hat{\psi}_m^\dagger(r)\hat{\psi}_m(r)\Big\} \quad (30)$$

The indices $i, j = a, b, b_2, ab, m$ stand for bosonic atoms (A and B), dimers (B_2 and AB) and trimer AB_2. The terms proportional to $\chi'_{i,j} = 2\pi a_{i,j}/M_{i,j}$ describe interspecies s-wave collisions with scattering length $a_{i,j}$, $M_{i,j} = M_i M_j/(M_i + M_j)$ being the reduced mass.

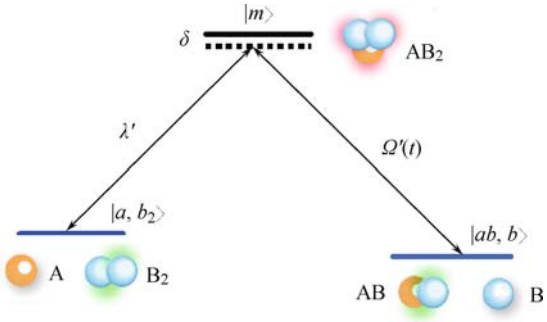

Fig. 14 Coherent abstraction reaction $A + B_2 \rightarrow AB + B$ with degenerate matter waves. A and B denote the bosonic or fermionic atoms, and B_2 and AB are molecular dimers. Reproduced from Ref. [107], Copyright © 2008 The American Physical Society.

In the MFA, $\hat{\psi}_i \rightarrow \sqrt{n}\psi_i$ where n is the initial particle density, the Heisenberg equations of motion are then

$$\dot{\psi}_a = 2\mathrm{i}\sum_j \chi_{a,j}|\psi_j|^2\psi_a + \mathrm{i}\lambda\psi_{b_2}^*\psi_m$$

$$\dot{\psi}_b = 2\mathrm{i}\sum_j \chi_{b,j}|\psi_j|^2\psi_b - \mathrm{i}\Omega\psi_{ab}^*\psi_m$$

$$\dot{\psi}_{b_2} = 2\mathrm{i}\sum_j \chi_{b_2,j}|\psi_j|^2\psi_{b_2} + \mathrm{i}\lambda\psi_a^*\psi_m$$

$$\dot{\psi}_{ab} = 2\mathrm{i}\sum_j \chi_{ab,j}|\psi_j|^2\psi_{ab} - \mathrm{i}\Omega\psi_b^*\psi_m + \mathrm{i}(\Delta+\delta)\psi_{ab}$$

$$\dot{\psi}_m = 2\mathrm{i}\sum_j \chi_{m,j}|\psi_j|^2\psi_m + (\mathrm{i}\delta - \gamma)\psi_m + \mathrm{i}\lambda\psi_a\psi_{b_2} - \mathrm{i}\Omega\psi_b\psi_{ab} \quad (31)$$

Here, $\chi_{i,j} = n\chi'_{i,j}$, $\lambda = \lambda'\sqrt{n}$, $\Omega = \Omega'\sqrt{n}$, and we have introduced the phenomenological decay rate γ to account for the loss of intermediate trimers, based on the assumption that this decay dominates all other loss mechanisms such as rogue photodissociation to noncondensate modes [144, 145]. As already mentioned, our goal is to minimize that decay by using a STIRAP pulse sequence.

The initial condition $\psi_b(0) = \psi_{ab}(0) = 0$ is readily seen to result in

$$\psi_b(t) = \psi_{ab}(t) = 0$$

for all times. This indicates that the mean-field GP equations break down completely in studying the onset of this type of abstraction reaction. A similar situation has been previously encountered in a broad range of systems in quantum optics [116], but also in coupled degenerate atomic and molecular systems such as the example in the matter-wave superradiance of Bose-condensed atoms [84, 116–118]. As in those situations, our strategy here is to decompose the problem into an initial quantum-noise-dominated stage followed by a classical stage that arises once the product components have acquired a macroscopic population. The initial quantum evolution is treated in a linearized approach whose main purpose is to establish the statistical properties of the initial fields required for the classical stage [84].

A simple physical picture of the initial stages of this system can be obtained when considering the limiting case where δ is the largest parameter in the system, $\mathrm{i}\dot{\hat{\psi}}_m/\delta \approx 0$. In the collisionless limit this gives

$$\hat{\psi}_m \approx -(\lambda'_a/\delta)\hat{\psi}_a\hat{\psi}_{b_2} + (\Omega'/\delta)\hat{\psi}_b\hat{\psi}_{ab}$$

which amounts to adiabatically eliminating the intermediate trimer state. In this case the system is described by the effective Hamiltonian [146]

$$\hat{\mathcal{H}}_{\mathrm{eff}} = -(G\hat{c}_{ab}^\dagger\hat{c}_b^\dagger\hat{c}_a\hat{c}_{b_2} + h.c.) + \hat{c}_0 \quad (32)$$

where

$$\hat{c}_0 = \Omega_1\hat{c}_a^\dagger\hat{c}_a\hat{c}_{b_2}^\dagger\hat{c}_{b_2} + \Omega_2\hat{c}_{ab}^\dagger\hat{c}_{ab}\hat{c}_b^\dagger\hat{c}_b \quad (33)$$

$$\hat{\psi}_i(r,t) = \phi_i(r)\hat{c}_i(t)$$

and the various constants are

$$G = (\lambda'\Omega'/\delta)\int \mathrm{d}r\phi_{ab}^*(r)\phi_b^*(r)\phi_a(r)\phi_{b_2}(r)$$

$$\omega_1 = (\lambda'^2/\delta)\int \mathrm{d}r\phi_a^*(r)\phi_a(r)\phi_{b_2}^*(r)\phi_{b_2}(r)$$

$$\omega_2 = (\Omega'^2/\delta)\int \mathrm{d}r\phi_{ab}^*(r)\phi_{ab}(r)\phi_b^*(r)\phi_b(r)$$

For short enough interaction times, we can treat the fields $\hat{\psi}_a$ and $\hat{\psi}_{b_2}$ classically, $\hat{c}_{a,b_2} \to \sqrt{N_{a,b_2}}$, and then neglect the term in Eq. (32) describing only the interactions between the modes $\hat{c}_a$ and $\hat{b}_2$. This results in the linearization of the equations of motion for the remaining quantized matter-wave fields $\hat{c}_{ab}$ and $\hat{c}_b$, with a noise source $\hat{f}_j^\dagger(t)$,

$$\dot{\hat{c}}_{ab,b}(t) = \hat{f}_{b,ab}^\dagger(t) = \mathrm{i}\mathcal{G}\hat{c}_{b,ab}^\dagger(t) \tag{34}$$

For simplicity we assume in the following that the correlations of the quantum noise operators appearing in Eq. (34) are markovian,

$$\langle \hat{f}_i^\dagger(t)\hat{f}_j(t')\rangle = 0, \quad \langle \hat{f}_i(t)\hat{f}_j^\dagger(t')\rangle = \mathcal{G}^2\delta_{ij}\delta(t-t')$$

where $\mathcal{G} = G\sqrt{N_a N_{b_2}}$ and $i, j = ab$ or b here and in the following. It is these noise operators that trigger the non-mean-field "spontaneous" evolution of the system from initial vacuum fluctuations.

It is interesting to observe that although the second factorial moments of the single modes ab and b are typical of chaotic fields, quantum entanglement within these two modes does exist, i.e.,

$$\left[g_{ab,b}^{(2)}\right]^2 - g_{ab}^{(2)} g_b^{(2)} = \sinh^{-4}(\mathcal{G}t) + 4\sinh^{-2}(\mathcal{G}t) > 0$$

violating the classical Cauchy–Schwarz inequality [116].

Similar equations of motion can be derived in case atoms A are bosonic and atoms B fermionic. The main difference in that case is in the commutation relations of the noise operators $(-\hat{f}_b^\dagger,\ \hat{f}_{ab}^\dagger)$. One finds that the vacuum-noise-triggered populations of principal modes are then [15, 147] $N_{ab,b} = \sin^2(\mathcal{G}t) < 1$, a direct consequence of the Fermi statistics [15, 147]. Being similar to the bosonic case, we also find

$$\left[g_{ab,b}^{(2)}\right]^2 - g_{ab}^{(2)} g_b^{(2)} = \left[1 - \frac{\cos^2(\mathcal{G}t)}{\sin^2(\mathcal{G}t)}\right]^2 > 0 \tag{35}$$

The fermionic dimer–atom correlations are of course also different from the bosonic case, specifically we have now $C_{ab,b} = 1 - N_{ab,b} < 1$, a signature of antibunching.

4.2 Creation of atom–molecule pairs

Rather than adopting a fully quantum treatment of, e.g., positive-P representation technique [119], we proceed in the following by solving the mean-field Eqs. (31) with stochastic classical seeds whose statistics are consistent with the results of the linearized, short-time quantum analysis [84]. To be specific, using Eqs. (31) we compute 300 trajectories with randomly chosen initial seeds satisfying the short-time distribution.

Figure 15 shows the standard derivations $\Delta N_i(t)$ around the average values of the particle populations,

$$\Delta N_i(t) = \left\{\frac{1}{300}\sum_{n=1}^{300}\left[(N_{i,n}(t) - \bar{N}_i(t)\right]^2\right\}^{1/2}$$

with $\bar{N}_i(t) = (1/300)\sum_n N_{i,n}(t)$, for $\delta = 3$ and $\delta = -3$. The inset shows the fluctuating range $\pm\Delta N_i$ about the mean populations, $\bar{N}_i \pm \Delta N_i(t)$ for $\delta = 3$ and for bosonic atoms. The small seeds resulting from quantum vacuum noise are significantly amplified, increasing more rapidly than their deviations, before reaching a stationary value. For $\delta = -3$, however, no stable reaction is observed.

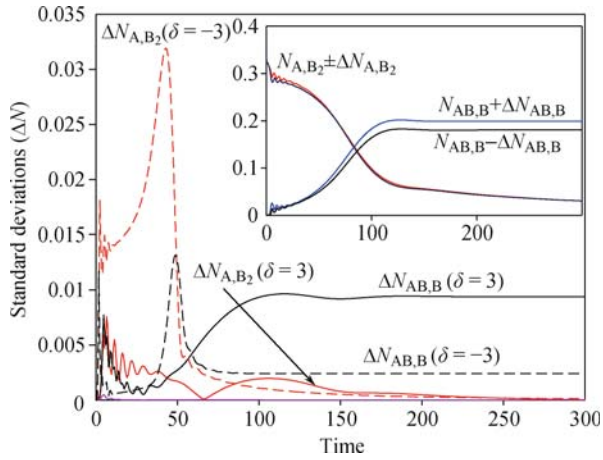

Fig. 15 Standard derivation of the particles populations from their average values for $\delta = \pm 3$. Time is in units of λ^{-1}. Inset: fluctuating range of the populations $\bar{N}_i(t) \pm \Delta N_i(t)$ for $\delta = 3$. Reproduced from Ref. [107], Copyright © 2008 The American Physical Society.

An important feature of coherent abstraction reaction is the existence of a CPT state [77, 107], which permits the transfer of a population from an initial to a final state via an intermediate dark state. Specifically, by using the steady-state method described in Section 3, the CPT solution of this system is derived

$$N_{ab,b}^s = \frac{2\mathcal{R}}{(1+\mathcal{R})\left[1 + 2\mathcal{R} + \sqrt{(1-2\mathcal{R})^2 + 8\mathcal{R}\Omega^2/\lambda^2}\right]}$$

Here, $\mathcal{R} \equiv N_a(0)/[2N_{b_2}(0)]$ is introduced to define the initial ratio of the particles numbers. The condition $\partial N_{ab,s}/\partial\mathcal{R} = 0$ yields a maximum dimer number

$$N_{ab,s}|_{\max} = 1/3$$

corresponding to a complete abstraction reaction for $\mathcal{R} = 1/2$ or the so-called "balanced case".

We have numerically solved Eqs. (31) and the typical results are shown in Fig. 16. In this specific example atom A is ^{87}Rb, atom B is ^{41}K. For this bosonic system, stable bimolecular conversion is always possible for negative detunings, but the system can be unstable for positive detunings. The increasing departure of the product populations from the ideal CPT line is due to the fact that only an approximate adiabatic condition exists for the CPT state.

When considering a mixture of bosonic and fermionic atoms, the abstraction reaction results in the conversion of bosonic to fermionic molecules,

$$\mathbf{b} + \mathcal{B} \to \mathcal{F} + \mathbf{f}$$

where **b** ($\mathcal{B}$) or **f** ($\mathcal{F}$) denotes bosonic or fermionic atoms (dimers). Ignoring s-wave collisions between fermionic atoms of the same species and retaining only their dominant kinetic energy, and assuming further that collisions are the dominating term for the bosons [137], we find that the mean-field dynamical equations are similar with some substitution, a consequence of the fact that we consider only the dominating kinetic energy term and ignore the s-wave collisions between identical fermionic particles [137].

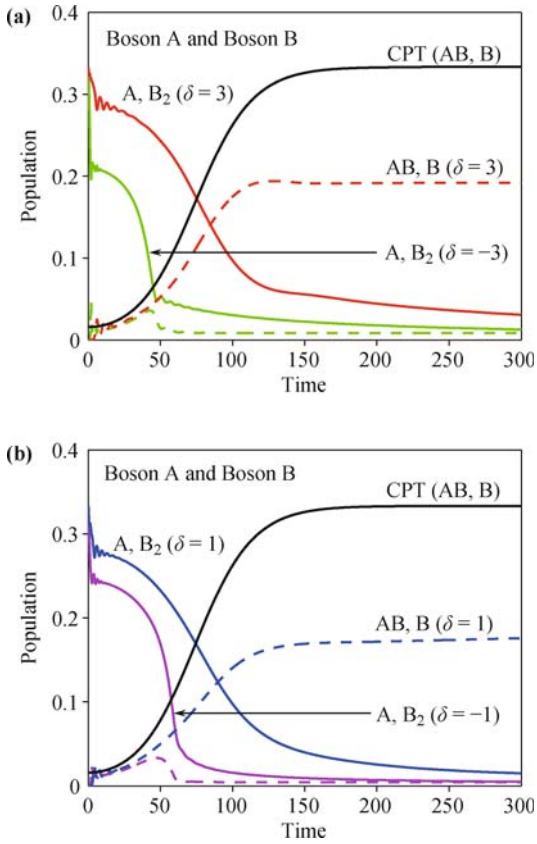

Fig. 16 Populations of the bosonic dimers and atoms for **(a)** $\delta = \pm 3$ or **(b)** $\delta = \pm 1$. Time is in units of λ^{-1}, and $\gamma = 1$. The line labelled "CPT" shows the ideal population of products (dimers AB and atoms B). Reproduced from Ref. [108], Copyright © 2009 The American Physical Society.

Our numerical simulations of this case are summarized in Fig. 17 for the collision parameters $\chi_{aa} = 0.5303$, $\chi_{bb} = 0$, $\chi_{ab} = \chi_{b,ab} = \chi_{a,ab} = -0.09$, $\chi_{a,ab} = -0.2637$, $A_b = 0.008$, $A_{ab} = 0.004$, and all other collision parameters equal to zero. These results show that the stable formation of dimers AB is possible for both positive and negative detunings [(a) $\delta = \pm 3$ or (b) $\delta = \pm 1$], initially with no particle populations imbalance.

In contrast to the purely bosonic case, the creation of fermion–fermion pairs is due to a statistics-independent cooperating many-body effect that has been previously recognized in the case of, e.g., matter-wave four-wave mixing [148]. We also note that in a recent work Li *et al.* [26] used a similar atom–molecule dark-state technique to realize a laser-catalyzed conversion of fermionic to bosonic molecules:

$$^6\mathrm{Li} + ^6\mathrm{Li}^7\mathrm{Li} \rightarrow ^6\mathrm{Li}_2 + ^7\mathrm{Li}$$

with an ultrahigh conversion rate of 99.97% [26].

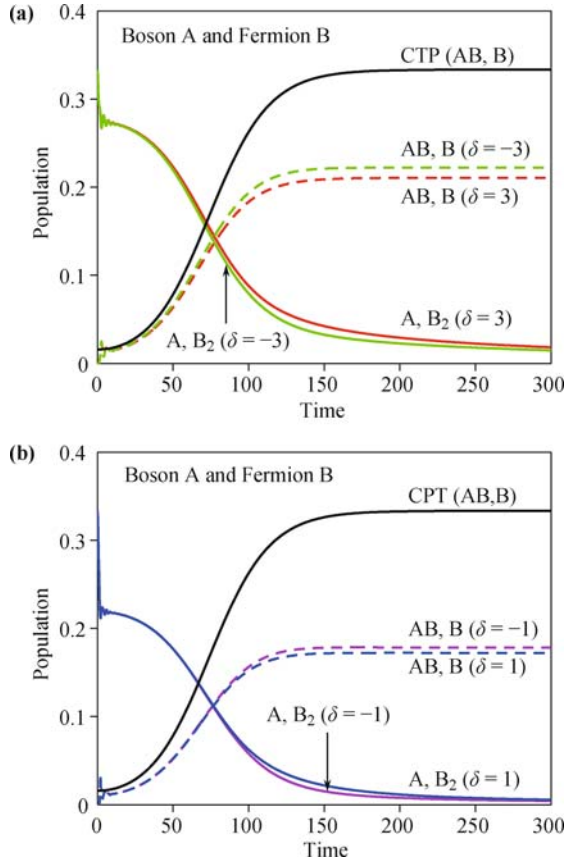

Fig. 17 The generation of fermionic dimers AB and atoms B for **(a)** $\delta = \pm 3$ or **(b)** $\delta = \pm 1$ initially with no particle populations imbalance. The CPT values of the dimer AB and atomic B are also plotted. Reproduced from Ref. [108], Copyright © 2009 The American Physical Society.

4.3 Role of population imbalance

The initial population imbalance $\mathcal{R}$ can also significantly affect the reaction dynamics. In Fig. 18, we see that the conversion rate $|\psi_{ab}(t = \infty)|^2$ has the maximum at a value somewhat larger than $\mathcal{R} = 0.5$ for both bosonic and fermionic cases. However, for bosonic atoms A and B, the final rates can be changed sharply with $\mathcal{R}$ and rapidly approach zero for $\mathcal{R} < 0.4$ and $\mathcal{R} > 1.4$; in contrast, for fermionic atoms B, the conversion rate changes its shape more slowly with $\mathcal{R}$ (even for $\mathcal{R} > 1.4$, the occupation of the product is still in excess of 7%).

In order to estimate the upper limit on collisions, we can use the condition $|\mathcal{G}t| < 1$ or

$$|G\sqrt{N_a N_{b_2}}t| < 1$$

which determines the validity of the short-time approximation for the early quantum stage, to estimate the time over which the fluctuations take place. This up-

per time limit is of the order of 10^{-5}s for $|\delta = 3|$ and $\Omega_0 = 20\lambda$. According to Cvitas *et al.* [83], typical low-temperature inelastic collision cross-sections are of the order of 10^{-17}m^3/s, corresponding to reaction times of the order of 10^{-3}s for a typical condensate density of 10^{14}cm^{-3}. From that estimate, it appears that the fluctuations do indeed dominate for short enough times. We also note that the collisional reaction time of 10^{-3}s corresponds to an almost complete noise-amplified conversion in Fig. 16. In that case the fluctuation-induced dynamics completely dominate the short-time behavior of the system. This feature, which is characteristic of a wide variety of collective abstraction reactions, may provide a useful means to produce reaction products that are difficult to obtain or have only poor yield when resulting from a purely collisional method.

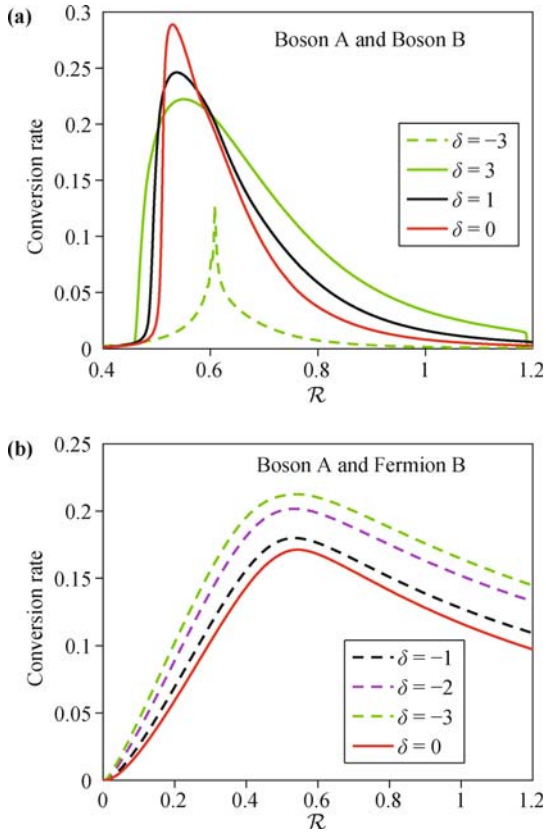

Fig. 18 Final dimer population $|\psi_{ab}(t = \infty)|^2$ as the function of $\mathcal{R}$ for **(a)** the Bose case and **(b)** the Fermi case for several values of δ. Reproduced from Ref. [107], Copyright © 2008 The American Physical Society.

5 Adiabatic condition in superchemistry

The standard adiabatic theorem in quantum mechanics is derived generally for a linear system with a sufficiently slowly changed Hamiltonian in comparison with typical level spacings, i.e.,

$$|\dot{H}| \ll \hbar|\Omega_{fg}|, \quad \text{for any } f \neq g \tag{36}$$

where Ω_{fg} is the frequency of the transition between the instantaneous eigenstates $|f(t)\rangle$ and $|g(t)\rangle$. Because of its fundamental importance in quantum theory and applications of quantum state control, the adiabatic theorem is actively studied under various conditions [149, 150].

Recently, Pu *et al.* derived an approximated adiabatic condition for atom–dimer conversion under collisionless limit [88]. In their method, the deviations from the CPT evolution form a set of *linearized* differential equations, which is easily solved to obtain an adiabaticity parameter. Then, by taking account of the collisions [90], Ling *et al.* confirmed the validity of this method by achieving again the similar adiabatic condition. This Section will be devoted to introducing the nonlinear adiabatic condition and to compare the difference of atom–dimer and atom–trimer conversion [89].

5.1 Synthesis of heteronuclear molecules

We first consider the synthesis of heteronuclear dimers. To compare with Pu *et al.* [88], here we also ignore the particle collisions with the two-photon resonance condition ($\delta = 0$). The effective Hamiltonian of this system in the simplest level is

$$\hat{H}_{\rm nl} = -\Delta\hat{\psi}_e^\dagger\hat{\psi}_e + \frac{\hbar}{2}\lambda'\left(\hat{\psi}_e^\dagger\hat{\psi}_a\hat{\psi}_b + \hat{\psi}_a^\dagger\hat{\psi}_b^\dagger\hat{\psi}_e\right) - \frac{\hbar}{2}\Omega'\left(\hat{\psi}_e^\dagger\hat{\psi}_g + \hat{\psi}_g^\dagger\hat{\psi}_e\right) \tag{37}$$

The indices $i = a, b, e, g$ are for atoms A, B and heteronuclear dimers in excited or ground states, respectively. The detuning Δ is introduced to account for the difference between the frequencies of the pump laser and the transition $|1\rangle \to |2\rangle$.

To find the adiabaticity parameter of the system under study, we need to find the CPT state of the system. In the CPT state, it is easy to show that

$$\lambda|\psi_a^s||\psi_b^s| = \Omega|\psi_g^s|, \quad |\psi_e^s| = 0 \tag{38}$$

where the index s stands for the steady state. Then the instantaneous CPT state vector can be written as:

$$\Psi_s = (\psi_a^s, \psi_b^s, \psi_e^s, \psi_g^s)^{\rm T} \tag{39}$$

where

$$\psi_a^s = \left(\frac{1}{\sqrt{1+2R^2}+1}\right)^{\frac{1}{2}}, \quad \psi_b^s = \left(\frac{1}{\sqrt{1+2R^2}+1}\right)^{\frac{1}{2}}$$
$$\psi_e^s = 0\,, \quad \psi_g^s = \frac{R}{\sqrt{1+2R^2}+1} \tag{40}$$

and $R = \lambda/\Omega$. For simplicity, here we take $N_a^s - N_b^s = \varepsilon = 0$.

The existence of the CPT state does not insure that this state can be reached adiabatically, and thus we should adopt the perturbative expansion approach to linearize the nonlinear system. In order to see whether the CPT state is dynamically stable, we add a small fluc-

tuation to the steady-state CPT solution and the state vector can be written as:

$$\delta\psi_i = \psi_i - \psi_i^s \tag{41}$$

Here $\delta\psi_i$ describes a small departure around the CPT state. Then the linearized equations can be written as:

$$\mathrm{i}\frac{\mathrm{d}}{\mathrm{d}t}\delta\psi = M\delta\psi + \dot{\Psi}_s \tag{42}$$

where

$$\boldsymbol{\delta\psi} = \begin{pmatrix} \delta\psi_a \\ \delta\psi_b \\ \delta\psi_e \\ \delta\psi_g \end{pmatrix},\ \boldsymbol{M} = \begin{pmatrix} 0 & 0 & \frac{\lambda}{2}\psi_b^s & 0 \\ 0 & 0 & \frac{\lambda}{2}\psi_a^s & 0 \\ \frac{\lambda}{2}\psi_b^s & \frac{\lambda}{2}\psi_a^s & -\Delta & -\frac{\Omega}{2} \\ 0 & 0 & -\frac{\Omega}{2} & 0 \end{pmatrix}$$

The eigenvalues (eigenfrequencies) of matrix $\boldsymbol{M}$ can be then analytically found as

$$\omega_{0,1} = 0,\ \ \omega_\pm = \frac{1}{2}\left[-\Delta \pm \left(\Delta^2 + \Omega\,\Omega_{\mathrm{eff}}^{\mathrm{nl}}\right)^{1/2}\right]$$

where $\Omega_{\mathrm{eff}}^{\mathrm{nl}} = \sqrt{\Omega^2 + 2\lambda^2}$. For $\omega_\pm$, the corresponding eigenstates are

$$\boldsymbol{w}_\pm = \boldsymbol{N}_\pm(\frac{\lambda}{2}\psi_b^s, \frac{\Omega}{2}\psi_a^s, \omega_\pm, \frac{\Omega}{2})^{\mathrm{T}} \tag{43}$$

where $\boldsymbol{N}_\pm$ describes the normalization constants. It can easily be seen that $\omega_{0,1,\pm}$ are all real and the form of $\omega_\pm$ are the same with Pu *et al.* [88], except for a smaller value of $\Omega_{\mathrm{eff}}^{\mathrm{nl}}$ in comparison with the homonuclear case.

The deviation vector expanded by normal modes is

$$\boldsymbol{\delta\psi} = \sum_{\alpha=0,1,\pm} c_\alpha\,\boldsymbol{w}_\alpha$$

and thus from the Eq. (42) we have

$$\mathrm{i}\dot{c}_\alpha = \omega_\alpha\, c_\alpha - \mathrm{i}\,\boldsymbol{w}_\alpha^\dagger\ \dot{\Psi}_s$$

Using the CPT solution given in Eqs. (40), we have

$$\begin{aligned} &\dot{\psi}_a^s = -(\sqrt{1+2R^2}+1)^{-\frac{3}{2}}(1+2R^2)^{-\frac{1}{2}}R\dot{R} \\ &\dot{\psi}_b^s = \dot{\psi}_a^s \\ &\dot{\psi}_e^s = 0 \\ &\dot{\psi}_g^s = (\sqrt{1+2R^2}+1)^{-1}(1+2R^2)^{-\frac{1}{2}}\dot{R} \end{aligned} \tag{44}$$

Then for the Goldstone zero modes $\boldsymbol{w}_{0,1} = \xi_0 + \xi_1$, with

$$\xi_0 = \boldsymbol{N}_0(\frac{\Omega}{2}, 0, 0, \frac{\lambda}{2}\psi_b^s)^{\mathrm{T}},\quad \xi_1 = \boldsymbol{N}_1(1,-1,0,0)^{\mathrm{T}} \tag{45}$$

it is straightforward to calculate

$$\begin{aligned} &\frac{\Omega}{2}\dot{\psi}_a^s + \frac{\lambda}{2}\psi_b^s\dot{\psi}_g^s = \varphi\dot{R}(R\Omega - \lambda) = 0 \\ &\frac{\lambda}{2}\psi_b^s\dot{\psi}_a^s - \frac{\lambda}{2}\psi_a^s\dot{\psi}_b^s = 0 \end{aligned} \tag{46}$$

with

$$\varphi = -\frac{1}{2}(\sqrt{1+2R^2}+1)^{-\frac{3}{2}}(1+2R^2)^{-\frac{1}{2}}$$

which leads to a crucial result

$$\boldsymbol{w}_{0,1}^\dagger(t)\,\dot{\Psi}_s(t) = 0\,,\quad \mathrm{i}\dot{c}_{0,1} = 0 \tag{47}$$

This means that these resonant zero modes [151] are not coupled with the dynamics of the system. For the other two modes $\omega_\pm$, we introduce the adaibaticity parameter of Pu *et al.* [88]

$$r_{\mathrm{nl}}(t) = \frac{1}{2}\sqrt{|c_+(t)|^2 + |c_-(t)|^2} \tag{48}$$

which denotes the population outside the dark state, and the final result is (for $\Delta = 0$)

$$r_{\mathrm{nl}} = \frac{|\dot{R}|}{1+\sqrt{1+2R^2}}\,\frac{1}{\Omega_{\mathrm{eff}}^{\mathrm{nl}}} \ll 1 \tag{49}$$

We see that, compared with the homonuclear case [88], the only difference is the replacement $1+\sqrt{1+8R^2} \to 1+\sqrt{1+2R^2}$ in the denominator, which means that the adiabatic condition for the heteronuclear system is more difficult to fulfill in the later evolution stage.

Now, we turn to see the adiabatic condition of coherent atom-heteronuclear trimer conversion. Our goal is to see whether the deviations from these CPT states $\partial\psi_{\mathrm{m}}$ not only remain insignificant, but also different for the two reaction paths I-II. To this end, we follow the above standard procedure to obtain the adiabaticity parameter as ($\delta = 0$)

$$\begin{aligned} r_{\mathrm{nl}}(t) &= \frac{1}{2}\sqrt{|c_+(t)|^2 + |c_-(t)|^2} \\ &\approx \frac{\dot{R}_1}{\sqrt{1+4R_1^2}}\frac{1}{\Omega_{\mathrm{eff}}^{\mathrm{I}}} \ll 1 \end{aligned} \tag{50}$$

where $\Omega_{\mathrm{eff}}^{\mathrm{I}} = \sqrt{\Omega_1^2 + 4\lambda_1^2}$. This is the adiabatic condition for the path AA. Clearly, $\sqrt{1+4R^2}$ in the denominator here (instead of R^2 for a linear system) makes it more difficult to be fulfilled at the later stage.

For the different path AB, we have

$$r_{\mathrm{nl}}(t) \approx \frac{\dot{R}_2}{\sqrt{1+R_2^2}}\frac{1}{\Omega_{\mathrm{eff}}^{\mathrm{II}}} \ll 1 \tag{51}$$

where $\Omega_{\mathrm{eff}}^{\mathrm{II}} = \sqrt{\Omega_2^2 + \lambda_2^2}$. Though somewhat similar, $\sqrt{1+R^2}$ in the denominator here is different from that for the path AA. As a comparison, we can write this term as $\sqrt{1+kR^2}$, where $k \sim 8$ for the atom–dimer conversion case [88], and $k = 4$ or 1 for the path AA or AB of the atom–trimer conversion.

Figure 19 plots the adiabatic evolutions of the atom-heteronuclear molecule conversion, where the molecular numbers have been converted into equivalent atom numbers so that the final level directly corresponds to the atom–molecule conversion efficiency: $\eta = 2|\psi_g|^2/1$ (for dimers) or $\eta = 3|\psi_g|^2/1$ (for trimers). In our simulations we use the same Gaussian pulses for the optical fields with the same parameters of Ref. [88]

$$\lambda_{1,2} = \Omega_0 \mathrm{e}^{-(t-t_1)^2},\quad \Omega_{1,2} = \Omega_0 \mathrm{e}^{-(t-t_2)^2}$$

with $\Omega_0 = 5$, $t_1 = 3.8$ and $t_2 = 3$. The initial populations are chosen as $|\psi_a(0)|^2 = |\psi_b(0)|^2 = 0.5$.

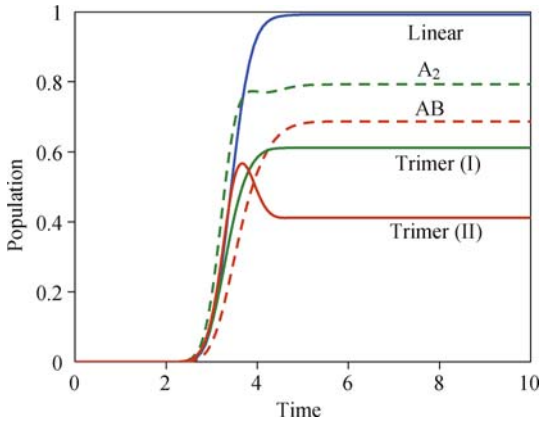

Fig. 19 Adiabatic evolutions of the atom-heteronuclear molecule conversion. Blue solid line denotes the reference line of the linear system; green dashed (solid) line denotes another reference of the homonuclear dimers $2|\psi_g|^2$ (heteronuclear trimers (I) $3|\psi_g|^2$); red dashed (solid) line denotes the heteronuclear dimers $2|\psi_g|^2$ (trimers) (II) $3|\psi_g|^2$), respectively. Reproduced from Ref. [89], Copyright © 2008 The American Physical Society.

For a comparison, the atom-homonuclear dimer conversion efficiency is close to 80% in the collisionless limit [88] or more than 85% with higher dump Rabi frequency (with the collisions) [87, 90]. For the ^{87}Rb atoms, a high transfer efficiency of up to 87% was achieved with molecular lifetime of about 1 s by Winkler *et al.* [152]. By ramping adiabatically over a magnetic FR at 1007.4 G with a slow Feshbach ramp (2×10^3 G/s), even up to 95% conversion efficiency was observed in a three-dimensional optical lattice due to the lattice shielding of the trapped molecules from collisions and thus the minimized inelastic decay by vibrational quenching [153, 154].

However, for heteronuclear dimers, we have only about 70% population transfer in the collisionless limit (see Fig. 19). We note that by using an ultracold gas of 40 000 ^{85}Rb atoms and 300 000 ^{87}Rb atoms, Papp and Wieman achieved up to 25 000 heteronuclear molecules and thus the transfer rate 62.5% for the ^{85}Rb atoms [82, 83]. A lower rate can be estimated by considering other cases of initial population imbalance (but with identical trap frequencies [155]). Similar experiments were also performed for the heteronuclear molecules of, e.g., ^{39}K-^{85}Rb (with a production rate of about 4×10^4 molecules/s) [52, 156], ^{23}Na-^{133}Cs (500 NaCs per 10 000 pulses was obtained from 5×10^5 Na atoms at 220 ± 80 μK and 2×10^6Cs atoms at 210 ± 80 μK) [51], or ^{85}Rb-^{133}Cs [65].

Finally, we note that for the cases of heteronuclear trimers, the conversion efficiency is about 61% via the reaction path AA (I) or about 41% via the path AB (II), which is consistent with Ref. [77]. Clearly, the chemical reaction paths have important impacts on the adiabatic evolutions of the atom–molecule conversion. These behaviors also can be seen in Fig. 20 for the evolution of the adiabaticity parameters. The transfer efficiency becomes lower from homonuclear dimers A_2 to heteronuclear dimers AB, and then even lower for heteronuclear trimers (I-II) in the same conditions.

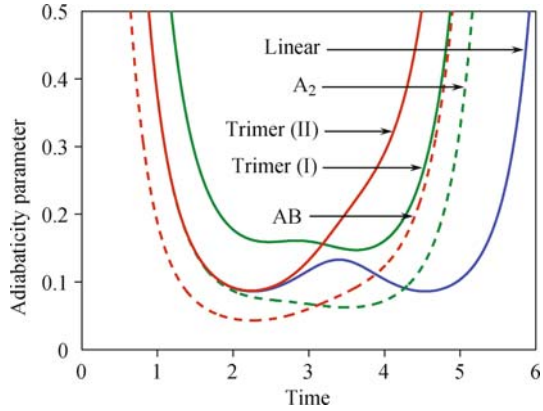

Fig. 20 Adiabaticity parameters for the linear system and the nonlinear systems for homonuclear dimers, heteronuclear dimers and heteronuclear trimers I(II), respectively. Reproduced from Ref. [89], Copyright © 2008 The American Physical Society.

5.2 Abstraction reaction

For coherent abstraction reaction, the standard linearization procedure gives the following linearized equations for the probability amplitude derivation $\partial\psi_{\rm i} = \psi_{\rm i} - \psi_{\rm i,s}$,

$$-{\rm i}\frac{{\rm d}}{{\rm d}t}\boldsymbol{\partial\psi} = \mathcal{M}\boldsymbol{\partial}\psi + {\rm i}\dot{\boldsymbol{\psi}}_{\rm s} \tag{52}$$

where $\boldsymbol{\partial\psi} = (\partial\psi_a, \partial\psi_b, \partial\psi_{b_2}, \partial\psi_{ab}, \partial\psi_m)^{\rm T}$ and

$$\mathcal{M} = \begin{pmatrix} 0 & M^{\rm T} \\ M & \delta \end{pmatrix} \tag{53}$$

with $M = (\lambda\psi_{b_2,s}, -\Omega\psi_{ab,s}, \lambda\psi_{a,s}, -\Omega\psi_{b,s})$. The eigenvalue of matrix $\mathcal{M}$ can be easily found as:

$$\omega_{0,1,2} = 0, \quad \omega_\pm = \frac{1}{2}\left[\delta \pm \left(\delta^2 + \frac{8\lambda\Omega}{3}\right)^{\frac{1}{2}}\right] \tag{54}$$

With their corresponding normal modes, we can expand the derivation vector as in the previous section. The degenerate zero modes are not coupled by the dynamics in this system, i.e.,

$${\rm i}\dot{c}_{0,1,2} = 0$$

by taking into account of

$$\begin{aligned}\boldsymbol{w}^\dagger_{0,1,2}(t)\dot{\psi}_{\rm s}(t) &= N_{0,1,2}(\Omega\psi_{ab,s}\dot{\psi}_{b_2,s} + \lambda\psi_{b_2,s}\dot{\psi}_{ab,s}) \\ &= \frac{\dot\lambda\Omega - \lambda\dot\Omega}{6}\left[\frac{\sqrt{\lambda\Omega^3}}{\Omega(\lambda+\Omega)^2}(-1) + \frac{\sqrt{\Omega\lambda^3}}{\lambda(\lambda+\Omega)^2}\right] \\ &= 0\end{aligned}$$

where $N_{0,1,2}$ is the normalized coefficient. Using $\boldsymbol{w}_\pm = N_\pm(-M, \omega_\pm)^{\rm T}$, $N_\pm = \sqrt{\frac{3}{4\lambda\Omega}}$ (for $\delta = 0$) and

$$\boldsymbol{w}^\dagger_\pm(t)\dot{\psi}_s(t) = N_\pm\frac{\dot\lambda\Omega - \lambda\dot\Omega}{3(\lambda+\Omega)}$$

we can get

$$c_{\pm}(t) = N_{\pm}\frac{\dot{\lambda}\Omega - \lambda\dot{\Omega}}{3(\lambda+\Omega)}\frac{1-\mathrm{e}^{-\mathrm{i}\omega_{\pm}t}}{\mathrm{i}\omega_{\pm}}$$

and

$$\gamma_{\mathrm{nl}}(t) \approx \frac{1}{2}\left(\frac{N_+^2}{\omega_+^2}+\frac{N_-^2}{\omega_-^2}\right)^{\frac{1}{2}}\frac{|\dot{\lambda}\Omega-\lambda\dot{\Omega}|}{3(\lambda+\Omega)} = \frac{|\dot{\eta}|}{1+\eta}\frac{1}{4\lambda} \ll 1$$

where $\eta = \lambda/\Omega$. This expression is different from that for the linear system [88], for the later case η in the denominator should be replaced by η^2, which is similar to the case of atom–dimer conversion [88].

We remark that this scheme relies crucially on the capability to avoid rapid collisional quenching or the formation of an unstable atom–dimer sample. When energetically allowed, collision-induced reactions always occur at some rate, and we need to guarantee that the time scale over which quantum fluctuations dominate the dynamics is short enough, so that the dynamics of the system is not collision-dominated.

6 Chemical quantum memory

From the point of view of quantum information science, coherent two-color PA [157–159] can be taken as encoding/decoding the optical information into/from the atom–molecule dark state, indicating a hybrid device for quantum control of photons. In this Section we will show such a scenario is accessible by introducing a quantized associating light into the atom-heteronuclear molecule dark state [160, 161], which also allows us to study the effects of initial populations imbalance on the optical storage process. In particular, we will compare the results for atom–molecule systems with that of the familiar atomic quantum memory scheme [162]. For a given number of atoms, we find that the signal light is slowed more in the chemical system, indicating some advantages over atomic slow-light media. Hence, the chemical proposal, together with, e.g., a cascaded molecular transition, indicates a promising new device for optical storage, processing, and retrieval.

6.1 Slow-light photoassociation

As Fig. 21 illustrates, the initial ultracold bosonic two-species atomic condensates (with populations N_a or N_b) are photoassociated into the excited molecular state $|e\rangle$ by a quantized signal light, which is then dumped into the ground molecular state $|g\rangle$ by another classical coupling light. The signal pulse is described by the dimensionless operator

$$\hat{E}(z,t) = \sqrt{\frac{\hbar\nu}{2\epsilon_0 L}}\hat{\mathcal{E}}(z,t)\exp(\mathrm{i}\frac{\nu}{c}(z-ct)) \tag{55}$$

where L is the quantization length in the z direction, ν is the PA light frequency and $\hat{\mathcal{E}}(z,t)$ is the slowly varying amplitude. We focus on the role of coherent couplings of photons and matter waves by ignoring the collisions of a dilute or FR-tuned medium [163]. This is a safe approximation for the short lifetime of associated dimers [72, 91]. The operators of signal light and matter waves satisfy the commutation relations, respectively,

$$[\hat{E}(z,t),\ \hat{E}^{\dagger}(z',t)] = \frac{\nu}{\epsilon_0}\delta(z-z')$$
$$[\hat{\phi}_i(z,t),\ \hat{\phi}_j{}^{\dagger}(z',t)] = \delta_{ij}\delta(z-z')$$

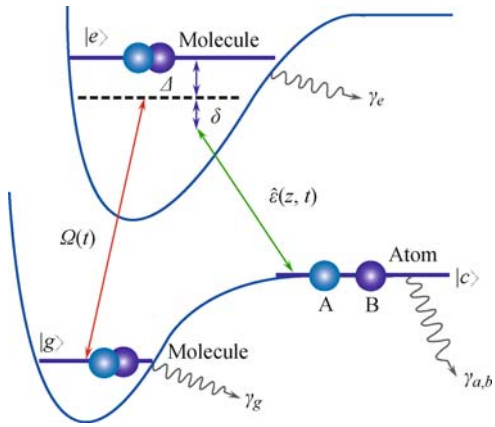

Fig. 21 Heteronuclear molecular creation in a two-species atomic BEC via two-color PA, with free-quasi-bound–bound transition induced by a quantum signal light and a classical coupling field. Reproduced from Ref. [161], Copyright © 2009 The American Physical Society.

The dynamics of this system is described in the simplest level by the interaction Hamiltonian

$$\begin{aligned}\hat{\mathcal{H}} = &\Delta\int \mathrm{d}z\hat{\phi_e}{}^{\dagger}(z,t)\hat{\phi}_e(z,t) + \delta\int \mathrm{d}z\hat{\phi_a}{}^{\dagger}(z,t)\hat{\phi}_a(z,t)\\ &-\int \mathrm{d}z\big[g\hat{\mathcal{E}}(z,t)\hat{\phi_e}{}^{\dagger}(z,t)\hat{\phi}_a(z,t)\hat{\phi}_b(z,t)\\ &+\Omega\hat{\phi_e}{}^{\dagger}(z,t)\hat{\phi}_g(z,t) + h.c.\big]\end{aligned} \tag{56}$$

Ω is the Rabi frequency of the coupling field, and $g = \wp\sqrt{\frac{\nu}{2\hbar\epsilon_0 V}}$ is the photon-matter waves coupling coefficient with $\wp$ being the transition-dipole moment of $|c\rangle - |e\rangle$ transition by $\hat{E}(z,t)$ [162]. Without loss of generality, we assume that the signal field amplitude $\hat{\mathcal{E}}$ and control field amplitude Ω are real whose phase factor can be absorbed by a global gauge transformation of the field operators [87, 161]. Here, we first drop off the usual kinetic and the trapping terms by considering a uniform system and the effects due to these terms will be discussed later.

With the slowly varying amplitude approximation [162], the propagation equation of the signal light can be written as:

$$(\frac{\partial}{\partial t}+c\frac{\partial}{\partial z})\hat{\mathcal{E}}(z,t) = \mathrm{i}gL\hat{\phi}_a^{\dagger}(z,t)\hat{\phi}_b^{\dagger}(z,t)\hat{\phi}_e(z,t) \tag{57}$$

Meanwhile, the evolutions of atomic field operators are described by the following Heisenberg equations,

$$\dot{\hat{\phi}}_a = -\mathrm{i}\delta\hat{\phi}_a - \gamma_a\hat{\phi}_a + \mathrm{i}g\hat{\mathcal{E}}^\dagger\hat{\phi}_b{}^\dagger\hat{\phi}_e \tag{58a}$$

$$\dot{\hat{\phi}}_b = -\gamma_b\hat{\phi}_b + \mathrm{i}g\hat{\mathcal{E}}^\dagger\hat{\phi}_a{}^\dagger\hat{\phi}_e \tag{58b}$$

$$\dot{\hat{\phi}}_e = -\mathrm{i}\Delta\hat{\phi}_e - \gamma_e\hat{\phi}_e + \mathrm{i}g\hat{\mathcal{E}}\hat{\phi}_a\hat{\phi}_b + \mathrm{i}\Omega\hat{\phi}_g \tag{58c}$$

$$\dot{\hat{\phi}}_g = -\gamma_g\hat{\phi}_g + \mathrm{i}\Omega\hat{\phi}_e \tag{58d}$$

where γ_a, γ_b, γ_e and γ_g denote the decay rates of corresponding matter-wave states. In order to obtain a closed-form signal-light propagation equation, it is a key step to study the evolutions of the following hybrid operators,

$$\begin{aligned}\frac{\partial}{\partial t}(\hat{\phi}_a^\dagger\hat{\phi}_b^\dagger\hat{\phi}_e) = {}& \mathrm{i}g\hat{\mathcal{E}}\hat{\phi}_a{}^\dagger\hat{\phi}_a\hat{\phi}_b{}^\dagger\hat{\phi}_b + \mathrm{i}\Omega\hat{\phi}_a{}^\dagger\hat{\phi}_b{}^\dagger\hat{\phi}_g \\ & -(\gamma_2 - \mathrm{i}\Delta - \mathrm{i}\delta)\hat{\phi}_a{}^\dagger\hat{\phi}_b{}^\dagger\hat{\phi}_e \\ & -\mathrm{i}g\hat{\mathcal{E}}(\hat{\phi}_a{}^\dagger\hat{\phi}_a + \hat{\phi}_b{}^\dagger\hat{\phi}_b)\hat{\phi}_e{}^\dagger\hat{\phi}_e\end{aligned} \tag{59}$$

$$\begin{aligned}\frac{\partial}{\partial t}(\hat{\phi}_a^\dagger\hat{\phi}_b^\dagger\hat{\phi}_g) = {}& -(\gamma_1 - \mathrm{i}\delta)\hat{\phi}_a^\dagger\hat{\phi}_b^\dagger\hat{\phi}_g + \mathrm{i}\Omega\hat{\phi}_a^\dagger\hat{\phi}_b^\dagger\hat{\phi}_e \\ & -\mathrm{i}g\hat{\mathcal{E}}(\hat{\phi}_a^\dagger\hat{\phi}_a + \hat{\phi}_b^\dagger\hat{\phi}_b)\hat{\phi}_e^\dagger\hat{\phi}_g\end{aligned} \tag{60}$$

with the transversal decay rates $\gamma_1 = \gamma_a + \gamma_b + \gamma_g$ and $\gamma_2 = \gamma_a + \gamma_b + \gamma_e$. These equations can be rewritten as:

$$\begin{aligned}\hat{\phi}_a^\dagger\hat{\phi}_b^\dagger\hat{\phi}_e = {}& -\frac{\mathrm{i}}{\Omega}\frac{\partial}{\partial t}(\hat{\phi}_a^\dagger\hat{\phi}_b^\dagger\hat{\phi}_g) - \frac{\mathrm{i}}{\Omega}(\gamma_1 - \mathrm{i}\delta)\hat{\phi}_a^\dagger\hat{\phi}_b^\dagger\hat{\phi}_g \\ & +\frac{g}{\Omega}\hat{\mathcal{E}}(\hat{\phi}_a^\dagger\hat{\phi}_a + \hat{\phi}_b^\dagger\hat{\phi}_b)\hat{\phi}_e^\dagger\hat{\phi}_g\end{aligned} \tag{61}$$

$$\begin{aligned}\hat{\phi}_a^\dagger\hat{\phi}_b^\dagger\hat{\phi}_g = {}& -\frac{\mathrm{i}}{\Omega}\frac{\partial}{\partial t}(\hat{\phi}_a{}^\dagger\hat{\phi}_b{}^\dagger\hat{\phi}_e) - \frac{g}{\Omega}\hat{\mathcal{E}}\hat{\phi}_a{}^\dagger\hat{\phi}_a\hat{\phi}_b{}^\dagger\hat{\phi}_b \\ & -\frac{\mathrm{i}}{\Omega}(\gamma_2 - \mathrm{i}\Delta - \mathrm{i}\delta)\hat{\phi}_a{}^\dagger\hat{\phi}_b{}^\dagger\hat{\phi}_e \\ & +\frac{g}{\Omega}\hat{\mathcal{E}}(\hat{\phi}_a{}^\dagger\hat{\phi}_a + \hat{\phi}_b{}^\dagger\hat{\phi}_b)\hat{\phi}_e{}^\dagger\hat{\phi}_e\end{aligned} \tag{62}$$

The equations can be greatly simplified under the weak excitation approximation (WEA): the control field is much stronger than the signal light at all times and thus the density of signal photons can be taken as much less than that of atoms. This means that only a small ratio of atoms are converted into molecules, which is the case in current two-color PA experiment [72, 91]. With the WEA at hand, after some algebra we find in the lowest non-vanishing order

$$\hat{\phi}_a{}^\dagger\hat{\phi}_b{}^\dagger\hat{\phi}_g \approx -\frac{g\hat{\mathcal{E}}}{\Omega}\hat{\phi}_a^\dagger\ \hat{\phi}_a\hat{\phi}_b{}^\dagger\ \hat{\phi}_b \tag{63}$$

Hence Eq. (61) can be rewritten as:

$$\hat{\phi}_a{}^\dagger\hat{\phi}_b{}^\dagger\hat{\phi}_e \approx \mathrm{i}\frac{gN_aN_b}{\Omega^2}\frac{\partial}{\partial t}\hat{\mathcal{E}}(z,t) - \mathrm{i}\frac{gN_aN_b}{\Omega^3}\frac{\partial\Omega(t)}{\partial t}\hat{\mathcal{E}}(z,t) \tag{64}$$

where $N_{a,b} = \hat{\phi}_{a,b}^\dagger\hat{\phi}_{a,b}$ is the population of atoms A or B, which can be assumed as constant in the WEA. Substituting Eq. (64) into Eq. (57) yields

$$\begin{aligned}&(\frac{\partial}{\partial t} + \frac{c}{1+\frac{g^2LN_aN_b}{\Omega^2}}\frac{\partial}{\partial z})\hat{\mathcal{E}}(z,t) \\ &\quad = \frac{1}{1+\frac{g^2LN_aN_b}{\Omega^2}}\frac{g^2LN_aN_b}{\Omega^3}\frac{\partial\Omega}{\partial t}\hat{\mathcal{E}}(z,t)\end{aligned} \tag{65}$$

Clearly, for a time-independent coupling field, we have a steady group velocity of the signal, and the temporal profile or the spectrum of the signal pulse remains unchanged during its slowing down process, just as in a three-level atomic ensemble [162].

For a time-dependent coupling field, however, the right-hand side of Eq. (65) leads to an adiabatic Raman enhancement of the signal pulse

$$\hat{\mathcal{E}}(z,t) = \frac{\cos\theta(t)}{\cos\theta(0)}\ \hat{\mathcal{E}}(z - \int_0^t v_g\mathrm{d}t', 0) \tag{66}$$

where $v_g = c\cos^2\theta$ is the group velocity of the signal light and θ is the mixing angle between light and matter-wave components, i.e., $\tan^2\theta = g^2N_aN_bL/\Omega^2(t)$, or

$$v_g^{-1} = \left(1 + \frac{\tilde{g}^2N_aN_b}{\Omega^2}\right)/c \tag{67}$$

with $\tilde{g} = g\sqrt{L}$. Obviously, if the classical field is adiabatically turned off by rotating the mixing angle θ for $\pi/2$, the signal light will be fully stopped within the medium or in the created atom–molecule dark state [72, 91].

6.2 Quantum state transfer

The important feature of quantum state transfer can be observed through the form of the closed-channel molecular field, i.e.,

$$\begin{aligned}&\hat{\phi}_g(z,t) \approx k\hat{\mathcal{E}}(z - \int_0^t v_g\mathrm{d}t', 0) \\ &k = -\frac{g\sqrt{N_aN_b}}{\Omega(0)}\sqrt{\frac{\Omega^2(0) + \tilde{g}^2N_aN_b}{\Omega^2(t) + \tilde{g}^2N_aN_b}}\end{aligned} \tag{68}$$

Obviously, for the initial stage ($\Omega^2 \gg \tilde{g}^2N_aN_b$), we have a purely photonic state, i.e., $\theta(0) = 0$ or $\hat{\phi}_g(z,0) = 0$, but when the coupling light is shut down adiabatically, the quantum state of the associating light is fully encoded into the created molecules via the mapping

$$\sqrt{L}\hat{\phi}_g(z,t) = -\hat{\mathcal{E}}(z - \int_0^t v_g\mathrm{d}t', 0) \tag{69}$$

For the atomic slow-light medium [162], the group velocity of signal light is: $v_g = c/(1 + \frac{g^2N}{\Omega^2})$, i.e., being proportional to $\sim N^{-1}$, where N can be regarded as the number of initial trapped atoms in the WEA; however, in our situation, this velocity is proportional to $\sim N^{-2}$ (for $N_a = N_b = N/2$). Hence, with the atom–molecule dark state, the signal light can be much slowed down by starting from the same total number of atoms.

As Fig. 22 shows, the initial population imbalance of the atoms A, B ($\eta = N_b/N_a$) also plays a role in the optical storage process, and the optimal conversion is reached for the balanced case ($\eta = 1$). In our calculations, the initial total atomic number is taken as $N = N_a + N_b = 3.0 \times 10^6$. In current experimental

conditions [164], the strength of the coupling field can be chosen as (in the unit of MHz)

$$\Omega(t) = 10\pi\{1 - 0.5\tanh[0.15(t-15)] + 0.5\tanh[0.15(t-125)]\} \quad (70)$$

which guarantees that the group velocity can be adiabatically reduced to zero in the photon-storage stage and then the signal light can be re-accelerated in the retrieval stage. The control field being similar to Eq. (70) is also used in the atomic slow-light medium [162]. For the imbalanced case, e.g., $\eta = 15$ as in the very recent experiment of creating polar molecules KRb [52], some deviation from the optimized case can appear.

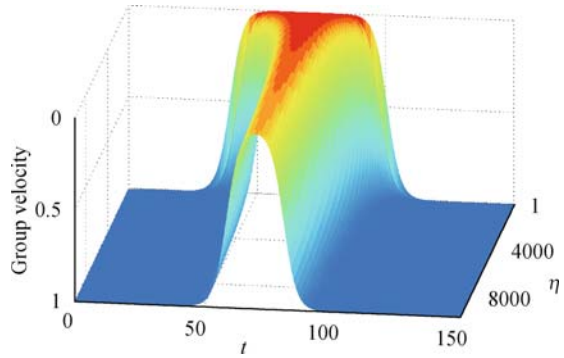

Fig. 22 The group velocity of signal light as a function of time for different populations imbalances η. The quantized length $L = 1$ mm, the coupling coefficient $g = 10$, the velocity is scaled by c and the time is in the unit of μs. Reproduced from Ref. [161], Copyright © 2009 The American Physical Society.

Figure 23 shows the different features of slow light propagation in four different kinds of matter-wave mediums: (i) the atomic ensemble, (ii)-(iii) the assembly of homonuclear or heteronuclear dimers [87, 161, 165], and (iv) the assembly of heteronuclear trimer ABC [79]). In addition, we see that by choosing a higher initial atomic population, the optical storage process can be significantly improved.

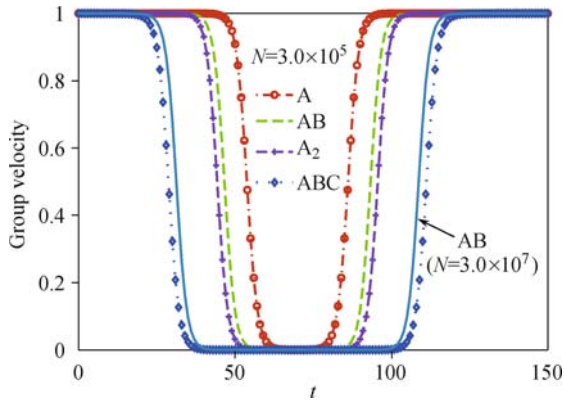

Fig. 23 The group velocity of the signal light as a function of time in different matter-wave mediums, with the optimal or balanced initial population imbalance. Reproduced from Ref. [161], Copyright © 2009 The American Physical Society.

It is worth mentioning that in the above discussions we have ignored the decay of molecular states. However, it can be readily shown that, after including these decay terms, the group velocity of the signal light is still in the form of Eq. (70) but with the following substitution

$$\Omega \to \sqrt{\Omega^2 + \gamma_1\gamma_2}$$

Clearly, due to the decay terms, one may reach a *nonzero* group velocity even when the classical field is turned off. For the typical parameters of the molecules KRb [164], we can take $N_{\rm K} = 1.0 \times 10^6$, $N_{\rm Rb} = 5.0 \times 10^6$, $\tilde{g} \approx 50$ $\rm s^{-1}$, and

$$\gamma_1 = 2\pi \times 97 \text{ Hz}, \quad \gamma_2 = 2\pi \times 5.7 \text{ MHz}$$

The velocity limit can be estimated as $v_g^c \approx 0.524$ $\rm km{\cdot}s^{-1}$. In particular, for a sufficient state transfer, the PA time duration should satisfy $t \ll \gamma_1^{-1} \sim 1.6$ ms [166, 167], which can be fulfilled in current experiments [168–170].

We also note that some optimized methods exist for a maximum efficiency of optical storage and retrieval, such as the recent works of Novikova *et al.* by using an optimized signal pulse shape in an atomic medium [171, 172]. For the present atom-molecule system, in order to avoid incoherent absorptive loss, the frequency components of the signal pulse must fit well with the slow-light spectral window, i.e., $t_s^{-1} \ll \sqrt{d}v_g/L \sim N^{-1}$, where t_s is the temporal length of the signal pulse, $d = g^2 N_a N_b L/(\gamma c)$ is optical depth of the medium. Thereby, to avoid "leakage" of the pulse outside the medium, the following condition should be fulfilled

$$v_g t_s \sim N^{-1} \ll L$$

This means that v_g must be small enough for the entire signal pulse to be spatially compressed into the medium, with also a large optical depth d. In contrast, by using a purely atomic medium, we have $d = g^2 NL/(\gamma c)$ [171] and thus $v_g t_s \sim N^{-1/2}$ [172]. Obviously, for the same initial total atoms, the light storage using the atom-molecule dark state has some advantage over the atomic spin-wave scheme.

6.3 Molecular solitons

Now we show that, by taking into account the particle collisions in the quantum state transfer process, it is also possible to realize a molecular matter-wave soliton laser. To this end, we consider coherent atom–molecule conversion process which is described by the following total Hamiltonian

$$\hat{H}_{\rm tot} = \hat{H}_0 + \hat{H}_{\rm coll} + \hat{\mathcal{H}} \quad (71)$$

where $\hat{\mathcal{H}}$, as in Eq. (56), denotes the coherent free-quasi-bound-bound transition, $\hat{H}_0$ and $\hat{H}_{\rm coll}$ describe the free motions and the particle collisions, respectively,

$$H_0 = \sum_i \int \mathrm{d}z \hat{\phi}_i^\dagger (-\frac{1}{2m_i}\frac{\partial^2}{\partial z^2} + V_i)\hat{\phi}_i$$
$$H_{\mathrm{coll}} = \sum_{i,j} U_{ij} \int \mathrm{d}z \hat{\phi}_i^\dagger \hat{\phi}_j^\dagger \hat{\phi}_j \hat{\phi}_i \quad (72)$$

were $V_i(z)(i,j=a,b,g)$ denotes the longitudinal external effective potential and one can choose $V_a(z)$=$V_b(z)=0$ in the following derivation [162], m_i is the particle mass, U_{ij} denotes the s-wave scattering collisions between the particles [173]. Then the evolution of molecular matter-wave field is written as:

$$\mathrm{i}\frac{\partial \hat{\phi}_g}{\partial t} = \Big[-\frac{1}{2(m_a+m_b)}\frac{\partial^2}{\partial z^2} + U_{ab}\hat{\phi}_a^\dagger \hat{\phi}_b + U_{gg}\hat{\phi}_g^\dagger \hat{\phi}_g + V_g(z)\Big]\hat{\phi}_g - \Omega \hat{\phi}_e \quad (73)$$

For simplicity, we consider an initially trapped atomic ensemble and also introduce the MFA by replacing the operators by the c-numbers, i.e., $\hat{\phi}_i(z,t) \to \Phi_i(z,t)$. Thereby, for the closed-channel molecules, i.e., with the mixing angle $\theta = \pi/2$, we obtain the nonlinear mean-field Gross–Pitaevskii equation

$$\mathrm{i}\frac{\partial \Phi_g}{\partial t} = -\frac{1}{2(m_a+m_b)}\frac{\partial^2 \Phi_g}{\partial z^2} + V_{\mathrm{eff}}\Phi_g + U_{gg}|\Phi_g^0|^2\Phi_g \quad (74)$$

where the effective potential $V_{\mathrm{eff}} = V_g + \sqrt{N_a N_b}U_{ab}$ can also be moved by suitably tuning the value of V_g [162]. For $a_{gg} > 0$, due to some balance between the repulsive molecular collisions and the molecular kinetic energy, the above well-known nonlinear equation can support a gray-soliton solution [174, 175]

$$\Phi_g = \Phi_g^0(z,t)\big\{\mathrm{i}\sqrt{1-q^2} + q\tanh\big[\frac{q}{\sqrt{\alpha}}(z - z_0(t))\big]\big\} \quad (75)$$

with $\alpha = (\sqrt{4\pi a_{gg}}|\Phi_g^0|)^{-1}$. V_g is chosen such that $V_{\mathrm{eff}} = 0$, the slowly-varying background function is

$$\Phi_g^0(z,t) = \langle\hat{\phi}_g\rangle \exp(-\mathrm{i}\int_{t_0}^t U_{gg}|\langle\hat{\phi}_g\rangle|^2 \mathrm{d}t') \quad (76)$$

and z is the inside-trap position. In addition, the "grayness" parameter is

$$q = \sqrt{1-(v_\nu/v_s)^2} \leqslant 1 \quad (77)$$

with the Bogoliubov sound speed [176]

$$v_s = [U_{gg}|\Phi_g^0|^2/(m_a+m_b)]^{1/2}$$

and the dark-soliton speed $v_\nu = \dot{z}_0(t)$, $z_0(t)$ being the central position of the molecular matter-wave soliton. Clearly, $q=1$ corresponds to a dark soliton with 100% density depletion. As Fig. 24 shows, by applying two counter-propagating control fields, a second-order molecular grey soliton ($q=0.8$) starting from the same position ($z=0$) can split into two solitons propagating in opposite directions.

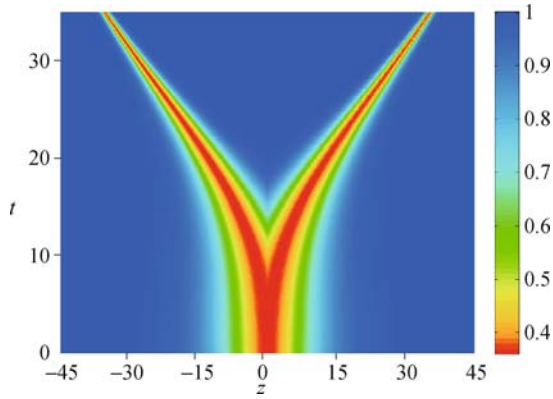

Fig. 24 Splitting grey solitons under the influence of background amplitude decreasing, for $q=0.8$. The units of time and trap size are in μs and μm, respectively. Reproduced from Ref. [161], Copyright © 2009 The American Physical Society.

7 Quantum spinor reaction

7.1 Double-pendulum model: photoassociation in a dipolar spinor gas

The long-range and anisotropic dipole–dipole interaction (DDI) [177] resulting from intrinsic or induced magnetic dipole moments can significantly affect the stability [178] and dynamics of BEC and modify their excitation spectrum [179, 180]. In this section we study the role of PA and magnetic DDI in the spin-mixing dynamics of an antiferromagnetic ^{23}Na BEC.

Specifically, we consider a spinor gas of N atoms initially in the state $m_{\mathrm{F}} = |-1\rangle$, coupled to a molecular condensate by a PA field of Rabi frequency $\Omega(t)$. The Hamiltonian of the system is $\hat{H} = \hat{H}_{\mathrm{SM}} + \hat{H}_{\mathrm{DD}} + \hat{H}_{\mathrm{PA}}$, where

$$\hat{H}_{\mathrm{SM}} = \int \mathrm{d}\boldsymbol{r}\hat{\psi}_\alpha^\dagger(\boldsymbol{r})\Big[-\frac{\nabla^2}{2m} + V_T(\boldsymbol{r}) + E_\alpha\Big]\hat{\psi}_\alpha(\boldsymbol{r}) + \frac{c_0'}{2}\int \mathrm{d}\boldsymbol{r}\hat{\psi}_\alpha^\dagger(\boldsymbol{r})\hat{\psi}_\beta^\dagger(\boldsymbol{r})\hat{\psi}_\alpha(\boldsymbol{r})\widehat{\psi}_\beta(\boldsymbol{r}) + \frac{c_2'}{2}\int \mathrm{d}\boldsymbol{r}\hat{\psi}_\alpha^\dagger(\boldsymbol{r})\hat{\psi}_\beta^\dagger(\boldsymbol{r})\boldsymbol{F}_{\alpha\alpha'}\cdot\boldsymbol{F}_{\beta\beta'}\hat{\psi}_{\beta'}(\boldsymbol{r})\hat{\psi}_{\alpha'}(\boldsymbol{r}) \quad (78a)$$

$$\hat{H}_{\mathrm{DD}} = \frac{c_d'}{2}\int \mathrm{d}\boldsymbol{r}\int \mathrm{d}\boldsymbol{r}'\frac{1}{|\boldsymbol{r}-\boldsymbol{r}'|^3} \cdot[\hat{\psi}_\alpha^\dagger(\boldsymbol{r})\hat{\psi}_\beta^\dagger(\boldsymbol{r}')\boldsymbol{F}_{\alpha\alpha'}\cdot\boldsymbol{F}_{\beta\beta'}\hat{\psi}_{\beta'}(\boldsymbol{r})\hat{\psi}_{\alpha'}(\boldsymbol{r}') - 3\hat{\psi}_\alpha^\dagger(\boldsymbol{r})\hat{\psi}_\beta^\dagger(\boldsymbol{r}')(\boldsymbol{F}_{\alpha\alpha'}\cdot\boldsymbol{e})(\boldsymbol{F}_{\beta\beta'}\cdot\boldsymbol{e})\hat{\psi}_{\beta'}(\boldsymbol{r})\hat{\psi}_{\alpha'}(\boldsymbol{r}')] \quad (78b)$$

$$\hat{H}_{\mathrm{PA}} = \int \mathrm{d}\boldsymbol{r}\hat{\psi}_b^\dagger(\boldsymbol{r})\Big[-\frac{\nabla^2}{2M} + V_T(\boldsymbol{r})\Big]\hat{\psi}_b(\boldsymbol{r}) + \int \mathrm{d}\boldsymbol{r}[\Omega(t)\hat{\psi}_-^\dagger(\boldsymbol{r})\hat{\psi}_-^\dagger(\boldsymbol{r})\hat{\psi}_b(\boldsymbol{r}) + h.c.] \quad (78c)$$

where $\hat{\psi}_\alpha(\boldsymbol{r})$ ($\alpha = \pm1, 0$) are the field annihilation operators of the spin-1 atom in the hyperfine state α and $\hat{\psi}_b(\boldsymbol{r})$ the corresponding operator of the molecule state,

$V_T(\boldsymbol{r})$ is the trapping potential and assumed to be spin-independent, E_α is the Zeeman shift [122], $\boldsymbol{F}$ is the spin-1 matrix [181], $\boldsymbol{e} = (\boldsymbol{r} - \boldsymbol{r}')/|\boldsymbol{r} - \boldsymbol{r}'|$ is a unit vector, and m and M are the atomic and molecular masses. The parameters appearing in the spin-exchange and the DDI Hamiltonians are $c_0' = 4\pi(a_0 + 2a_2)/(3m)$, $c_2' = 4\pi(a_2 - a_0)/(3m)$, and $c_d' = \mu_0\mu_{\rm B}^2 g_{\rm F}^2/(4\pi)$, where $a_{0,2}$ are the s-wave scattering lengths, μ_0 is the vacuum magnetic permeability, $\mu_{\rm B}$ is the Bohr magneton, and $g_{\rm F}$ is the Landé g-factor. Finally, $\Omega(t) = \Omega\exp(-{\rm i}\omega_L t)$ is the effective Rabi frequency of the PA light of frequency Ω_L.

We describe the atomic system in a single-mode approximation (SMA) [121–124, 182]. It is known that the spatial degrees of freedom decouple from the spinor dynamics when the spin healing length is larger than the condensate size, and the SMA has been shown to be in good agreement with experiments [121–124, 182]. We then have $\hat{\psi}_\alpha(\boldsymbol{r}) \to \phi(\boldsymbol{r})\hat{a}_\alpha$, $\hat{\psi}_b(\boldsymbol{r}) \to \phi(\boldsymbol{r})\hat{b}$, where $\phi(\boldsymbol{r})$ is the spatial wave function of the condensate, and $\hat{a}_\alpha$ or $\hat{b}$ are atomic or molecular annihilation operators, and the Hamiltonians $\hat{H}_{\rm SM}$, $\hat{H}_{\rm DD}$ and $\hat{H}_{\rm PA}$ simplify to

$$\begin{aligned}\hat{H}_{\rm SM} = &\sum_\alpha \omega_\alpha \hat{a}_\alpha^\dagger \hat{a}_\alpha + \frac{c_0}{2}\sum_{\alpha,\beta}\hat{a}_\alpha^\dagger\hat{a}_\beta^\dagger a_\alpha a_\beta + \frac{c_2}{2}[\hat{a}_+^{\dagger 2}\hat{a}_+^2 \\ &+2\hat{a}_+^\dagger\hat{a}_0^\dagger\hat{a}_0\hat{a}_+ + 2\hat{a}_-^\dagger\hat{a}_0^\dagger\hat{a}_0\hat{a}_- - 2\hat{a}_+^\dagger\hat{a}_-^\dagger\hat{a}_-\hat{a}_+ \\ &+\hat{a}_-^{\dagger 2}\hat{a}_-^2 + 2\hat{a}_0^{\dagger 2}\hat{a}_+\hat{a}_- + 2\hat{a}_+^\dagger\hat{a}_-^\dagger\hat{a}_0^2] \qquad (79a)\end{aligned}$$

$$\begin{aligned}\hat{H}_{\rm DD} = &\frac{c_{\rm d}}{2}[-2\hat{a}_+^\dagger\hat{a}_0^\dagger\hat{a}_+\hat{a}_0 - 2\hat{a}_-^\dagger\hat{a}_0^\dagger\hat{a}_-\hat{a}_0 - 2\hat{a}_0^{\dagger 2}\hat{a}_+\hat{a}_- \\ &+2\hat{a}_+^{\dagger 2}\hat{a}_+^2 + 2\hat{a}_-^{\dagger 2}\hat{a}_-^2 - 4\hat{a}_+^\dagger\hat{a}_-^\dagger\hat{a}_+\hat{a}_- \\ &-2\hat{a}_+^\dagger\hat{a}_-^\dagger\hat{a}_0\hat{a}_0 + \hat{a}_+^\dagger\hat{a}_+ + \hat{a}_-^\dagger\hat{a}_- - 2\hat{a}_0^\dagger\hat{a}_0] \qquad (79b)\end{aligned}$$

$$\hat{H}_{\rm PA} = \omega_b\hat{b}^\dagger\hat{b} + [\Omega(t)\hat{a}_-\hat{a}_-\hat{b}^\dagger + \Omega(t)^*\hat{b}\hat{a}_-^\dagger\hat{a}_-^\dagger] \qquad (79c)$$

where $\omega_{a,b}$ are the energies of the atomic and molecular free motion, and $c_{0,2}$ and c_d denote the spin-exchange and the dipole–dipole interactions, respectively,

$$\begin{aligned}\omega_\alpha &= \int {\rm d}\boldsymbol{r}\phi^*(\boldsymbol{r})[-\nabla^2/(2m) + V_T(\boldsymbol{r}) + E_\alpha]\phi(\boldsymbol{r}) \\ \omega_b &= \int {\rm d}\boldsymbol{r}\phi^*(\boldsymbol{r})[-\nabla^2/(2M) + V_T(\boldsymbol{r})]\phi(\boldsymbol{r}) \\ c_{0,2} &= c_{0,2}'\int {\rm d}\boldsymbol{r}\,|\phi(\boldsymbol{r})|^4 \\ c_{\rm d} &= \frac{c_{\rm d}'}{2}\iint {\rm d}\boldsymbol{r}{\rm d}\boldsymbol{r}'\frac{|\phi(\boldsymbol{r})|^2|\phi(\boldsymbol{r}')|^2(1-3\cos^2\theta)}{|\boldsymbol{r}-\boldsymbol{r}'|^3}\end{aligned}$$

Here, θ is the polar angle of the vector $\boldsymbol{r} - \boldsymbol{r}'$, and $c_{\rm d}$ can be tuned by modifying the geometric shape of the condensate or the trap aspect ratio κ [101, 183].

Within a standard MFA we replace the operators $\hat{\alpha}$, $\hat{b}$ by corresponding c-numbers. Further introducing the slowly-varying variables

$$\hat{a}_\pm \to (a_\pm/\sqrt{N}){\rm e}^{-{\rm i}\omega_\pm t},\quad \hat{a}_0 \to (a_0/\sqrt{N}){\rm e}^{-{\rm i}(\omega_0+\delta)t}$$
$$\hat{b} \to (b/\sqrt{N}){\rm e}^{-{\rm i}(2\omega_- t+\omega_L)t}$$

where N is the initial number of atoms and $\delta = (\omega_- + \omega_+ - 2\omega_0)/2$ denotes the quadratic Zeeman effect [122]. Scaling in addition the various coupling constants to $\Omega(t) \to (\Omega\sqrt{N}){\rm e}^{-{\rm i}\omega_L t}$ and $c_{0,2,{\rm d}} \to c_{0,2,{\rm d}}N$, and the time to $t \to c_0 N t$, we then arrive at the mean-field equations of motion, with the molecular losses γ. Considering for illustration a Gaussian ansatz for the condensate wave function,

$$\phi(r) = \pi^{-3/4}\kappa^{1/2}q^{-3/2}\exp[-(x^2+y^2+\kappa^2Z^2)/(2q^2)]$$

one finds $U \equiv c_{\rm d}/|c_2| = 2\pi c_{\rm d}\chi(\kappa)/(3|c_2|) \in [-1,\ 2]$, where $\chi(\kappa)$ is a monotonically increasing function of κ that equals zero at $\kappa = 1$ [101, 183–185]. Hence the presence of the DDI results in a situation where the atomic spin mixing can be varied continuously within the bounded range of U. In particular, the dipolar spinor gas is of ferromagnetic for $U > 1$; for $U < 1$, however, it can be ferromagnetic ($-1 < U < -0.5$) or even antiferromagnetic ($-0.5 < U < 1$) [101, 183–185].

Expressing the amplitudes a_i and b in terms of their real amplitudes and phases as $a_{\pm1,0} = \sqrt{n_{\pm,0}}{\rm e}^{-{\rm i}\theta_{\pm,0}}$ and $b = \sqrt{n_m}{\rm e}^{-{\rm i}\phi}$, it is possible to introduce two sets of conjugate variables $(n_-,\ \alpha)$ and (n_m, β), where $\alpha = \theta_+ + \theta_- - 2\theta_0$ and $\beta = \phi - 2\theta_-$. Then, for the special case of zero magnetization, $m = n_+ - (n_- + 2n_m) = 0$, we can get

$$\begin{aligned}\dot{n}_- &= A_1\sin\alpha - 2A_2\sin\beta \\ \dot{\alpha} &= A_0 + A_1B_1\cos\alpha + \frac{A_2}{n_-}\cos\beta \\ \dot{n}_m &= A_2\sin\beta \\ \dot{\beta} &= \bar{A}_0 + A_1B_2\cos\alpha + \frac{A_2}{2n_m}\cos\beta\end{aligned} \qquad (80)$$

where

$$\begin{aligned}A_1 &= 2c_2(1-U)(1-2n_- - 4n_m)\sqrt{2n_-(n_- + n_m)} \\ A_2 &= 2\Omega n_-\sqrt{n_m} \\ B_1 &= \frac{2n_- + n_m}{2n_-(n_- + n_m)} - \frac{2}{1-2n_- - 4n_m} \\ B_2 &= \frac{1 - 10n_- - 12n_m}{2(n_- + n_m)(1-2n_- - 4n_m)}\end{aligned}$$

and

$$\begin{aligned}A_0 &= c_d(1 + 8n_- + 12n_m) + 2[c_2(1 - 4n_- - 6n_m) + \delta] \\ \bar{A}_0 &= \Delta + 4\delta - 2 + 4n_m(1 + c_2) + 2[c_2(1 - 6n_- - 8n_m)] \\ &\quad +3c_d(1 + 4n_- + 8n_m)\end{aligned}$$

where $\Delta = (\omega_b - 2\omega_-) - \omega_L$ is the detuning of the atom-molecule transition. These equations provide a coupled double-pendulum description of the dynamics of single-channel PA-tuned dipolar spinor gas [186–188].

Our double-pendulum model has some special cases: (i) for small values of Ω or $A_2 \ll A_1$, it reduces to the single-pendulum dynamics of spin-1 atoms [122]; (ii) in

contrast, for $U \sim 1$, the system is well approximated as a light-dominated single-pendulum model, with $A_1 \ll A_2$; (iii) in the "resonant" case ($\alpha = \beta$), we have

$$\mathcal{E} = \mathcal{E}_0 + (A_1 + A_2)\cos\alpha$$

In particular, for the special case $A_1 = A_2$, which can be obtained only in the case $U < 1$, this yields an *enhanced* single-pendulum system with $\mathcal{E} = \mathcal{E}_0 + 2A_1\cos\alpha$. This is to be contrasted to the case $A_1 = -A_2$, which can occur only in the (ferromagnetic) case $U > 1$. In that case of $\mathcal{E} = \mathcal{E}_0$, it indicates a complete *destructive* interference leading to the disappearance of the pendulum-like dynamics of the system.

Clearly, the PA field can induce quite different optical responses, depending on the magnetic phase of the atomic system. This is confirmed by numerical calculations of the time dependence of the atomic level populations. As a specific example, we have used the parameters of ^{23}Na atoms,

$$a_0 = (15.0 \pm 1.6)a_{\rm B}, \quad a_2 = (55.1 \pm 1.6)a_{\rm B}$$

where $a_{\rm B} \approx 0.529$ Å is the Bohr radius. Here we take $n \sim 8.6 \times 10^{13}{\rm cm}^{-3}$ [123, 124]. Then in our calculations c_2 is about 127 Hz, the time unit corresponds to 0.24 ms, and the unit of Ω, δ or Δ is 4200 Hz.

Figure 25 shows the population of the atomic state $|m_{\rm F} = 0\rangle$ obtained by numerically solving the mean-field equation for the constructive ($A_1 = A_2$) or destructive ($A_1 = -A_2$) interference cases, corresponding to $U < 1$ and $U > 1$, respectively. In this example the atoms are prepared in the initial state

$$f_0 \equiv [a_+, a_0, a_-, b]_{t=0} = [\sqrt{0.25}, \sqrt{0.5}, \sqrt{0.25}, 0]$$

These two situations, $U < 1$ or $U > 1$, differ drastically in that the population of the $|m_{\rm F} = 0\rangle$ state first decreases or increases below or above the initial value 0.5, respectively. Also, the range of oscillations of atomic spin mixing is wide for $U < 1$, with $n_0 \in [0, 0.5]$; in contrast, it is considerably narrower in the ferromagnetic domain, $n_0 \in [0.5, 0.62]$. (Note in particular the complete absence of oscillations for $U = 1$.) As such, they hint at the possibility of novel laser-based diagnostics of the very weak strength of the DDI.

Figure 26 further illustrates the effect of the optical field strength Ω on the atomic spin oscillations. Figure 26(a) shows the oscillation period of the spin-0 atomic state as a function of $\Delta = 0$ and $U = 0.1$ for four values of δ. For $\delta \leqslant 0.023$, we observe a single-peak resonance in the atomic oscillations at a *critical* optical Rabi frequency Ω_c [122–124]. It corresponds to the situation where the effective total energy of the system is just sufficient to bring them to their top position, with the period of oscillations becoming then infinite. Further increasing Ω for a fixed δ leads to a decreased period. We have found numerically that the single-peak structure appears below the *critical* value $U_c = 0.16$.

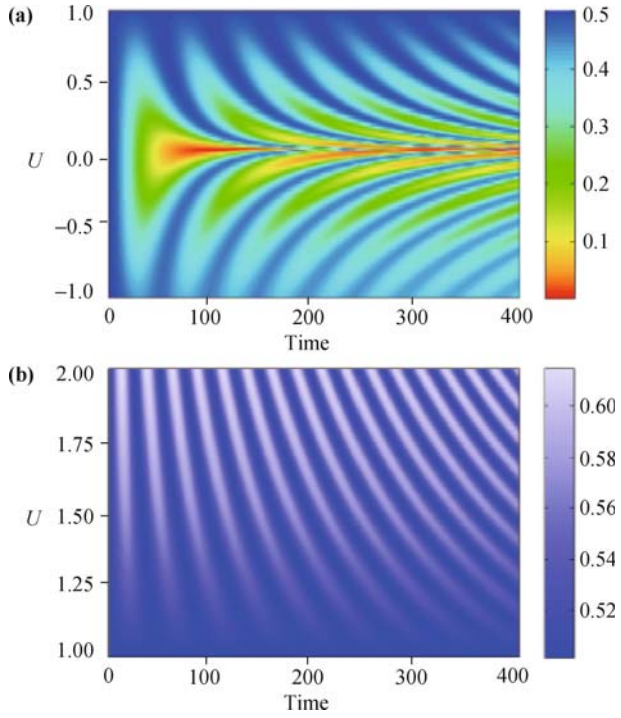

Fig. 25 Time dependence of the population of the spin-0 atomic component as a function of U for ^{23}Na atoms within the regime **(a)** $-1 \leqslant U \leqslant 1$ or the regime **(b)** $1 \leqslant U \leqslant 2$. Reproduced from Ref. [180], Copyright © 2009 The American Physical Society.

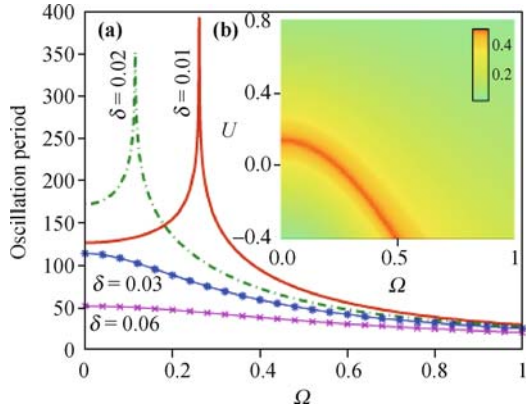

Fig. 26 Period and amplitude of oscillations of the spin-0 atoms. **(a)** Oscillation period as a function of Ω for several values of δ with $U = 0.1$. **(b)** A amplitude as a function of U and Ω for $\delta = 0.02$. Reproduced from Ref. [180], Copyright © 2009 The American Physical Society.

We note that the experiment of Hamley *et al.* [189] also hints at the possibility of the coexistence of two PA channels for the same specific PA field. For example, the mixed-spin channel $(-1, +1)$ and single-spin channel $(0, 0)$ corresponding to the s-wave collision $F = 0$ are coupled to the *same* molecular state via PA.

7.2 Laser-catalyzed atomic spin mixing

Now, we show that the interplay of two channels, the spin-dependent collisions and the optical PA, provides

a flexible tool for the control of atomic spin, including enhanced and inhibited spin oscillations, laser-induced ferromagnetic-to-antiferromagnetic transition, as well as coherent spin transfer triggered by quantum fluctuations. This method can be also extended to study, e.g., the optical control of domain formation and of spin textures in a spinor gas [190].

Figure 27 illustrates the process under consideration, the dynamics of a spin-1 atomic condensate resulting from the virtual PA of two $m_{\rm F}=0$ atoms into a molecular state, followed by dissociation into a pair of $m_{\rm F}=-1$ and $m_{\rm F}=+1$ atoms. Accounting in addition for spin-dependent collisions between atoms, this system is described by the Hamiltonian [191]

$$H = H_{\rm SM} + H_{\rm pa}$$

where $H_{\rm SM}$ denotes the spin-dependent collisions and $H_{\rm pa}$ refer to the controllable light-assisted interactions, i.e.,

$$H_{\rm pa} = \int {\rm d}\boldsymbol{r}\Big[\Delta'\hat{\psi}_m^\dagger\hat{\psi}_m + \Omega_{\rm p}(\hat{\psi}_0^{\dagger 2}\hat{\psi}_m + \hat{\psi}_m^\dagger\hat{\psi}_0^2) - \Omega_{\rm d}(\hat{\psi}_m^\dagger\hat{\psi}_+\hat{\psi}_- + \hat{\psi}_-^\dagger\hat{\psi}_+^\dagger\hat{\psi}_m)\Big] \quad (81)$$

The Rabi frequencies $\Omega_{\rm p,d}$ describe the strength of the photoassociation of $m_{\rm F}=0$ atoms and dissociation into $m_{\rm F}=\pm1$ atoms, and Δ' is the detuning between the molecular and atomic states.

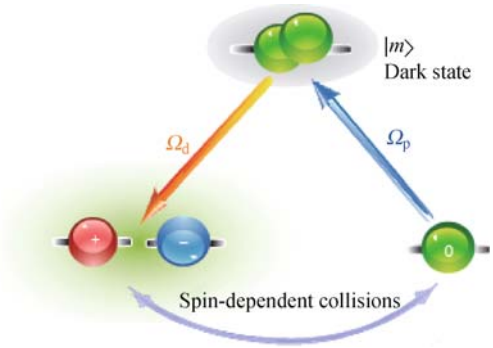

Fig. 27 Coherent two-channel spin-exchange process in a laser-controlled spin gas. In addition to the familiar collisional channel, the optical channel proceeds via the virtual PA of two $|m_{\rm F}=0\rangle$ atoms into an intermediate molecular state $|m\rangle$, which dissociates into a pair of $|m_{\rm F}=+\rangle$ and $|m_{\rm F}=-\rangle$ atoms. Reproduced from Ref. [191], Copyright © 2010 The American Physical Society.

We first consider the adiabatic off-resonant regime by assuming that Δ' is the largest parameter in the system. From $\partial\hat{\psi}_m/\Delta'\partial t \simeq 0$, we have $\hat{\psi}_m \simeq \frac{\Omega_{\rm d}\hat{\psi}_+\hat{\psi}_- - \Omega_{\rm p}\hat{\psi}_0^2}{\Delta'}$, and substitute this form into the Heisenberg equations of motion derived from the Hamiltonian [192]. It is easily seen that the resulting equations can also be derived from the effective Hamiltonian

$$\mathcal{H}_{\rm eff} = H_{\rm SM} + \int {\rm d}\boldsymbol{r}\Big[\Omega'(\hat{\psi}_+^\dagger\hat{\psi}_-^\dagger\hat{\psi}_0^2 + \hat{\psi}_0^{\dagger 2}\hat{\psi}_+\hat{\psi}_-) + \mathcal{O}\Big]$$

with

$$\Omega' = \Omega_{\rm p}\Omega_{\rm d}/\Delta', \quad \mathcal{O} = -\frac{\Omega_{\rm p}^2}{\Delta'}\hat{\psi}_0^{\dagger 2}\hat{\psi}_0^2 - \frac{\Omega_{\rm d}^2}{\Delta'}\hat{\psi}_-^\dagger\hat{\psi}_+^\dagger\hat{\psi}_+\hat{\psi}_-$$

In addition to the familiar spin-dependent collisions, spin coupling now also results from laser couplings, resulting in the two-channel spin-exchange Hamiltonian

$$\mathcal{H} = \mathcal{C}'\int {\rm d}\boldsymbol{r}(\hat{\psi}_+^\dagger(\boldsymbol{r},t)\hat{\psi}_-^\dagger(\boldsymbol{r},t)\hat{\psi}_0(\boldsymbol{r},t)\hat{\psi}_0(\boldsymbol{r},t) + h.c.)$$

Here $\mathcal{C}' = \Omega' + c_2'$ describes the combined effect of spin-dependent collisions and optical PA. Clearly, the effective spin-coupling strength $\mathcal{C}'$ can be negative or positive with suitable optical parameters, leading to significantly different spin dynamics. For convenience we introduce the scaled parameters $c_{0,2} = c_{0,2}'\int {\rm d}\boldsymbol{r}|\phi(\boldsymbol{r})|^4$, $\Omega = \Omega'\int {\rm d}\boldsymbol{r}|\phi(\boldsymbol{r})|^4$, $\Delta = \frac{\Omega_{\rm d}^2}{\Delta'}\int {\rm d}\boldsymbol{r}|\phi(\boldsymbol{r})|^4$, and $\tau = c_0 nt$, where n is the initial atomic density.

The mean-field evolution of the spin-0 atomic population n_0 is illustrated in Fig. 28 for several values of $\mathcal{C} = \Omega + c_2$ and for the initial state $(n_+,\ n_0,\ n_-) = (0.05,\ 0.9,\ 0.05)$. The specific example of atoms ^{87}Rb is considered here, with $a_0 = (101.8 \pm 2)a_{\rm B}$ and $a_2 = (100.4 \pm 1)a_{\rm B}$ [193], where $a_{\rm B}$ is the Bohr radius. In our calculations, we assume the optical detuning $\Delta' = 100\Omega_{\rm p}$ and $\Omega_{\rm d} = 10\Omega_{\rm p}$, which is reasonable for the adiabatic off-resonant case. The typical initial atomic density $n \sim 10^{14}$ cm^{-3}, corresponding to $c_0 n \sim 9700$ Hz.

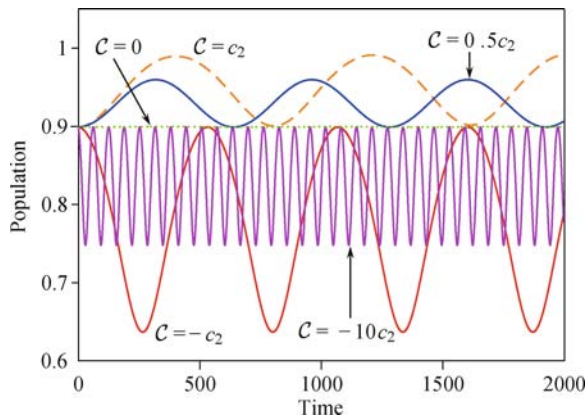

Fig. 28 Population of spin-zero atoms with (*solid lines*) or without (*dashed lines*) laser fields. Here, $n = 2\times10^{14}$ cm^{-3} [194] and the time is scaled to $\tau = c_0 nt$, corresponding to the unit 0.1 ms. Reproduced from Ref. [191], Copyright © 2010 The American Physical Society.

Significantly different regimes are reached by varying the optical detuning Δ': (i) In the collision-dominated regime $|c_2| > |\Omega|$, the population of spin-0 atoms is always *larger* than its initial value 0.9. In this perturbed regime, the spin coupling is still ferromagnetic ($\mathcal{C} < 0$); (ii) For $\mathcal{C} = 0$, i.e., $\Omega = -c_2$ (for $\Delta' > 0$) the two channels interfere destructively, leading to frozen or inhibited spin mixing; (iii) The sign of $\mathcal{C}$ can be reversed by tuning the laser fields, resulting in an effective antiferromagnetic regime $\mathcal{C} > 0$ [101].

By expressing the c-number amplitudes a_i in terms of

real amplitudes and phases, i.e., $a_{\pm,0} = \sqrt{n_{\pm,0}}\mathrm{e}^{-\mathrm{i}\theta_{\pm,0}}$, the energy functional of this system can be derived as:

$$\mathcal{E} = q(1-n_0) + \mathcal{C}\sqrt{(1-n_0)^2 - m^2}\cos\theta + c_2 n_0(1-n_0) + \frac{\Delta}{4}n_0(2-n_0) - \frac{\Omega^2}{\Delta}n_0^2 \quad (82)$$

where q denotes the quadratic Zeeman effect, $\theta = \theta_+ + \theta_- - 2\theta_0$ is the relative phase of the spin components and $m = n_+ - n_-$ is the atomic magnetization. Figure 29 plots equal-energy contours in the phase space (θ, n_0), for several values of $\mathcal{C}$ for $m = 0$, and $q = 0.01$ corresponding to the fixed magnetic field about 460 mG.

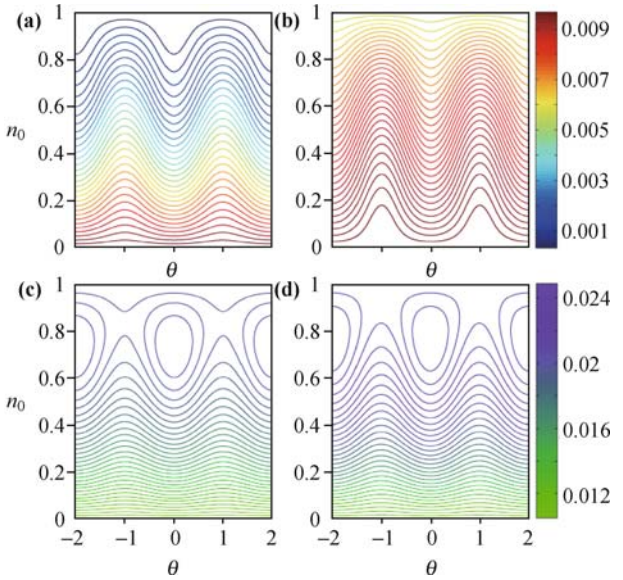

Fig. 29 Equal energy contours of $\mathcal{E}$ without **(a)** ($\mathcal{C} = c_2$) and with **(b)** ($\mathcal{C} = 0.5c_2$), **(c)** ($\mathcal{C} = -0.5c_2$), and **(d)** ($\mathcal{C} = -c_2$) optically-controlled process for $q = 0.01$ and $m = 0$. Reproduced from Ref. [191], Copyright © 2010 The American Physical Society.

Figure 30 also shows the two-photon resonant control of atomic spinor dynamics for $\Omega'_{\mathrm{p}} = \Omega_{\mathrm{p}}/(c_0\sqrt{n}) = 1$ (corresponding to 9700 Hz) and

$$\Omega'_{\mathrm{d}}(t) = \Omega_{\mathrm{d}}/(c_0\sqrt{n}) = \Omega'_{\mathrm{d},0}\mathrm{sech}(t/t_0) \quad (83)$$

with $\Omega'_{\mathrm{d},0} = 40$, $t_0 = 20$. In contrast to the off-resonant

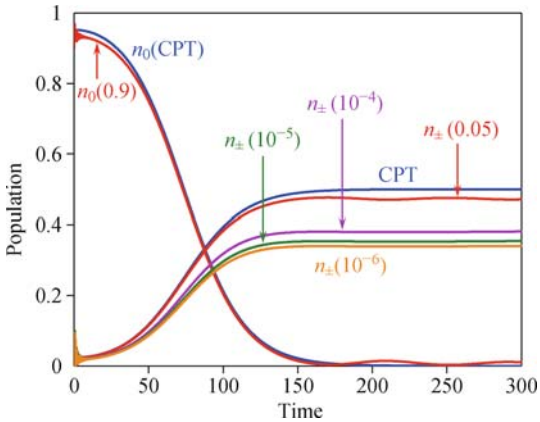

Fig. 30 Atomic populations in the resonant regime for ^{87}Rb, with detuning $\delta = \delta'/c_0 n = 3$ and $\gamma = 1$. Reproduced from Ref. [191], Copyright © 2010 The American Physical Society.

spin oscillations, we have now a full transfer of the population from the initial state, say $|m_{\mathrm{F}} = 0\rangle$ to coherent superposition of $|m_{\mathrm{F}} = \pm 1\rangle$ hyperfine states.

7.3 Creation of spinor molecules

In this section, we show a new regime of coherent reactive spin oscillations (RSO) or perhaps atom-molecule spin super-mixing. To set the stage, we first assume that the condensed atoms are initially prepared in the spin-0 state $|1, 0\rangle$ [125]. The spin-($\pm$) atomic pair is created via spin-exchanged collisions, i.e., $2\mathrm{A}_0 \to \mathrm{A}_\downarrow + \mathrm{A}_\uparrow$ [189]. With the PA lights, the spin-($-$) atom can be associated with another spin-0 atom into the molecular excited state $|m\rangle$, which is then dumped into the ground state $|g\rangle$ by a coupling light, i.e., $\mathrm{A}_0 + \mathrm{A}_\downarrow \to \mathrm{A}_0\mathrm{A}_\downarrow$ [125]. This *chain reaction* leads to

$$3\mathrm{A}_0 \to \mathrm{A}_0\mathrm{A}_\downarrow + \mathrm{A}_\uparrow$$

indicating a spin-dependent three-body recombination or an atom-dimer pair formation from three spin-0 atoms.

By eliminating the intermediate state $|m\rangle$ [192], we obtain the equations of motion of the system

$$\begin{aligned}
\mathrm{i}\frac{\mathrm{d}\hat{a}_+}{\mathrm{d}\tau} &= \chi_2(\rho_+ + \rho_0 - \rho_-)\hat{a}_+ + \chi_2\hat{a}_0^2\hat{a}_-^\dagger \\
\mathrm{i}\frac{\mathrm{d}\hat{a}_0}{\mathrm{d}\tau} &= \chi_2(\rho_+ + \rho_-)\hat{a}_0 - \Omega\rho_-\hat{a}_0 + 2\chi_2\hat{a}_+\hat{a}_-\hat{a}_0^\dagger + \Omega\hat{g}\hat{a}_-^\dagger \\
\mathrm{i}\frac{\mathrm{d}\hat{a}_-}{\mathrm{d}\tau} &= -\Gamma\hat{a}_- + \chi_2\hat{a}_0^2\hat{a}_+^\dagger + \Omega\hat{g}\hat{a}_0^\dagger \\
\mathrm{i}\frac{\mathrm{d}\hat{g}}{\mathrm{d}\tau} &= \Omega\hat{a}_0\hat{a}_- + (\Delta + \delta - \delta')\hat{g}
\end{aligned} \quad (84)$$

where $\Omega = \frac{\Omega_1\Omega_2}{c_0 N\delta}$, $\Gamma = \omega\rho_0 - \chi_2(\rho_- + \rho_0 - \rho_+)$, $\Omega = \frac{\omega_1^2}{c_0 N\delta}$, $\tau = c_0 N t$, $\chi_2 = c_2/c_0$, and

$$\delta' = \frac{\Omega_2^2}{c_0 N\delta}\left(1 + \frac{\mathrm{i}\gamma}{2\delta}\right)$$

Figure 31(a) shows the far-off resonance case for atom-molecule pair formation from the initially prepared spin-0 atoms, with the mean-field replacement $\hat{a}_i,\ \hat{g} \to \sqrt{\rho_{i,g}}$. The resulting atom-molecule oscillations, which we term as RSO or spin super-mixing, can be controlled by the laser fields.

In order to observe coherent RSO, the PA strength should be chosen in a suitable regime to allow a competitive process between the spin-exchanged collisions and the atom-molecule conversion. In this regime, the population of spin-down atoms are kept essentially zero at all times. In fact, with the initial atomic state $f = [0, 1, 0]$, the populations of spin-down atoms can be kept as zero under the condition $\Omega = -\chi_2\sqrt{\rho_0}$. Figure 3(b) shows that, with this generalized STIRAP technique, the atom-molecule pair can be produced efficiently, corresponding to a high conversion rate $\eta = \rho_+ + 2\rho_g \approx 99\%$ in Fig. 31(b). Here, the state $|1, -1\rangle$ can be viewed as

an atomic spin dark state, which guarantees quantum pair creation of atoms and molecules ($\rho_+ = \rho_g$). Note that the light strength should be chosen as $\Omega \leqslant |\chi_2|$, or $\Omega_1\Omega_2 \leqslant |N\delta c_2|$, which yields $\Omega_1 \leqslant 0.3\pi$ MHz, and $\Omega_2 \leqslant 0.6\pi$ MHz.

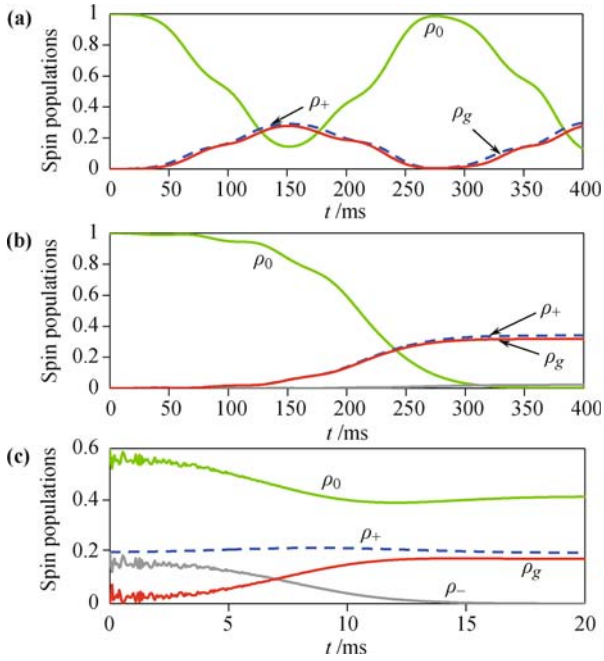

Fig. 31 Spin populations as function of time for the spinor gas of ^{87}Rb. **(a)** Coherent RSO, and **(b)** spinor molecules conversion under dark-state conditions with $\delta = -100\chi_2$, $\Omega = 0.75|\chi_2|$, and the initial atomic state $f = [0, 1, 0]$. **(c)** PA-dominated atom-molecule conversion, in order to simulate the experimental results of Ref. [125], the initial atomic state is taken as $f = [\sqrt{0.2}, \sqrt{0.6}, \sqrt{0.2}]$. $\Omega = \Omega_{\rm m}{\rm sech}(t/4)$ where $\Omega_{\rm m}$ is the maximal PA strength in the experiment [125], with $|\frac{\Omega_{\rm m}}{\chi_2}| = 1.44 \times 10^4$. The other parameters are $\chi_2 = -0.01$, $\gamma = 10|\chi_2|$, and $c_0 N = 10^5 {\rm s}^{-1}$.

With this condition, the first derivatives of the slowly varying amplitudes for spin-down atoms can be neglected, i.e., $\mathrm{i}\dot{\hat{a}}_- \approx 0$ [195–197]. Then we obtain an effective interacting Hamiltonian

$$\hat{\mathcal{H}}_{\rm eff} = \chi_3(\hat{a}_0^{\dagger 3}\hat{a}_+\hat{a}_g + \hat{a}_0^3\hat{a}_+^\dagger a_g^\dagger)$$

with $\chi_3 = \Omega\chi_2/\Gamma$, indicating a laser-induced three-body spin-dependent recombination [12, 13, 195, 196].

We note that very recently Kobayashi *et al.* [125] studied the two-color PA of the spinor atoms ^{87}Rb and observed the molecular creation in the state $|2, -1\rangle$ through spin-selective measurement (by associating two reactant atoms in the state $|1, -1\rangle$ and $|1, 0\rangle$). In particular, only the populations of reactant atoms decreased and the other component $|1, 1\rangle$ remains almost unchanged [125], which is confirmed by our numerical calculations Fig. 31(c). Their experiment had two PA lights with the maximal power $I_1 = 10$ W, $I_2 = 20$ W and $\delta = 2\pi \times 300$ MHz. For the typical situations [91, 182, 198] $\Omega/\sqrt{I} = 7$ MHz$({\rm W}\cdot{\rm cm}^{-2})^{1/2}$, this yields $\Omega_1 = 139$ MHz, $\Omega_2 = 197$ MHz, which is well beyond the RSO regime.

Within the standard MFA, the spatial wave function can be also written as $\sqrt{N}\mathrm{e}^{-\mathrm{i}\mu t/\hbar}\zeta$, where $\zeta = (\sqrt{\rho_i}\mathrm{e}^{\mathrm{i}\theta_i}, \sqrt{\rho_g}\mathrm{e}^{\mathrm{i}\theta_g})$ and θ_i represents the phase of the i-th Zeeman state [199]. Then the spin-dependent three-body recombination can be described by a nonrigid pendulum model with the energy functional $\mathcal{E}$. In contrast to the atomic spinor gas [200, 201], it is possible to observe the dynamical instability or the domain structures for even anti-ferromagnetic RSO system. In order to see this, we consider an off-equilibrium state oscillation by changing the external magnetic field from nonzero to zero values [200]. The condensate size is assumed to be much larger than the healing length $\mathcal{L}_s = 2\pi\hbar/\sqrt{2m|c_2'|n}$ at least in one direction so that the instability-induced domains can appear. Then we calculate the criterion

$$\frac{{\rm d}\mathcal{E}}{{\rm d}m} = \frac{3\chi_3}{2}m\left[1 - \frac{\rho_0^{3/2}\cos\theta}{\sqrt{(1-\rho_0)^2 - m^2}}\right] + \chi_2\rho_0 + \frac{3\rho_0}{2\Gamma}(\chi_2^2\rho_0 - \Omega^2) \tag{86}$$

where $\theta = 3\theta_0 - (\theta_+ + \theta_g)$ and $m = \rho_+ - \rho_- - \rho_g$.

Figure 32 shows the surfaces of ${\rm d}\mathcal{E}/{\rm d}m = 0$ for ferromagnetic and anti-ferromagnetic cases. We note that for the purely atomic ensemble ($\chi_2 < 0$, $\theta = 0$), there is a wide dynamically unstable region (see Ref. [200]). In contrast, for our system, this region can be significantly reduced [$\chi_3 < 0$ in Fig. 32(a)] by tuning the lasers. Even the essentially different feature can be seen for the anti-ferromagnetic case since no dynamical instability can exist for the purely atomic gas ($\chi_2 > 0$, $\theta = \pi$), but for our RSO regime, we obtain the similar instability behavior for $\chi_3 < 0$ [see Fig. 32(b)]. Clearly, the dynamical stability is now determined by χ_3 instead of χ_2.

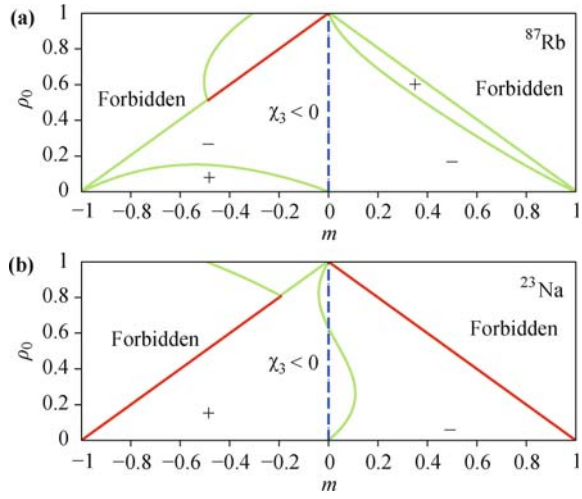

Fig. 32 Surfaces of ${\rm d}\mathcal{E}/{\rm d}m = 0$ (*green solid lines*) for **(a)** the atoms ^{87}Rb, with $\theta = 0$, $\chi_2 = -0.01$; and **(b)** the atoms ^{23}Na atoms, with $\theta = \pi$, $\chi_2 = 0.01$. The plus or minus sign denotes ${\rm d}\mathcal{E}/{\rm d}m > 0$ or ${\rm d}\mathcal{E}/{\rm d}m < 0$. Here, we take $\delta = 100|\chi_2|$.

Finally, we emphasize that the initial magnetization m also can greatly affect the spinor reaction. In fact, as Fig. 33 shows, with the CPT condition

$$\Omega(t) = -\chi_2\sqrt{\frac{\rho_0\rho_+}{\rho_g}}$$

for $m \geqslant 0$, the ground-state molecules can be produced efficiently with the conversion value $\rho_g = (1-m)/3$. However, for $m < 0$, all spin components evolve into irregular oscillations. Clearly, both the PA light and the atomic magnetization have essential impacts on creating spinor molecules.

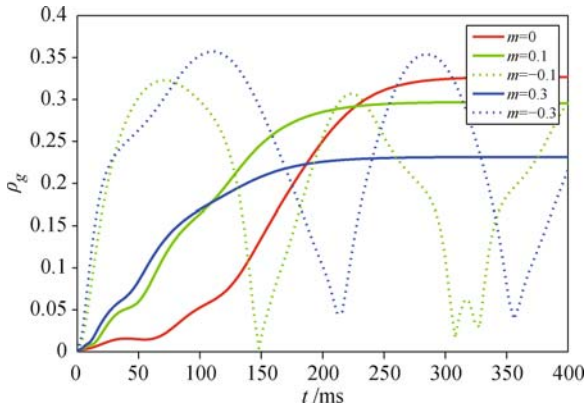

Fig. 33 Populations of spinor molecules with different values of m, with $\chi_2 = -0.01$ and $\delta = 100|\chi_2|$.

8 Conclusions

In summary, superchemistry or degenerate matter-wave reaction is going through extraordinary developments as a fascinating new research field in the quantum control of colds atoms and molecules. In the past few years, superchemistry has been extended from the simplest atom–dimer conversion to coherent assembly and manipulations of complex molecules, to the bimolecular or multi-molecular conversion [19, 20, 107] (abstraction reaction), and to completely new kinds of reactions involving inherent quantum spin degrees of freedom. Many purely quantum effects have been identified in tunneling-dominated reaction of de Broglie waves, such as finite-number effect, quantum confinement effect [106], interference or super-selectivity of different reaction channels [104], vacuum-noise effect in triggering cold reaction [107], optical enhancement or destruction of spin mixing [191], and cavity-assisted molecular amplification [202]. This has also led to some fascinating practical applications in, e.g., quantum information storage.

These pioneering works, together with rapid advances of current experimental techniques in making and probing cold molecules, indicate that quantum superchemistry is still in its golden age with encouraging developments in both theoretical and experimental aspects. In fact, more surprising discoveries are highly expected to be coming in the near future, e.g., optomechanics driven by PA light [203], synthesis of chiral molecules [204], gauge potential in atom–molecule conversion [80], and quantum reactive control of cold plasmas [205].

Acknowledgements This work was supported in part by the National Natural Science Foundation of China (Grant Nos. 10974045 and 10874041), the Program for New Century Excellent Talents in University (NCET) from the Ministry of Education, and the Talented-Youth Project in Henan Province.

References

1. V. Letokhov, Laser Control of Atoms and Molecules, Oxford: Oxford University Press, 2007
2. M. H. Anderson, J. R. Ensher, M. R. Matthews, C. E. Wieman, and E. A. Cornell, Science, 1995, 269: 198
3. C. C. Bradley, C. A. Sackett, J. J. Tollett, and R. G. Hulet, Phys. Rev. Lett., 1995, 75: 1687
4. K. B. Davis, M.-O. Mewes, M. R. Andrews, N. J. van Druten, D. S. Durfee, D. M. Kurn, and W. Ketterle, Phys. Rev. Lett., 1995, 75: 3969
5. P. Meystre, Atom Optics, Berlin: Springer-Verlag, 2001
6. D. J. Heinzen and R. Wynar, Phys. Rev. Lett., 2000, 84: 5029
7. S. Inouye, M. R. Andrews, J. Stenger, H. J. Miesner, D. M. Stamper-Kern, and W. Ketterle, Nature, 1998, 392: 151
8. C. Chin, Rudolf Grimm, P. Julienne, and E. Tiesinga, Rev. Mod. Phys., 2010, 82: 1225
9. P. D. Lett, K. Helmerson, W. D. Phillips, L. P. Ratliff, S. L. Rolston, and M. E. Wagshul, Phys. Rev. Lett., 1993, 71: 2200
10. G. Modugno, Science, 2009, 326: 1640
11. M. Mackie, O. Dannenberg, J. Piilo, K.-A. Suominen, and J. Javanainen, Phys. Rev. A, 2004, 69: 053614
12. B. Borca, J. W. Dunn, V. Kokoouline, and C. H. Greene, Phys. Rev. Lett., 2003, 91: 070404
13. C. P. Search, W. P. Zhang, and P. Meystre, Phys. Rev. Lett., 2004, 92: 140401
14. J. H. Huckans, J. R. Williams, E. L. Hazlett, R.W. Stites, and K. M. O'Hara, Phys. Rev. Lett., 2009, 102: 165302
15. K. V. Kheruntsyan, Phys. Rev. Lett., 2006, 96: 110401
16. V. Efimov, Phys. Lett., 1970, 33B: 563
17. V. Efimov, Sov. J. Nucl., Phys., 1971, 12: 589
18. T. Kraemer, M. Mark, P. Waldburger, J. G. Danzl, C. Chin, B. Engeser, A. D. Lange, K. Pilch, A. Jaakkola, H.-C. Nägerl, and R. Grimm, Nature, 2006, 440: 315
19. S. Knoop, F. Ferlaino, M. Berninger, M. Mark, H.-C. Nägerl, R. Grimm, J. P. D'Incao, and B. D. Esry, Phys. Rev. Lett., 2010, 104: 053201
20. S. Ospelkaus, K.-K. Ni, D.Wang, M. H. G. de Miranda, B. Neyenhuis, G. Quéméner, P. S. Julienne, J. L. Bohn, D. S. Jin, and J. Ye, Science, 2010, 327: 853
21. K. E. Strecker, G. B. Partridge, and R. G. Hulet, Phys. Rev. Lett., 2003, 91: 080406
22. J. Cubizolles, T. Bourdel, S. J. J. M. F. Kokkelmans, G. V. Shlyapnikov, and C. Salomon, Phys. Rev. Lett., 2003, 91: 240401
23. S. Jochim, M. Bartenstein, A. Altmeyer, G. Hendl, C. Chin, J. Hecker Denschlag, and R. Grimm, Phys. Rev. Lett.,

2003, 91: 240402
24. T. Bourdel, L. Khaykovich, J. Cubizolles, J. Zhang, F. Chevy, M. Teichmann, L. Tarruell, S. J. J. M. F. Kokkelmans, and C. Salomon, Phys. Rev. Lett., 2004, 93: 050401
25. M. W. Zwierlein, C. A. Stan, C. H. Schunck, S. M. F. Raupach, S. Gupta, Z. Hadzibabic, and W. Ketterle, Phys. Rev. Lett., 2003, 91: 250401
26. X. Li, G. A. Parker, P. Brumer, I. Thanopulos, and M. Shapiro, Phys. Rev. Lett., 2008, 101: 043003
27. J. Colgan and M. S. Pindzola, Phys. Rev. Lett., 2002, 88: 173002
28. K. Xu, T. Mukaiyama, J. R. Abo-Shaeer, J. K. Chin, D. E. Miller, and W. Ketterle, Phys. Rev. Lett., 2003, 91: 210402
29. C. A. Regal, M. Greiner, and D. S. Jin, Phys. Rev. Lett., 2004, 92: 083201
30. C. A. Regal, C. Ticknor, J. L. Bohn, and D. S. Jin, Nature, 2003, 424: 47
31. S. T. Thompson, E. Hodby, and C. E. Wieman, Phys. Rev. Lett., 2005, 95: 190404
32. E. A. Donley, N. R. Claussen, S. T. Thompson, and C. E. Wieman, Nature, 2002, 417: 529
33. C. P. Koch, F. M.-Seeuws, and R. Kosloff, Phys. Rev. Lett., 2005, 94: 193001
34. S. Dürr, T. Volz, A. Marte, and G. Rempe, Phys. Rev. Lett., 2004, 92: 020406
35. R. Wynar, R. S. Freeland, D. J. Han, C. Ryu, and D. J. Heinzen, Science, 2000, 287: 1016
36. F. Lang, K. Winkler, C. Strauss, R. Grimm, and J. H. Denschlag, Phys. Rev. Lett., 2008, 101: 133005
37. N. Syassen, T. Volz, S. Teichmann, S. Dürr, and G. Rempe, Phys. Rev. A, 2006, 74: 062706
38. J. Herbig, T. Kraemer, M. Mark, T. Weber, C. Chin, H.-C. Nägerl, and R. Grimm, Science, 2003, 301: 1510
39. M. Viteau, A. Chotia, M. Allegrini, N. Bouloufa, O. Dulieu, D. Comparat, and P. Pillet, Science, 2008, 321: 232
40. J. G. Danzl, E. Haller, M. Gustavsson, M. J. Mark, R. Hart, N. Bouloufa, O. Dulieu, H. Ritsch, and H.-C. Nägerl, Science, 2008, 321: 1062
41. A. Fioretti, D. Comparat, A. Crubellier, O. Dulieu, F. Masnou-Seeuws, and P. Pillet, Phys. Rev. Lett., 1998, 80: 4402
42. A. G. Truscott, K. E. Strecker, W. I. McAlexander, G. B. Partridge, and R. G. Hulet, Science, 2001, 291: 2570
43. F. Schreck, G. Ferrari, K. L. Corwin, J. Cubizolles, L. Khaykovich, M.-O. Mewes, and C. Salomon, Phys. Rev. A, 64: 011402(R)
44. C. A. Stan, M. W. Zwierlein, C. H. Schunck, S. M. F. Raupach, and W. Ketterle, Phys. Rev. Lett., 2004, 93: 143001
45. Z. Hadzibabic, C. A. Stan, K. Dieckmann, S. Gupta, M. W. Zwierlein, A. Görlitz, and W. Ketterle, Phys. Rev. Lett., 2002, 88: 160401
46. E. Wille, F. M. Spiegelhalder, G. Kerner, D. Naik, A. Trenkwalder, G. Hendl, F. Schreck, R. Grimm, T. G. Tiecke, J. T. M. Walraven, S. J. J. M. F. Kokkelmans, E. Tiesinga, and P. S. Julienne, Phys. Rev. Lett., 2008, 100: 053201
47. C. Silber, S. G ü nther, C. Marzok, B. Deh, Ph. W. Courteille, and C. Zimmermann, Phys. Rev. Lett., 2005, 95: 170408
48. B. Deh, C. Marzok, C. Zimmermann, and Ph. W. Courteille, Phys. Rev. A, 2008, 77: 010701(R)
49. C. Marzok, B. Deh, Ph. W. Courteille, and C. Zimmermann, Phys. Rev. A, 2007, 76: 052704
50. J. Deiglmayr, A. Grochola, M. Repp, K. Mörtlbauer, C. Glück, J. Lange, O. Dulieu, R. Wester, and M. Weidemüller, Phys. Rev. Lett., 2008, 101: 133004
51. C. Haimberger, J. Kleinert, M. Bhattacharya, and N. P. Bigelow, Phys. Rev. A, 2004, 70: 021402(R)
52. M. W. Mancini, G. D. Telles, A. R. L. Caires, V. S. Bagnato, and L. G. Marcassa, Phys. Rev. Lett., 2004, 92: 133203
53. S. Inouye, J. Goldwin, M. L. Olsen, C. Ticknor, J. L. Bohn, and D. S. Jin, Phys. Rev. Lett., 2004, 93: 183201
54. F. Ferlaino, C. D'Errico, G. Roati, M. Zaccanti, M. Inguscio, and G. Modugno, and A. Simoni, Phys. Rev. A, 2006, 73: 040702(R)
55. G. Roati, F. Riboli, G. Modugno, and M. Inguscio, Phys. Rev. Lett., 2002, 89: 150403
56. C. Klempt, T. Henninger, O. Topic, J. Will, W. Ertmer, E. Tiemann, and J. Arlt, Phys. Rev. A, 2007, 76: 020701(R)
57. C. Ospelkaus, S. Ospelkaus, K. Sengstock, and K. Bongs, Phys. Rev. Lett., 2006, 96: 020401
58. C. Ospelkaus, S. Ospelkaus, L. Humbert, P. Ernst, K. Sengstock, and K. Bongs, Phys. Rev. Lett., 2006, 97: 120402
59. F. Deuretzbacher, K. Plassmeier, D. Pfannkuche, F. Werner, C. Ospelkaus, S. Ospelkaus, K. Sengstock, and K. Bongs, Phys. Rev. A, 2008, 77: 032726
60. J. J. Zirbel, K.-K. Ni, S. Ospelkaus, T. L. Nicholson, M. L. Olsen, P. S. Julienne, C. E. Wieman, J. Ye, and D. S. Jin, Phys. Rev. A, 2008, 78: 013416
61. K.-K. Ni, S. Ospelkaus, M. H. G. de Miranda, A. Pe'er, B. Neyenhuis, J. J. Zirbel, S. Kotochigova, P. S. Julienne, D. S. Jin, and J. Ye, Science, 2008, 322: 231
62. I.Bloch, M. Greiner, O. Mandel, T. W. Hänsch, and T. Esslinger, Phys. Rev. A, 2001, 64: 021402(R)
63. A. J. Kerman, J. M. Sage, S. Sainis, T. Bergeman, and D. DeMille, Phys. Rev. Lett., 2004, 92: 033004
64. J. M. Sage, S. Sainis, T. Bergeman, and D. DeMille, Phys. Rev. Lett., 2005, 94: 203001
65. A. J. Kerman , J. M. Sage, S. Sainis, T. Bergeman, and D. DeMille, Phys. Rev. Lett., 2004, 92: 153001
66. E. R. Hudson, N. B. Gilfoy, S. Kotochigova, J. M. Sage, and D. DeMille, Phys. Rev. Lett., 2008, 100: 203201
67. S. J. J. M. FKokkelmans, H. M. J. Vissers, and B. J. Verhaar, Phys. Rev. A, 2001, 63: 031601
68. M. Mackie, Phys. Rev. A, 2002, 66: 043613
69. K. Bergmann, H. Theuer, and B. Shore, Rev. Mod. Phys., 1998, 70: 1003
70. N. V. Vitanov, T. Halfmann, B. W. Shore, and K. Bergmann, Annu. Rev. Phys. Chem., 2001, 52: 763
71. M. Mackie and J. Javanainen, Phys. Rev. A, 1999, 60: 3174
72. M. Mackie, R. Kowalski, and J. Javanainen, Phys. Rev. Lett., 2000, 84: 3803
73. C. Zhao, X. Zou, H. Pu, and G. C. Guo, Phys. Rev. Lett., 2008, 101: 010401

74. T. B. Ottenstein, T. Lompe, M. Kohnen, A. N. Wenz, and S. Jochim, Phys. Rev. Lett., 2008, 101: 203202
75. Ákos Rapp, G. Zaránd, C. Honerkamp, and W. Hofstetter, Phys. Rev. Lett., 2007, 98: 160405
76. I. Bloch, Science, 2008, 319: 1202
77. H. Jing, J. Cheng, and P. Meystre, Phys. Rev. Lett., 2007, 99: 133002
78. H. Jing, J. Cheng, and P. Meystre, Phys. Rev. A, 2008, 77: 043614
79. H. Jing. Y. Jiang, W. Zhang, and P. Meystre, New J. Phys., 2008, 10: 123005
80. M. Taglieber, A.-C. Voigt, T. Aoki, T. W. Hänsch, and K. Dieckmann, Phys. Rev. Lett., 2008, 100: 010401
81. C. Chin, T. Kraemer, M. Mark, J. Herbig, P. Waldburger, H. C. Nagerl, and R. Grimm, Phys. Rev. Lett., 2005, 94: 123201
82. S. B. Papp and C. E. Wieman, Phys. Rev. Lett., 2006, 97: 180404
83. M. T. Cvitaŝ P. Soldan, J. M. Hutson, P. Honvault, and J. M. Launey, Phys. Rev. Lett., 2005, 94: 200402
84. C. P. Search and P. Meystre, Phys. Rev. Lett., 2004, 93: 140405
85. F. Zhou and G. W. Semenoff, Phys. Rev. Lett., 2006, 97: 180411
86. D. Blume, B. D. Esry, C. H. Greene, N. N. Klausen, and G. J. Hanna, Phys. Rev. Lett., 2002, 89: 163402
87. H.-Y. Ling, H. Pu, and B. Seaman, Phys. Rev. Lett., 2004, 93: 250403
88. H. Pu, P. Maenner, W. Zhang, and H.-Y. Ling, Phys. Rev. Lett., 2007, 98: 050406
89. H. Jing, F. Zheng, Y. Jiang, and Z. Geng, Phys. Rev. A, 2008, 78: 033617
90. H.-Y. Ling, P. Maenner, W. Zhang, and H. Pu, Phys. Rev. A, 2007, 75: 033615
91. K. Winkler, G. Thalhammer, M. Theis, H. Ritsch, R. Grimm, and J. H. Denschlag, Phys. Rev. Lett., 2005, 95: 063202
92. R. Dumke, J. D. Weinstein, M. Johanning, K. M. Jones, and P. D. Lett, Phys. Rev. A, 2005, 72: 041801(R)
93. T. Mukaiyama, J. R. Abo-Shaeer, K. Xu, J. K. Chin, and W. Ketterle, Phys. Rev. Lett., 2004, 92: 180402
94. S. Dürr, S. T. Volz, and G. Rempe, Phys. Rev. A, 2004, 70: 031601(R)
95. U. V. Poulsen and K. Mømer, Phys. Rev. A, 2001, 63: 023604
96. K. V. Kheruntsyan and P. D. Drummond, Phys. Rev. A, 2002, 66: 031602(R)
97. K. V. Kheruntsyan, Phys. Rev. A, 2005, 71: 053609
98. V. A. Yurovsky and A. Ben-Reuven, Phys. Rev. A, 2003, 67: 043611
99. K. V. Kheruntsyan, M. K. Olsen, and P. D. Drummond, Phys. Rev. Lett., 2005, 95: 150405
100. A. Pekalski and J. Przystawa, Modern Trends in the Theory of Condensed Matter, Berlin: Springer-Verlag, 1980
101. S. Yi, L. You, and H. Pu, Phys. Rev. Lett., 2004, 93: 040403
102. M. W. Zwierlein, C. A. Stan, C. H. Schunck, S. M. F. Raupach, A. J. Kerman, and W. Ketterle, Phys. Rev. Lett., 2004, 92: 120403
103. M. Greiner, C. A. Regal, J. T. Stewart, and D. S. Jin, Phys. Rev. Lett., 2005, 94: 110401
104. M. G. Moore and A. Vardi, Phys. Rev. Lett., 2002, 88: 160402
105. A. Vardi and M. G. Moore, Phys. Rev. Lett., 2002, 89: 090403
106. I. Tikhonenkov and A. Vardi, Phys. Rev. Lett., 2007, 98: 080403
107. H. Jing, J. Cheng, and P. Meystre, Phys. Rev. Lett., 2008, 101: 073603
108. H. Jing, J. Cheng, and P. Meystre, Phys. Rev. A, 2009, 79: 023622
109. E. Bodo, F. A. Gianturco, N. Balakrishnan, and A. Dalgarno, J. Phys. B, 2004, 37: 3641
110. L. Che, Z. F. Ren, X. G. Wang, W. R. Dong, D. X. Dai, X. Y. Wang, D. H. Zhang, X. M. Yang, L. S. Sheng, G. L. Li, H. J. Werner, F. Lique, and M. H. Alexander, Science, 2007, 317: 1061
111. M. Shapiro and P. Brumer, Principles of the Quantum Control of Molecular Processes, New York: Wiley, 2003
112. M. Shapiro and P. Brumer, Phys. Rev. Lett., 1996, 77: 2574
113. C. A. Arango, M. Shapiro, and P. Brumer, Phys. Rev. Lett., 2006, 97: 193202
114. T. Köhler, K. Góral, and P. S. Julienne, Rev. Mod. Phys., 2006, 78: 1311
115. K. M. Jones, E. Tiesinga, P. D. Lett, and P. S. Julienne, Rev. Mod. Phys., 2006, 78: 483
116. P. Meystre and M. Sargent, Elements of Quantum Optics, Berlin: Springer-Verlag, 2007
117. M. G. Moore and P. Meystre, Phys. Rev. Lett., 1999, 83: 5202
118. H. Uys and P. Meystre, Phys. Rev. A, 2007, 75: 033805
119. J. J. Hope and M. K. Olsen, Phys. Rev. Lett., 2001, 86: 3220
120. T. L. Ho, Phys. Rev. Lett., 1998, 81: 742
121. C. K. Law, H. Pu, and N. P. Bigelow, Phys. Rev. Lett., 1998, 81: 5257
122. W. Zhang, D. L. Zhou, M.-S. Chang, M. S. Chapman, and L. You, Phys. Rev. A, 2005, 72: 013602
123. A. T. Black, E. Gomez, L. D. Turner, S. Jung, and P. D. Lett, Phys. Rev. Lett., 2007, 99: 070403
124. Y. Liu, S. Jung, S. E. Maxwell, L. D. Turner, E. Tiesinga, and P. D. Lett, Phys. Rev. Lett., 2009, 102: 125301
125. J. Kobayashi, Y. Izumi, K. Enomoto, M. Kumakura, and Y. Takahashi, Appl. Phys. B, 2009, 95: 37
126. D. Meiser and P. Meystre, Phys. Rev. Lett., 2005, 94: 093001
127. H. Jing and S. Cui, Phys. Rev. A, 2010, 82: 025601
128. L. Zhou, W. Zhang, H. Y. Ling, L. Jiang, and H. Pu, Phys. Rev. A, 2007, 75: 043603
129. S.-Y. Meng, L.-B. Fu, J. Chen, and J. Liu , Phys. Rev. A, 2009, 79: 063415
130. S.-Y. Meng, L.-B. Fu, and J. Liu, Phys. Rev. A, 2008, 78, 053410

131. P. Soldán, M. T. Cvitaš, and J. M. Hutson, P. Honvault, and J.-M. Launay, Phys. Rev. Lett., 2002, 89: 153201
132. F. D. Colavecchia, J. P. Burke, W. J. Stevens, M. R. Salazar, G. A. Parker, and R. T. Pack, J. Chem. Phys., 2003, 118: 5484
133. G. Modugno, M. Modugno, F. Riboli, G. Roati, and M. Inguscio, Phys. Rev. Lett., 2002, 89: 190404
134. H. Xiong, S. Liu, W. Zhang, and M. Zhan, Phys. Rev. Lett., 2005, 95: 120401
135. B. L. Grigorenko, A. V. Nemukhin and V. A. Apkarian, Chem. Phys., 1997, 219: 161
136. O. Dannenberg, M. Mackie, and K.-A. Suominen, Phys. Rev. Lett., 2003, 91: 210404
137. L.-H. Lu and Y.-Q. Li, Phys. Rev. A, 2007, 76: 053608
138. A. S. Parkins and D. F. Walls, Phys. Rep., 1998, 303: 1
139. M. Salerno, Phys. Rev. A, 2005, 72: 063602
140. P. Capuzzi, A. Minguzzi, and M. P. Tosi, Phys. Rev. A, 2003, 67: 053605
141. S. K. Adhikari, Phys. Rev. A, 2004, 70: 043617
142. M. W. Zwierlein, A. Schirotzek, C. H. Schunck, and W. Ketterle, Science, 2006, 311: 492
143. H. Jing and Y. Jiang, Phys. Rev. A, 2008, 77: 065601
144. M. Mackie, K. A. Suominen, and J. Javanainen, Phys. Rev. Lett., 2002, 89: 180403
145. J. Javanainen and M. Mackie, Phys. Rev. Lett., 2002, 88: 090403
146. Y. Shi and Q. Niu, Phys. Rev. Lett., 2006, 96: 140401
147. W. Zhang, C. P. Search, H. Pu, P. Meystre, and E. M. Wright, Phys. Rev. Lett., 2003, 90: 140401
148. M. G. Moore and P. Meystre, Phys. Rev. Lett., 2001, 86: 4199
149. L.-B. Fu and J. Liu, Ann. Phys., 2010, 325: 2425
150. L.-B. Fu, D.-F. Ye, C. Lee, W. Zhang, and J. Liu, Phys. Rev. A, 2009, 80: 013619
151. J. P. Blaizot and G. Ripka, Quantum Theory of Finite Systems, Cambridge: MIT Press, 1986
152. K. Winkler, F. Lang, G. Thalhammer, P. V. D. Straten, R. Grimm, and J. H. Denschlag, Phys. Rev. Lett., 2007, 98: 043201
153. G. Thalhammer, K. Winkler, F. Lang, S. Schmid, R. Grimm, and J. Hecker Denschlag, Phys. Rev. Lett., 2006, 96: 050402
154. M. Junker, D. Dries, C. Welford, J. Hitchcock, Y. P. Chen, and R. G. Hulet, Phys. Rev. Lett., 2008, 101: 060406
155. S. Watabe and T. Nikuni, Phys. Rev. A, 2008, 77: 013616
156. D. Wang, J. Qi, M. F. Stone, O. Nikolayeva, H. Wang, B. Hattaway, S. D. Gensemer, P. L. Gould, E. E. Eyler, and W. C. Stwalley, Phys. Rev. Lett., 2004, 93: 243005
157. Y. Wu and R. Côté, Phys. Rev. A, 2002, 65: 053603
158. Y. Wu, J. Phys. B, 2002, 35: 4271
159. Y. Wu and X.-X. Yang, Chin. Phys. Lett., 2002, 19: 1410
160. H. Jing, Y. Deng, and W. Zhang, Phys. Rev. A, 2009, 80: 025601
161. A.Nunnenkamp, D. Meiser, and P. Meystre, New J. Phys., 2006, 8: 88
162. M. Fleischhauer and M. D. Lukin, Phys. Rev. Lett., 2000, 84: 5094
163. S. A. Haine, M. K. Olsen, and J. J. Hope, Phys. Rev. Lett., 2006, 96: 133601
164. S. Ospelkaus, A. Pe'er, K.-K. Ni, J. J. Zirbel, B. Neyenhuis, S. Kotochigova, P. S. Julienne, J. Ye, and D. S. Jin, Nature Phys., 2008, 4: 622
165. H. Jing and M.-S. Zhan, Eur. Phys. J. D, 2007, 42: 183
166. S. Chen, Y. A. Chen, T. Strassel, Z. S. Yuan, B. Zhao, J. Schmiedmayer, and J. W. Pan, Phys. Rev. Lett., 2006, 97: 173004
167. J. Simon, H. Tanji, J. K. Thompson, and V. Vuletić, Phys. Rev. Lett., 2007, 98: 183601
168. R. Zhao, Y. O. Dudin, S. D. Jenkins, C. J. Campbell, D. N. Matsukevich, T. A. B. Kennedy, and A. Kuzmich, Nature Phys., 2009, 5: 100
169. B. Zhao, Y. A. Chen, X. H. Bao, T. Strassel, C. S. Chuu, X. M. Jin, J. Schmiedmayer, Z. S. Yuan, S. Chen, and J. W. Pan, Nature Phys., 2009, 5: 95
170. N. S. Ginsberg, S. R. Garner, and L. V. Hau, Nature, 2007, 445: 623
171. A. V. Gorshkov, A. André, M. Fleischhauer, A. S. Sørensen, and M. D. Lukin, Phys. Rev. Lett., 2007, 98: 123601
172. I. Novikova, A. V. Gorshkov, D. F. Phillips, A. S. Sørensen, M. D. Lukin, and R. L. Walsworth, Phys. Rev. Lett., 2007, 98: 243602
173. M. Mackie, K. Härkönen, A. Collin, K.-A. Suominen, and J. Javanainen, Phys. Rev. A, 2004, 70: 013614
174. T. Busch, and J. R. Anglin, Phys. Rev. Lett., 2000, 84: 2298
175. J. Denschlag, J. E. Simsarian, D. L. Feder, C. W. Clark, L. A. Collins, J. Cubizolles, L. Deng, E. W. Hagley, K. Helmerson, W. P. Reinhardt, S. L. Rolston, B. I. Schneider, and W. D. Phillips, Science, 2000, 287: 97
176. M. R. Andrews, D. M. Kurn, H.-J. Miesner, D. S. Durfee, C. G. Townsend, S. Inouye, and W. Ketterle, Phys. Rev. Lett., 1997, 79: 553
177. A. Griesmaier, J. Werner, S. Hensler, J. Stuhler, and T. Pfau, Phys. Rev. Lett., 2005, 94: 160401
178. S. Yi and L. You, Phys. Rev. A, 2000, 61: 041604(R)
179. L. Santos, G. V. Shlyapnikov, and M. Lewenstein, Phys. Rev. Lett., 2003, 90: 250403
180. H. Jing, Y. Jiang, and P. Meystre, Phys. Rev. A, 2009, 80: 063618
181. W. Zhang, S. Yi, and L. You, Phys. Rev. A, 2004, 70: 043611
182. M.-S. Chang, Q. Qin, W. Zhang, L. You, and M. S. Chapman, Nature Phys., 2005, 1: 111
183. S. Yi and H. Pu, Phys. Rev. Lett., 2006, 97: 020401
184. C. Eberlein, S. Giovanazzi, and D. H. J. O'Dell, Phys. Rev. A, 2005, 71: 033618
185. S. Giovanazzi, A. Görlitz, and T. Pfau, Phys. Rev. Lett., 2002, 89: 130401
186. J. Cheng, H. Jing, and Y.-J. Yan, Phys. Rev. A, 2008, 77: 061604(R)
187. J. Rudnick, Phys. Rev. E, 1994, 49: 5768
188. J. Cheng, Phys. Rev. A, 2009, 80: 023608
189. C. D. Hamley, E. M. Bookjans, G. Behin-Aein, P. Ahmadi, and M. S. Chapman, Phys. Rev. A, 2009, 79: 023401

190. L. E. Sadler, J. M. Higbie, S. R. Leslie, M. Vengalattore, and D. M. Stamper-Kurn, Nature, 2006, 443: 312
191. H. Jing, Y. Jiang, W. Zhang, and P. Meystre, Phys. Rev. A, 2010, 81: 031603(R)
192. J. Calsamiglia, M. Mackie, and K.-A. Suominen, Phys. Rev. Lett., 2001, 87: 160403
193. E. G. M. van Kempen, S. J. J. M. F. Kokkelmans, D. J. Heinzen, and B. J. Verhaar, Phys. Rev. Lett., 2002, 88: 093201
194. Y. Liu, E. Gomez, S. E. Maxwell, L. D. Turner, E. Tiesinga, and P. D. Lett, Phys. Rev. Lett., 2009, 102: 225301
195. H. Pu and P. Meystre, Phys. Rev. Lett., 2000, 85: 3987
196. L.-M. Duan, A. Sørensen, J. I. Cirac, and P. Zoller, Phys. Rev. Lett., 2000, 85: 3991
197. Y.-X. Liu, J. Q. You, L. F. Wei, C. P. Sun, and F. Nori, Phys. Rev. Lett., 2005, 95: 087001
198. G. Thalhammer, M. Theis, K. Winkler, R. Grimm, and J. H. Denschlag, Phys. Rev. A, 2005, 71: 033403
199. W. X. Zhang, S. Yi, and L. You, New J. Phys., 2003, 5: 77
200. W. Zhang, D. L. Zhou, M.-S. Chang, M. S. Chapman, and L. You, Phys. Rev. Lett., 2005, 95: 180403
201. L. E. Sadler, J. M. Higbie, S. R. Leslie, M. Vengalatorre, and D. M. Stamper-Kurn, Nature, 2006, 443: 321
202. C. P. Search, J. M. Campuzano, and M. Zivkovic, Phys. Rev. A, 2009, 80: 043619
203. R. Kanamoto and P. Meystre, Phys. Rev. Lett., 2010, 104: 063601
204. Y. Li, C. Bruder, and C. P. Sun, Phys. Rev. Lett., 2007, 99: 130403
205. R. S. Fletcher, X. L. Zhang, and S. L. Rolston, Phys. Rev. Lett., 2007, 99: 145001